

Evaluation of Nanoparticle (NP) Toxicity in Respect to NP Physicochemistry
and Reactivity in the Aquatic Environment

Danae Patsiou

Submitted for the degree of Doctor of Philosophy

Heriot-Watt University

School of Energy, Geoscience, Infrastructure and Society

Institute of Life and Earth Sciences

May 2018

The copyright in this thesis is owned by the author. Any quotation from the thesis or use of any of the information contained in it must acknowledge this thesis as the source of the quotation or information.

ABSTRACT

The increasing application of nanoparticles (NPs) has led to increased occurrence of engineered NPs in the aquatic environment. Understanding the toxicity of NPs in the aquatic environment is dependent on linking NP physicochemistry with toxicological responses and while research has been moving towards this direction, the link has not been fully understood yet. The present study critically reviewed adsorption and desorption processes of organic environmental contaminants on TiO₂ NPs and evaluated interactions of NPs with compounds of different physicochemistry already existing in the aquatic environment as contaminants. Aquatic toxicity of the new generation lead-halide perovskite NPs was evaluated relative to lead ion dissolution. Finally, the sedimentation of NP agglomerates during a traditional fish early-life stage toxicity test, a major limitation of assessing NP toxicity in the aqueous phase, was addressed by development of an exposure chamber designed to keep NP agglomerates in homogeneous dispersion. The model organisms used in the present study to evaluate NP toxicity were larvae and adult zebrafish *Danio rerio* and the unicellular green fresh water alga *Chlorella vulgaris*. The main findings were: 1) sorption of environmental contaminants on NPs can change the bioavailability of the contaminant in the aqueous phase. Specifically, sorption of copper and benzo(a)pyrene (under fluorescent light) on NPs reduced the adsorbent bioavailability. On the contrary, benzo(a)pyrene and anthracene, when adsorbed on TiO₂ or Si NPs, were photo-catalysed under UVA and in the case of benzo(a)pyrene, highly toxic photo-by-products showed increased bioavailability in larval zebrafish; 2) lead-halide perovskite acute toxicity was attributed to lead ion dissolution based on induction of metallothionein 2 gene expression through aqueous and dietary exposure, and 3) the perovskite-spiked diets did not disrupt zebrafish gut microbiome after a 14-d exposure while disruption of gut microbiota by equivalent Pb(NO₃)₂ diets was observed; finally, 4) higher toxicity was found when NPs were tested using an exposure chamber that allowed continuous NP dispersion, indicating toxicity is depended on the dispersion state of NPs. This study has expanded our knowledge on NP surface physicochemistry and interactions with surrounding compounds in the aqueous phase; has confirmed metal ion dissolution out of metallic NPs and linked perovskite NP toxicity to lead ion dissolution as well as linked NP toxicity to NP dispersion in the aqueous phase contributing to a better understanding of NP properties and reactivity relation to toxicity in the aquatic environment.

ACKNOWLEDGEMENTS

To begin with, I would like to acknowledge Dr Judit Kalman and Dr Ross Alexander for their contribution to the algal experiments presented in Chapters 3 and 5, Fengjia Liu for some molecular analysis presented in Chapter 2, Cristina del Rio Cubilledo for DNA and RNA isolation of zebrafish tissues presented in Chapter 4, Dr Ana Catarino and Dr Stephen Summers for advice and suggestions during the DNA analysis of zebrafish gut microbiota presented in Chapter 4 and Dr David Boyle for his contribution on the chemical analysis of the pelleted fish food in Chapter 4. I would like to thank Prof. Martin McCoustra for his advice in the chemistry background in Chapters 1 and 2. Also, many thanks to the members of the EPAquatic research group for maintenance of the zebrafish experimental population. This thesis was supported by the European Project FP7: Future Nano Needs “Framework to respond to regulatory needs of future nanomaterials and markets”.

I must express my gratitude to my supervisors: Prof. Ted Henry and Prof. Teresa Fernandes who trusted me with this project guided me and encouraged me throughout my time as their student. Special acknowledgment goes to Prof. Ted Henry who I have been lucky to have as my primary supervisor; he was an inspiration all these years, he taught me good science, critical thinking and scientific writing.

Completing this work would have been all the more difficult without my comrades in the lab and PhD life here in Edinburgh, Ana Catarino, Chrysi Xintaropoulou and Valentina Ricottone, we kept supporting and encouraging each other and grew stronger together. Finally, I must express my gratitude to my partner Dionysis and my mother, father and brother, for their patience and support through all the ups and downs of my research. I am indebted to them for their help.

ACADEMIC REGISTRY
Research Thesis Submission


Name:	Danai Patsiou		
School:	EGIS		
Version: <i>(i.e. First, Resubmission, Final)</i>	Final	Degree Sought:	PhD

Declaration

In accordance with the appropriate regulations I hereby submit my thesis and I declare that:

- 1) the thesis embodies the results of my own work and has been composed by myself
- 2) where appropriate, I have made acknowledgement of the work of others and have made reference to work carried out in collaboration with other persons
- 3) the thesis is the correct version of the thesis for submission and is the same version as any electronic versions submitted*.
- 4) my thesis for the award referred to, deposited in the Heriot-Watt University Library, should be made available for loan or photocopying and be available via the Institutional Repository, subject to such conditions as the Librarian may require
- 5) I understand that as a student of the University I am required to abide by the Regulations of the University and to conform to its discipline.
- 6) I confirm that the thesis has been verified against plagiarism via an approved plagiarism detection application e.g. Turnitin.

* Please note that it is the responsibility of the candidate to ensure that the correct version of the thesis is submitted.

Signature of Candidate:		Date:	
-------------------------	---	-------	--

Submission

Submitted By <i>(name in capitals)</i> :	
Signature of Individual Submitting:	
Date Submitted:	

For Completion in the Student Service Centre (SSC)

Received in the SSC by <i>(name in capitals)</i> :			
Method of Submission <i>(Handed in to SSC; posted through internal/external mail):</i>			
E-thesis Submitted (mandatory for final theses)			
Signature:		Date:	

Please note this form should be bound into the submitted thesis.
Academic Registry/Version (1) August 2016

Table of Contents

Glossary.....	10
Chapter 1- Introduction to Nanoparticle Physicochemistry and Toxicity in the Aqueous Phase, and Toxicant Sorption/Desorption onto TiO ₂ Nanoparticles	13
1.1 Abstract	13
1.2 Introduction	14
1.3.1 Changes in Toxicant Sorption/Desorption Physicochemistry with TiO ₂ NPs in the Aqueous Phase.....	16
1.3.2 Properties of TiO ₂ NPs in the aqueous phase	18
1.3.2.1 Agglomeration	18
1.3.2.2 Oxidation of TiO ₂ NPs by UV radiation	20
1.3.3 Sorption of Organic Substances to TiO ₂ NPs	22
1.3.3.1 Influence of Natural Organic Matter on sorption.....	22
1.3.3.2 Influence of TiO ₂ NP Surface Area on Sorption.....	22
1.4 Use of Bioavailability to Inform on Sorption of Organic Compounds onto TiO ₂ NPs	25
1.5 Pilot study.....	30
1.6 Thesis Objectives	32
Chapter 2 - Toxicity of PAHs in the Presence of NPs Depends on Sorption Capacity and Potential Photocatalytic Properties of NPs.....	35
2.1 Abstract	35
2.2 Introduction	36
2.3 Materials and Methods.....	38
2.3.1 Chemicals	38
2.3.2 Experimental Organism.....	39
2.3.3 Experimental Design.....	39

2.3.4 Experiment 1: Anthracene toxicity under UVA exposure	40
2.3.5 Experiment 2: Sorption of BaP to NPs.....	41
3.3.5 Experiment 3: Sorption of PAHs to NPs under UVA.....	41
2.3.6 Experiment 4: Sorption of PAHs to photo-excited NPs.....	42
2.3.7 Gene expression	42
2.3.8 Statistical analyses	43
2.4 Results and Discussion.....	44
2.4.1 Anthracene toxicity under UVA exposure	44
2.4.2 Sorption of BaP to NPs	45
2.4.3 Sorption of PAHs to NPs under UVA.....	49
2.4.4 Conclusions.....	56
Chapter 3 - Differences in Engineered Nanoparticle (NP) Physicochemistry Revealed by Investigation of Changes in Copper Bioavailability during Sorption to NPs in the Aqueous Phase.	57
3.1 Abstract	57
3.2 Introduction	57
3.3 Materials and Methods.....	59
3.3.1 Chemicals	59
3.3.2 Analytical chemistry	61
3.3.3 Test organisms	61
3.3.4 Concentration-response assays	62
3.3.5 mt2 gene expression	63
3.3.6 Statistical analyses	64
3.4 Results and Discussion.....	65
Chapter 4 - Investigation of Eco-Toxicity of Perovskite Nanomaterials in Aquatic Organisms.	76

4.1 Abstract	76
4.2 Introduction	76
4.3 Materials & Methods.....	78
4.3.1 Perovskite NPs.....	78
4.3.2 Aqueous acute toxicity tests	79
4.3.3 Dietary exposure	80
4.3.4 Measurements of Pb by analytical chemistry	81
4.3.5 Gene expression analysis.....	82
4.3.6 Assessment of gut microbiota.....	83
4.3.7 Histological analysis	84
4.3.8 Statistical analyses	84
4.4 Results and Discussion.....	85
Chapter 5 - A Comparison of Nanoparticle (NP) Acute Toxicity Tests in the Aqueous Phase: The Importance of Homogeneous NP Dispersions.	98
5.1 Abstract	98
5.2 Introduction	99
5.3 Materials and Methods.....	102
5.3.1 Nanoparticles tested	102
5.3.2 Acute Toxicity Tests	104
5.3.3 Antioxidant Activity.....	105
5.3.4 Statistical analyses	105
5.4 Results and Discussion.....	106
Chapter 6 - Conclusions	115
Appendix A	118
Appendix B.....	120
Appendix C.....	123

Appendix D	134
References	137

Glossary

Abbreviation	Explanation
ALA-D	δ -aminolevulinic acid dehydratase
ANOVA	Analysis of variance
ANT	Anthracene
BaP	Benzo(a)Pyrene
Bp	Base pairs
BDE	Polybrominated diphenyl ether
Chl α	Chlorophyll α
CI	Confidence interval
CIP	Ciprofloxacin
CNT	Carbon nanotube
Cyp1A	Cytochrome P450 1A
Ddb2	DNA damage protein 2
DLS	Dynamic light scattering
DMPO	5,5-dimethyl-1-pyrroline N-oxide
DMSO	Dimethyl sulfoxide
DOM	Dissolved organic matter
Dpf	Days post fertilization
E1	Estrone
E2	17 β -estradiol

EC50	Median effective concentration
EE2	17 α -ethinyl estradiol
EROD	7-Ethoxyresorufin O-Dealkylase
EU	European union
H2-DCF-DA	2, 7 dichlorofluorescein diacetate
FNN	Future Nano Needs
GLM	General linear model
GST	Glutathione S-transferase
Hpf	Hours post fertilization
ICP-MS / OES	Inductively coupled plasm - mass spectrometry / optical emission spectrometry
LC50	Median lethal concentration
LC-MS	Liquid chromatography - mass spectrometry
MS-222	Tricaine methanesulfonate
Mt2	Metallothionein 2
NM	Nanomaterial
NOM	Natural organic matter
NMDS	Nonmetric Multidimensional Scaling
NP	Nanoparticle
OECD	Organization of economic and cultural development
OTU	Operational taxonomical unit
PAHs	Polycyclic aromatic hydrocarbons

PCP	pentachlorophenol
PFOS	Perfluorooctanesulfonic acid
PVP	Polyvynil pyrrolidone
qRT PCR	Quantitative reverse transcription polymerase chain reaction
ROS	Reactive oxygen species
SE	Standard error
Sod1	Superoxide dismutase 1
TCDD	2,3,7,8-tetrachlorodibenzo-p-dioxin
tRFLP	Terminal restriction fragment length polymorphism
UVA	Ultra violet A

Chapter 1- Introduction to Nanoparticle Physicochemistry and Toxicity in the Aqueous Phase, and Toxicant Sorption/Desorption onto TiO₂ Nanoparticles

1.1 Abstract

The increasing applications and use of nanoparticles (NPs) has led to higher production and subsequent release of these particles into the aquatic environment. Substances in surface waters will likely sorb to NPs and sorption has implications on the fate, transport, and environmental consequences of both the substance and the NPs. The aim of this chapter is to review the sorption of organic substances with TiO₂ NPs, the most abundant NP in surface waters, in the aqueous phase, how sorption changes TiO₂ NPs physicochemistry, and how sorption can affect substance transport, decomposition, and bioavailability in aquatic organisms. After having critically reviewed studies that have investigated sorption of organic substances with TiO₂ NPs, it is concluded that constituents of the aquatic environment, such as ionic compounds and natural organic matter, can change surface physicochemistry of TiO₂ NPs, promote agglomeration of NPs, and influence the sorption capacity of TiO₂ NPs to organic substances. UV radiation can enhance the degradation of some organic substances sorbed on the surface area of TiO₂ NPs. The bioavailability of some organic substances can be influenced by the presence or absence of TiO₂ NPs and measurement of bioavailability has been used as a sensitive method to inform on sorption of organic substances onto TiO₂ NPs and their transport in the aqueous phase. The sorption of a photo-labile organic compound, anthracene, onto anatase TiO₂ NPs under UVA light conditions was investigated by anthracene bioavailability in larval zebrafish. The reduction of bioavailable photo-excited anthracene in the presence of TiO₂ NPs indicates sorption of anthracene or photo-by-products onto TiO₂ NPs. Investigation of environmental factors that can influence sorption of organic contaminants onto TiO₂ NPs and their transport in the aqueous phase is important for understanding environmental fate and the implications of TiO₂ NPs presence in the aquatic environment. The present thesis, consequently, aimed to investigate: 1) sorption of polycyclic aromatic compounds onto TiO₂ and SI NPs under the effect of UVA radiation; 2) sorption of copper ions onto a wider range of NPs with different physicochemistry to associate sorption properties to NP physicochemistry; 3) toxicity of a new generation photovoltaic NP, perovskites, in the aquatic

environment; and 4) toxicity of NPs using enhanced exposure methods that minimise NP sedimentation throughout exposure duration.

1.2 Introduction

Nanomaterials (NMs) are materials with at least one dimension in the nanoscale while nanoparticles (NPs) have all three dimensions in the nanoscale (between 1 and 100 nm) (ISO, 2008). NMs can occur naturally in the environment in soil, volcanic ash, ocean spray, etc. Engineered NMs, are materials with tailored properties and unique physicochemistry that can be attributed to their nanoscale size. The nanoscale size of the NMs increases the surface area compared to bulk and their high surface-to-volume ratio increases reactivity when compared to larger particles. Thus, NM technology and development of NM applications involve a broad range of industry and research. For example, carbon nanotubes (CNT) are being used to reduce weight in spaceships (Gohardani et al., 2014), Ag NPs are widely used in food and fabric industry to minimise health risks from bacteria and to produce odour-free clothing (Haider and Kang, 2015; Kołodziejczak-Radzimska and Jesionowski, 2014), ZnO NPs can block ultraviolet (UV) rays and are widely used in sunscreens (Kołodziejczak-Radzimska and Jesionowski, 2014), and SiO₂ (Thomas and Stephen, 2010) and C₆₀ NPs (Dai, 2006) are used in sporting goods to increase strength and stability. While NMs can occur naturally [i.e. C₆₀ and C₇₀ fullerenes have been found as films on carbonaceous rocks (Buseck et al., 1992)], the increasing nanotechnology applications and uses in many aspects of everyday life, call for urgent investigation of engineered NMs environmental fate and toxicity upon release in the aquatic environment.

Due to NM broad applications and the spreading of NP products in the market, the likelihood of uncontrolled release of NPs in aquatic environment during manufacturing, in waste during or after application, or by accident is increasing. Sun et al., (2014) have estimated the most current environmental concentration according to production volumes and the distribution of products. Specifically, nano-TiO₂ are the NM mostly produced in EU and the most abundant NMs in the surface waters with estimated concentrations in the µg range (Sun et al., 2014). The production of ZnO NPs and CNTs are second and third highest. In the aquatic environment NMs are likely to interact with constituents within the media and form agglomerates that are held together by relatively weak forces of attraction such as van der Waals forces. Within the

aqueous phase, the characteristics and physicochemistry of NMs and NM agglomerates are important because they influence the environmental fate, bioavailability, and toxicology of NMs.

Although the aquatic toxicology of engineered NM has been increasingly studied for the last 13 years, a conclusive relationship between toxicity and aqueous-phase NM physicochemistry is not yet established. Numerous cases of indirect toxicity of NMs have been reported during NM toxicity assays that can lead to uncertainty, and misinterpretation and inaccurate conclusions (Petersen et al., 2014; Selck et al., 2016). For instance, in the aqueous phase, NMs can agglomerate, dissolve and release ions, and/or sediment to the bottom of the container; and changes in NM physicochemistry can occur throughout exposure (reviewed in Petersen et al., 2014). When the toxicity of metal NMs is reported, it is not clear if effects are related directly to the NMs or the ions released from the particles (Jang et al., 2014). Studies have reported that aqueous-phase NMs can associate with substances (e.g., environmental contaminants) and these associations can modify bioavailability of the substance and specific toxicological response in zebrafish (Boran et al., 2014; Henry et al., 2013; Park et al., 2011). Use of bioavailability measurements to investigate sorption of substances to NPs can provide a unique and highly relevant analytical tool that enables interrogation directly within the aqueous phase (i.e., without need for filtration or procedures that can disrupt sorption phenomenon).

The objective of this chapter is to review the aqueous-phase behaviour of TiO₂ NPs with a focus on sorption/desorption processes with organic contaminants. The chapter reviews the physicochemistry of the TiO₂ NPs in the aqueous phase, factors that affect sorption of organic contaminants onto TiO₂ NPs, the influence of UV photo-activation of TiO₂ NPs and other chemical substances, and the use of chemical bioavailability as a tool for the evaluation of sorption/desorption processes. A pilot study on the sorption of anthracene onto anatase TiO₂ NPs under UVA irradiation illustrates utility of detection methods based on bioavailability of decomposition products of organic contaminants in zebrafish larvae. Additionally, this chapter presents the areas the present thesis aims to investigate.

1.3.1 Changes in Toxicant Sorption/Desorption Physicochemistry with TiO₂ NPs in the Aqueous Phase

As described earlier, TiO₂ NMs are the most widely produced engineered NMs worldwide with an estimated current production of more than 200,000 tons per year (Robichaud et al., 2009; Sun et al., 2014). More than 60% of TiO₂ NMs are used in cosmetics and sunscreens, and, due to their white colour, TiO₂ NMs are widely used as a pigment in paints, plastics as well as in the food industry (Sun et al., 2014). The most frequently used TiO₂ NMs are the Aeroxide P25 NPs (Evonik Degussa), and numerous studies on P25 have been conducted since this NP was first mentioned in the literature in 1985 (Cărdoba and Luque, 1985). Specifically, a search “TiO₂” and “P25” in Scopus produces 4,425 document results (from 1980 till March 2017), 40% in the field of chemistry and 21.3% in the field of environmental sciences.

Their low cost and high chemical stability have made TiO₂ NMs attractive to support remediation of contaminated environments, and TiO₂ NMs have been used in decontamination of air, water and soil (Choi et al., 2006). TiO₂ is a common semiconductor and an excellent photo-catalyst and with potential for application to the photo-degradation of organic compounds in the aqueous phase (Linsebigler et al., 1995). The photocatalytic reaction starts with photo-excitation of a valence electron and the subsequent generation of an electron-hole pair that leads to creation of hydrogen peroxide and consequent photo-degradation of organic compounds in the presence of water (Gaya and Abdullah, 2008). Anatase and rutile, the two most common crystalline structures of TiO₂, can be photo-excited in the ultraviolet A (UVA) and visible light spectrum, respectively (Hurum et al., 2003). The nanoscale properties of TiO₂ NPs increase the catalytic functionalities of the material and the efficiency of photo-degradation of unwanted substances (e.g. contaminants).

Release of TiO₂ NPs in the aquatic environment can be natural from the terrestrial environment; accidental, during industrial processes and fabrication of engineered NPs; or intentional, during and after use of products containing TiO₂ NPs. Studies based on the large amount of information available for production of economically important engineered NMs have been used to model and predict nano-TiO₂ concentrations in the aquatic environment (Gottschalk et al., 2009; Gottschalk et al., 2013). Taken into consideration the production volumes, the importance of product allocation and life cycle, the predicted environmental concentrations of nano-TiO₂ were the highest in sewage effluent, surface waters, sediments and soils, and

calculated to be less than 1 $\mu\text{g/L}$ on surface waters while TiO_2 pigment was estimated to be in only one order of magnitude higher concentrations (Sun et al., 2014).

Once in the aquatic environment, TiO_2 NPs can undergo transformations that can alter their physicochemistry compared to the pristine state. After TiO_2 NP release into the environment, ozone, UV light and humidity alter the NP surfaces and can affect surface coatings (Labille et al., 2010; Mitrano et al., 2015). The process of oxidation is affected by environmental conditions and the duration in the environment. The oxidation that occurs on the surface of the particle after the release and weathering of commercial coated TiO_2 NPs in the aquatic environment, can erode the coating and expose the core TiO_2 NPs (Kaegi et al., 2008). The ionic strength and changes in ionic strength of surface waters (e.g., transitions between freshwater and marine waters, different ionic content) can induce changes in physicochemistry of NPs including alterations in surface properties that can lead to larger masses of NPs. High calcium levels can neutralize the negative surface charge of TiO_2 NPs in fresh water, and the presence of divalent ions tends to promote agglomeration of NPs (Shih et al., 2012). Changes of the surface charge and surface area can in turn lead to alteration of surface physicochemistry of the particles and complicate the interactions and sorption of other compounds present in the aquatic environment (i.e. natural organic matter, organic contaminants, metals). For instance, thorium sorption onto TiO_2 NPs is independent of the presence of NaCl or KCl in aqueous solution (Tan et al., 2007; Zhijun et al., 2005), but the presence of K^+ , Li^+ or Na^+ can alter the surface of TiO_2 NPs and compete with thorium ions for sorption sites onto TiO_2 NPs, therefore changing the sorption capacity of TiO_2 NPs (Tan et al., 2007).

The interactions between TiO_2 NPs and organic contaminants present in the aquatic environment can have implications on the environmental fate and transport of the compounds involved. Numerous studies have investigated the complicated processes of adsorption of organic compounds on the surface of TiO_2 NPs. Sorption refers to the collective processes of adsorption, the process of adhesion of a molecule to a surface due to surface forces (Calvert, 1990); and absorption, the process of molecules crossing the surface and retained by the material (Calvert, 1990). The physicochemical properties of both adsorbent and adsorbate (e.g. size and the charge of the TiO_2 NPs and the organic compound) can influence sorption of substances to NPs. The chemistry of the sorption of organic contaminants onto TiO_2 NPs has been investigated in the context of photo degradation of organic contaminants in the aquatic environment (Lee et al., 2015; Li et al., 2010; Okupnik et al., 2015; Peterson et al., 2012), but

these studies have not been critically reviewed. Further, sorption of contaminants onto TiO₂ NPs and effects on bioavailability and toxicity in aquatic organisms have been researched, (Fang et al., 2015; Farkas et al., 2015; Qiang et al., 2015), and these studies must be critically evaluated to advance the collective understanding of the environmental implications of toxicant sorption onto TiO₂ NPs.

1.3.2 Properties of TiO₂ NPs in the aqueous phase

1.3.2.1 Agglomeration

Titanium dioxide NPs agglomerate, and agglomeration is influenced by NP surface charge, size, and presence of other substances in the aqueous phase. The term “agglomerate” (Figure 1.1) is defined as a cluster of NPs and other substances that is loosely held (i.e., a cluster of NPs that readily return to original nanoscale size by high frequency sonication), whereas, the term aggregate is used to refer to a cluster of strongly held NPs that are not returned to original nanoscale dispersion by high frequency sonication (Jiang et al., 2009b). It has been documented that surface charge of oxide NPs is an important property responsible for the agglomeration of the particles (Bian et al., 2011; Keller et al., 2010). At the nanoscale, attractive forces between particles (van der Waals forces) can cause NPs to agglomerate. The isoelectric point of anatase TiO₂ NPs in the aqueous phase is at pH 6 (Jiang et al., 2009b) and the NPs acquire a negative surface charge in waters of higher pH (down to approximately -40 mV) (Allouni et al., 2009; Jiang et al., 2009a; Lee et al., 2015; Loosli et al., 2015; Okupnik et al., 2015; Salih et al., 2015). A pH closer to the isoelectric point of the NPs enhances NP agglomeration, while at higher pH values the absolute value of the surface charge can increase repulsive forces between NPs and reduce agglomeration (Jiang et al., 2009b).

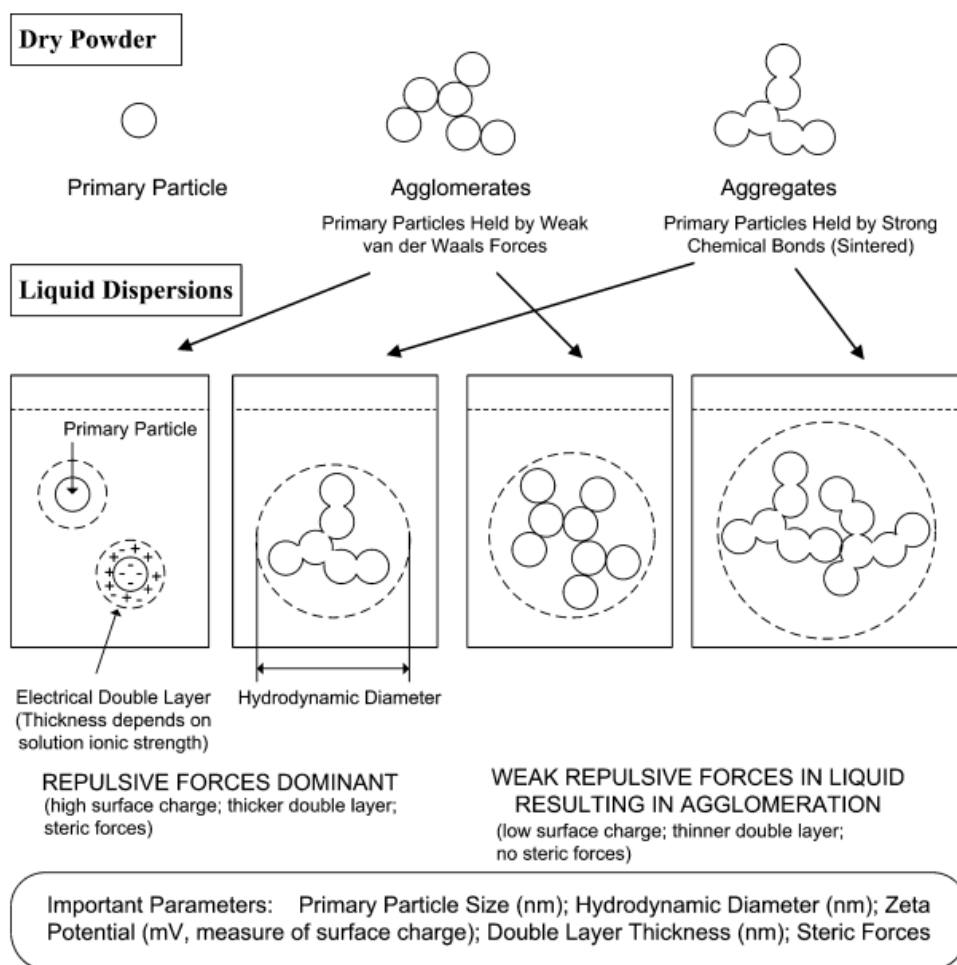


Figure 1.1: Different conditions and formations of particles in dry and aqueous phase as found in Jiang et al., 2009b.

The physicochemical properties of NP are likely to affect agglomeration in the aqueous phase. Specifically, the NP surface area available for interactions with the surrounding environment and the chemical structure of the surface are additional factors that influence NP agglomeration. The crystalline structure of TiO₂ NPs likely affects agglomeration and potential sedimentation of the NPs in the aqueous phase. More rapid sedimentation has been observed for rutile TiO₂ NPs compared to anatase TiO₂ NPs in the water column (Qiang et al., 2015). Specifically, for rutile TiO₂ NPs (20 - 80 nm primary size) 48 h after being introduced to a fresh water medium, more than 80% of the TiO₂ concentration was decreased in the upper water layer and in turn large agglomerates of 800 nm size were found in the bottom layer based on measurements by dynamic light scattering (DLS) (Qiang et al., 2015). On the contrary, the same study observed that the concentration of anatase TiO₂ NPs of a primary size 20 - 50 nm reduced by 52% in the upper water layer within 48 h (Qiang et al., 2015). The particle size and

surface area have been reported to be more important than the crystalline structure in the agglomeration of the TiO₂ NPs (Okupnik et al., 2015; Suttiponparnit et al., 2010).

The ionic strength of the medium can induce the formation of TiO₂ NP agglomerates in the aqueous phase. Divalent cations adsorb to specific sites on the surface of TiO₂ NPs and neutralize the negative charges on the surface and thereby prevent repellent forces between NPs and facilitating agglomeration (Romanello and de Cortalezzi, 2013). Calcium ions of a fresh water medium neutralize the surface charge of NPs and leading to agglomeration. The presence of natural organic matter (NOM) can stabilize aqueous dispersions of NPs when concentrations of divalent cations are relatively low (e.g., 0.3 mM of CaCl₂) (Romanello and de Cortalezzi, 2013), and this is likely because calcium ions bind to the NOM and are then less available to sorb to TiO₂ NPs. The TiO₂ NP agglomerates tend to sediment rapidly in fresh water and sea water media. Specifically, 80% of the TiO₂ NPs were removed from the water column in less than 100 minutes and formed larger agglomerates in seawater compared to fresh water (Keller et al., 2010). The hydrodynamic diameter (i.e., the average size) of TiO₂ NPs in suspension, increased from 793 to 2833 nm as the concentration of TiO₂ NPs increased from 5 to 50 mg/L, after 3 h in Roswell Park Memorial Institute (RPMI) cell and tissue culture medium (Allouni et al., 2009).

1.3.2.2 Oxidation of TiO₂ NPs by UV radiation

Ultraviolet illumination can cause changes in the surface chemistry of TiO₂ NPs and other metal oxide NPs such as ZnO and CeO₂. TiO₂ NPs under UV light produce electron-hole pairs (e⁻-h⁺) and the oxidation of H₂O or OH⁻ generates hydroxyl radicals (OH[•]) (Li et al., 2002). Additionally, the presence of O₂ acts as an electron trap that leads to generation of superoxide (O₂^{•-}) (Li et al., 2002; Gaya and Abdullah, 2008). The above observations indicate that UV light can induce the production of reactive oxygen species (ROS) by TiO₂ NPs. Pigeot-Remy et al., (2017) observed high levels of hydroxyl radicals at the surface of TiO₂ P25 NPs by spin trapping after 15 sec of UVA irradiation. Anatase band gap energy of 3.2 eV corresponds to 385 nm UVA wavelength while rutile TiO₂ has a smaller band gap energy (3.0 eV) with excitation at 410 nm wavelength (Hurum et al., 2003), Band gap energy of a semi-conductor material corresponds to the electron flow from valence to conduction and can depend on external source of energy (e.g. solar radiation) (Yablonovitch, 1993). Therefore, oxidation of TiO₂ NPs by UV light can potentially occur after their release to the aquatic environment and

exposure to sunlight. No free radicals were observed with P25 TiO₂ NPs under 4 h of visible light exposure; however, the intensity of 5,5-dimethyl-1-pyrroline N-oxide (DMPO)-OH^{*} was significantly increased after the incorporation of boron and nickel in TiO₂ NPs indicating that chemical composition of TiO₂ NPs can influence production of free radicals (Zhao et al., 2004). Brame et al. (2013) indirectly demonstrated the presence of ROS during degradation of 4-chlorophenol in the presence of sunlight and food-grade TiO₂ NPs, when upon addition of the hydroxyl radical (•OH) scavenger, isopropanol, the degradation ended. Weathering of TiO₂ NPs, used in cosmetic products, by artificial daylight degraded the polydimethylsiloxane coating of the TiO₂ NPs (Auffan et al., 2010). Silicon as part of the coating of the TiO₂ NPs, leached in solution (up to 90% of the initial weight) and the remaining coating layer was oxidized (Auffan et al., 2010). This alteration process of the surface of TiO₂ NPs after release in the aquatic environment can alter the physicochemical properties and reactivity of the NPs.

Photo-degradation of organic compounds by metal oxide NPs is a promising method for the elimination of organic contaminants from the water. In particular, TiO₂ P25 NPs under UV light facilitated photo-degradation and led to a reduction in half of the amount of paracetamol present within 300 min (Yang et al., 2008). Further, Peterson et al., (2012) observed total degradation of ampicillin after 500 min in the presence of anatase TiO₂ NPs under 254 nm UV light. For the TiO₂ materials, the NPs provide larger surface area, compared to larger particles, and this can lead to higher photocatalytic activity compared to bulk material (Belessi et al., 2007). Specifically, a TiO₂ NP of 30 nm diameter achieved total degradation of methylene blue in 10 min under 300 nm UV light in aqueous solution, while TiO₂ particles of 49 μm diameter needed 60 min to facilitate the same amount of degradation (Xu et al., 1999). Estrone (E1) and 17β-estradiol (E2) (ng/L range) were totally degraded under light (238-579 nm) in the presence of TiO₂ P25 (1 g/L) within 4 h, and, when the light was fixed at 253 nm, the degradation time reduced to less than 1 h (Zhang et al., 2007). Investigation of ofloxacin degradation by TiO₂ NPs in dark conditions showed that sorption onto TiO₂ NPs led to breakage of organic compounds and degradation of ofloxacin after 100 h (Peterson et al., 2015) compared to UV photo degradation of the same compound in the range of minutes to 1 h (Paul et al. 2007; An et al., 2010).

1.3.3 Sorption of Organic Substances to TiO₂ NPs

1.3.3.1 Influence of Natural Organic Matter on sorption

NOM can associate with TiO₂ NPs and influence the NP physicochemistry and environmental fate. NOM is a mixture of organic compounds naturally occurring in the aquatic environment (Sillanpää, 2014); and NOM includes carboxylic and amino acids, proteins, and substances that include molecules of high molecular weight such as humic and fulvic acids (Belin et al., 1993). The amount and the properties of NOM may differ according to area (geology, soil composition) and season. As mentioned above, NOM can sorb onto the surface of TiO₂ NPs in the aqueous phase and stabilize the NPs in dispersion. Therefore, in the presence of NOM the agglomeration of particles tends to be inhibited. High concentrations of Ca ions (>1.5 mM of CaCl₂), however, can promote neutralization of the surface charge and increase of the hydrodynamic diameter (Zhang et al., 2009).

The presence of NOM in aquatic environments can influence sorption of organic contaminants onto TiO₂ NPs. Fries et al., (2016) investigated sorption of the antibiotic ciprofloxacin (CIP) onto TiO₂ NPs, in the presence of NOM, and concluded that NOM and CIP competed for sorption sites on TiO₂ NPs, and, in the presence of NOM, CIP sorption on TiO₂ NPs was reduced. The study used 500 mg/L TiO₂ NPs and achieved sorption of 50 % of the primary CIP concentration. Wang et al., (2014) found that the presence of dissolved organic matter (DOM, specifically tannic acid) as a coating on TiO₂ NPs, enhanced the sorption of phenanthrene on TiO₂ NPs. The DOM coating of TiO₂ NPs promoted agglomeration of NPs reducing the surface area available for sorption therefore, the sorption of phenanthrene onto NPs compared to bulk TiO₂ was not different. Zhang et al. (2007) observed that in the presence of humic acid, the photo-degradation of E1 and E2 by TiO₂ P25 was enhanced and that was attributed to the additional photosensitivity of NOM itself.

1.3.3.2 Influence of TiO₂ NP Surface Area on Sorption

The surface area of TiO₂ NPs available is important for sorption, and total surface area in a preparation is influenced by the number of particles and the surface-to-volume ratio of the particles present. More perfluorooctanesulfonic acid (PFOS) was sorbed to small anatase particles of the same mass compared to larger rutile TiO₂ NPs as detected by measurement of the PFOS concentration in the top layer of the water column after centrifugation of PFOS-TiO₂

NPs and analysis by ultra-performance liquid chromatography - tandem mass spectrometry (Qiang et al., 2015). The conclusion that the size of the particles is more important than the crystalline structure was supported by another study that investigated sorption of algal toxin, microcystin LR, onto TiO₂ NPs (Okupnik et al. 2015). In particular, TiO₂ P25 (80% anatase, 20% rutile) displayed the highest capacity for microcystin adsorption measured in supernatant by liquid chromatography - mass spectrometry (LC-MS), followed by pure anatase NPs and pure rutile NPs; however, P25 NPs did have the smallest hydrodynamic diameter. All TiO₂ NPs displayed higher capacity for adsorption of the cyanobacterial toxin compared to bulk TiO₂ (Okupnik et al., 2015).

Larger surface area can potentially be achieved with higher concentrations of NPs, but greater numbers of particles can increase the potential for agglomeration and thereby reduce surface area available for sorption. Farkas et al. (2015) observed reduced concentration of benzo(a)pyrene (BaP) in the aqueous phase to 61% of the starting concentration in the presence of 0.2 mg/L TiO₂ NPs after sorption on the surface of the particles. Sedimentation of the TiO₂ NPs with sorbed BaP decreased further (37% of the starting BaP concentration) when more NPs were added in the preparations (2 mg/L) (Farkas et al., 2015). At higher TiO₂ NP concentrations (>150 mg/L), the effectiveness of the particle as a photo-catalyst was decreased due to agglomeration of the particles (Li et al., 2010). At higher concentrations, the agglomeration rate was faster due to increased probability of contact between particles. Increasing pH of medium from 2.29 to 6.15 led to the formation of larger agglomerates and the observed sorption/degradation of orange II dye was decreased (Li et al., 2010). Studies that have assessed sorption of organic compounds onto TiO₂ NPs are presented in Table 1.1.

Table 1.1: Evaluation of sorption of organic contaminants on TiO₂ NPs, based on analytical chemistry.

TiO₂ NPs specifics	Adsorbate	Factors assessed	Results	References
P25	Orange II	Agglomeration and photocatalytic performance	Less agglomeration of NPs, efficient photo-degradation of orange II	<i>Li et al., 2010</i>
P25 Anatase, rutile, rutile hydrophilic, rutile hydrophobic	Trichloroethylene phenanthrene	Activated carbon and humic acid Organic matter- different types of TiO ₂ NPs	Humic acid reduced sorption of Trichloroethylene on TiO ₂ NPs Sorption enhancement due to organic matter	<i>Salih et al., 2015</i> <i>Wang et al., 2014</i>
P25, anatase (<25 nm) and rutile (10-30 nm) NPs	Microcystin LR	Different crystalline phase of TiO ₂ NPs- NPs compared to bulk	Sorption of MLR enhanced with smaller size of TiO ₂ NPs	<i>Okupnik et al., 2015</i>
Anatase NPs (32 nm)	CIP	Natural organic matter	NOM competitive against CIP for sorption on TiO ₂ NPs	<i>Fries et al., 2016</i>
Rutile NPs 10 x 40 nm average particle size	17 β -estradiol	Effect of 17 β -estradiol on aggregation and NP characteristics	Quick sorption Changes in NPs size after sorption	<i>Lee et al., 2015</i>
P25	Dissolved matter	organic Photo degradation of DOM with TiO ₂ and UVA	Removal of 73-90% DOM	<i>Phong and Hur, 2015</i>
25 nm diam. anatase	ofloxacin	Adsorption vs degradation	TiO ₂ NPs remove ofloxacin by adsorption and degradation	<i>Van Wieren et al., 2012</i>
25 nm diam. anatase	Ampicillin	Effect of pH	TiO ₂ NPs remove penicillin by adsorption and degradation	<i>Peterson et al., 2012</i>
25 nm diam. anatase	ofloxacin	Dark conditions	Ofloxacin sorption to TiO ₂ , degradation occurred in dark conditions	<i>Peterson et al., 2015</i>

1.4 Use of Bioavailability to Inform on Sorption of Organic Compounds onto TiO₂ NPs

Aquatic toxicology of TiO₂ NPs has demonstrated that aqueous-phase agglomerates of TiO₂ NPs are of minimal toxicity at environmentally relevant concentrations. Aqueous concentrations of 0.1-1 mg/L (2-3 orders of magnitude above estimated TiO₂ NPs concentration on surface waters (Sun et al., 2014)) can interfere with respiratory surfaces in fish (Boyle et al., 2013b; Federici et al., 2007) and subsequent effects of TiO₂ NPs observed, such as on fish behaviour (Boyle et al., 2013b), reproduction (Ramsden et al., 2013), and tissues biochemistry (Boyle et al., 2013b). A critical comparison among studies conducted with identical TiO₂ NPs in rainbow trout *Oncorhynchus mykiss* exposed via diet, aqueous phase, and injection into cardiovascular system, demonstrated that Ti did not accumulate in internal tissues of rainbow trout after waterborne or dietary exposure. Minor sub-lethal toxicity indications (e.g. elevated TBARS and glutathione) were attributed to physical disruption of fish respiration (accumulation of TiO₂ NPs in gills; production of mucus in gills) after waterborne exposure (Boyle et al., 2013a). Although also at concentrations that are orders of magnitude higher than environmental relevance, TiO₂ NPs under simulated solar radiation with environmentally relevant UVA intensity of 1,700 $\mu\text{W}/\text{cm}^2$, enhanced mortality of smaller organisms than rainbow trout after daily renewal of exposure solutions. Specifically, zebrafish free swimming larvae 96-h LC₅₀ was observed at 134.6 mg/L TiO₂ NPs P25 (Ma and Diamond, 2013), in Japanese medaka larvae 96-h LC₅₀ was observed at 2.2 mg/L and 48-h LC₅₀ of 29.8 $\mu\text{g}/\text{L}$ was found in *Daphnia magna* (Ma et al., 2012) and no investigation of ROS has been conducted.

Sorption/desorption of substances with TiO₂ NPs has been investigated within the aqueous phase by evaluation of changes in substance bioavailability in organisms. Bioavailability of a substance can be defined as the amount of a substance that has entered the body and interacted with organs/tissues to generate a measurable response in the organism (Semple et al., 2004; Tian et al., 2014). The interpretation of a biomarker relies on the concentration-response principle, assuming a relationship between the response of the biomarker and the concentration of the chemical compound. For some organic substances, bioavailability can be influenced by the presence or absence of TiO₂ NPs, and, presumably, the change in substance bioavailability occurs because of sorption to TiO₂ NPs. The investigated organic substance should cause a well-defined concentration-response pattern, thus any changes in the biomarker response could

be attributed to the presence of TiO₂ NPs.

Organisms such as fish and bivalves have been used to evaluate the sorption of organic contaminants onto TiO₂ NPs in the aqueous phase (Table 1.2). The sorption of the organic compound onto TiO₂ NPs is shown as changes in the response (e.g., toxicity) of the organism to the compound. Sorption depends on the nature of the organic compound, the characteristics of TiO₂ NPs (size and crystal phase) as it has been mentioned earlier, and additionally can depend on the organism used for the assessment of bioavailability and the route of exposure (e.g. waterborne or dietary exposure). Direct comparison between studies is difficult because of differences in methods that include types of TiO₂ NPs, the organic compounds tested, and the organisms and end points used for measurement of bioavailability. Several different biomarkers and aquatic organisms have been used to assess bioavailability.

TiO₂ NP agglomerates with sorbed contaminants can be ingested by aquatic organisms and the bioavailability of the sorbed contaminant can increase after ingestion. Marine bivalves such as ark shell *Scapharca subcrenata* have been used to assess sorption of phenanthrene (Tian et al., 2014) and polybrominated diphenyl ether (BDE) (Tian et al., 2015), *Mytilus galloprovincialis* to evaluate sorption of 2,3,7,8-tetrachlorodibenzo-p-dioxin (TCDD) (Canesi et al., 2014) and *Haliotis diversicolor* to assess sorption of tributyltin on TiO₂ NPs (Zhu et al., 2011). The above-mentioned studies observed enhanced bioavailability of organic compounds in the presence of TiO₂ NPs suggesting that TiO₂ NPs facilitated transport of sorbed organic compounds into the studied organisms. One study observed reduced uptake (in µg/L) of benzo(a)pyrene in the presence of TiO₂ NPs in *Mytilus edulis*. No changes were observed in the activity of glutathione peroxidase and superoxide dismutase proteins; however, the catalase protein activity of the digestive glands was increased significantly in the presence of TiO₂ NPs indicating the presence of hydrogen peroxide and increased frequency of micronucleus in *M. edulis* haemocytes was also observed (Farkas et al., 2015). As bivalves are organisms of low mobility and feed by drawing large quantities of water via the inhalant siphon and filtering the water through the gill, waterborne TiO₂ NP agglomerates and potential sorbents can end up inside the organisms.

The bioavailability of a sorbed organic toxicant on TiO₂ NP agglomerates may differ when investigated in different developmental stages of the same organism. TiO₂ NPs facilitated bioaccumulation of PFOS in adult zebrafish and bioaccumulation of PCP was reduced in

zebrafish embryos (Qiang et al. 2015; Fang et al., 2015). Qiang et al., (2015) observed increased bioavailability of PFOS, as mass of PFOS in adult zebrafish wet weight, in the presence of TiO₂ NPs. Differences were found between two crystalline phases tested, specifically, anatase TiO₂ NPs increased PFOS bioavailability by 55.9% and rutile TiO₂ NPs increased PFOS by 25.4%. Zebrafish ingested TiO₂ agglomerates with sorbed PFOS and the TiO₂ NPs acted as a carrier increasing the concentration of hydrophobic PFOS in the whole fish body, although no information is provided on whether PFOS was accumulated or present on fish skin or in the lumen of the gut. Fang et al., (2015) investigated bioavailability of pentachlorophenol (PCP) in larval zebrafish to assess sorption of PCP onto TiO₂ NPs and observed that the mass of PCP accumulated by the organism was reduced in the presence of TiO₂ NPs by 33.7%. Further experimentation showed that the presence of TiO₂ NPs in the PCP exposure increased ROS measured by florescence, increased superoxide dismutase gene expression, suggesting increased bioavailability of PCP (Fang et al., 2015).

The bioavailability of the organic compound sorbed onto TiO₂ NPs can be different when assessed by different biomarkers and tissues of the same organism. The presence of TiO₂ P25 NPs had no effect on TCDD bioavailability in European sea bass (Della Torre et al., 2015; Vannuccini et al., 2015). The presence of TiO₂ NPs did not change the bioavailability of TCDD as assessed by measurement of upregulation of cytochrome P4501A (*cyp1A*) and glutathione s-transferase gene expression or EROD enzyme activity (Della Torre et al., 2015; Vannuccini et al., 2015), however the presence of TiO₂ NPs and adsorbate suppressed significantly the expression of ATP-binding cassette genes, *abcb1* and *abcc1* (Vannuccini et al., 2015). Further analysis of expression of gene related to immunomodulation showed upregulation in gills and spleen of fish exposed in TiO₂ NPs or TCDD alone, but the presence of NPs reduced the induction caused by TCDD when fish were exposed to the mixture (Della Torre et al., 2015). This response in combination with the reduced body burden of TCDD in the presence of TiO₂ NPs, suggest that the sorption of TCDD onto TiO₂ NPs can cause alteration of physicochemical characteristics of agglomerates and sorbent and result in lower TCDD bioavailability. One explanation for the reduction of the concentration of primary substance can be the decomposition of the substance after sorption on the surface of TiO₂ NPs. Sorption onto TiO₂ NPs leads to photo-induced degradation or slower degradation of organic compounds in the dark conditions. TiO₂ NPs may induce decomposition of sorbed parent substances to by-products that can have biomarker response. For instance, as it is shown in this work (Figure

1.2), parent polycyclic aromatic hydrocarbons (PAHs) and degradation by-products may not have the same bioactivity, thus cause different biomarker response in the organism and inform on sorption of compound onto TiO₂ NPs differently.

Qiang et al. (2016) conducted a comparative study to assess sorption of PFOS on TiO₂ NPs in three species of fish that naturally occupy different levels of the water column. Zebrafish resided in the top layer of the exposure chamber, grass carp *Ctenopharyngodon idella* occupied the middle layer, and a benthic fish species, *Hypostomus plecostomus*, was in the bottom layer of the exposure chamber. The PFOS whole body burden was increased in the presence of TiO₂ NPs, 59 % in zebrafish, 67.6 % in *C. idella* and 16.4% in *H. plecostomus*. The highest concentration of PFOS was found in the intestines, gills and skin of all three fish species after exposure to TiO₂-PFOS (Qiang et al., 2016). The results showed differences in the bioavailability of PFOS among species that can be attributed to the eating behaviour, natural habitat and physiology of each species. The PFOS-TiO₂ NPs combination increased PFOS concentration in zebrafish more than *H. plecostomus*.

Table 1.2: Evaluation of sorption of organic contaminants on TiO₂ NPs by assessment of bioavailability in aquatic organisms.

TiO ₂ NPs specifics	Adsorbate	Factors assessed	Target organism	Results	References
P25	2,3,7,8-tetrachlorodibenzo-p-dioxin (TCDD)	sorption	European sea bass	TiO ₂ NPs showed no effect in TCDD biotransformation gene expression	<i>Vanuccini et al., 2015</i>
25 nm d.	Pentachlorophenol (PCP)	PCP range of concentrations sorption	Zebrafish larvae	TiO ₂ reduced uptake of PCP	<i>Fang et al., 2015</i>
62 nm d.	Benzo-a-Pyrene (BaP)	Sorption on TiO ₂ range of conc.	<i>Mytilus edulis</i>	TiO ₂ reduced uptake of BaP	<i>Farkas et al., 2015</i>
<10 nm d. anatase NPs	Phenanthrene	sorption	Ark shell <i>Scapharca subcrenata</i>	TiO ₂ enhanced uptake	<i>Tian et al., 2014</i>
20-50 nm d. anatase NPs, 20-80 nm d. rutile NPs	Perfluorooctanesulfonate (PFOS)	TiO ₂ anatase and TiO ₂ rutile NPs sorption	Zebrafish adults	TiO ₂ NPs enhanced uptake	<i>Qiang et al., 2015</i>
P25	TCDD	sorption	European sea bass	TiO ₂ NPs did not affect biotransformation or bio-concentration of TCDD	<i>Della Torre et al., 2015</i>
P25	TCDD	In vitro and in vivo exposure	<i>Mytilus galloprovincialis</i>	TiO ₂ NPs enhanced bioavailability of TCDD	<i>Canesi et al., 2014</i>
7nm d.	polybrominated diphenyl ether (BDE)	Range of BDE conc. Range of TiO ₂ NPs conc.	Zebrafish larvae	TiO ₂ enhanced uptake	<i>Wang et al., 2014</i>
<10 nm d. anatase	Tributyltin (TBT)	Range of conc. of TBT	<i>Haliotis diversicolor</i> embryos	TiO ₂ enhanced TBT toxicity	<i>Zhu et al., 2011</i>
<10 nm d. anatase	BDE	Range of conc. of BDE	<i>Scapharca subcrenata</i>	TiO ₂ enhanced uptake of BDE	<i>Tian et al., 2015</i>
20-30 nm d. anatase	PFOS	Different fish species	Zebrafish, <i>Ctenopharyngodon idella</i> , <i>Hypostomus plecostomus</i>	TiO ₂ NPs increased bioaccumulation of PFOS in all three species	<i>Qiang et al., 2016</i>
P25	Ciprofloxacin (CIP)	UVA	<i>Vibrio fisheri</i>	Initial decrease in toxicity after sorption of CIP to TiO ₂ NPs, high toxicity of CIP by products	<i>Silva et al., 2016</i>

1.5 Pilot study

The present experiment was a small preliminary study designed to investigate sorption of anthracene onto TiO₂ NPs under UVA radiation (the main study is presented in Chapter 2). Other than this research, there A been no other studies that have used changes in substance bioavailability to investigate sorption of photo-labile aromatic compound on potentially photo-active NPs. Sorption of anthracene under UVA onto TiO₂ NPs was investigated assessing the bioavailability of photo-excited anthracene in zebrafish larvae (72-96 hpf). Zebrafish larvae (20 larvae per beaker) were exposed to 15 µg/L anthracene (dissolved in dimethyl sulfoxide, with final concentration of dimethyl sulfoxide <0.01% in the exposure preparations) and each treatment was repeated thrice. The control exposure is synthesized fresh water medium and DMSO (<0.01%) (79, 38, 12, 17 and 2 mg/L of Ca²⁺, Mg²⁺, Na⁺ and K⁺, respectively). Zebrafish were exposed to anthracene for 24 h and at the end of the exposure a UVA exposure followed (5 W/m²). Samples were collected 3 h after the end of UVA exposure for molecular analysis. The bioavailability of the aromatic hydrocarbon was assessed through changes in cytochrome P4501A (*cyp1A*) gene expression in zebrafish embryos conducted following the procedure presented by Sleight et al. (2017) after 24-h exposure to anthracene and anthracene and TiO₂ NPs mixtures (see chapter 2 section 3 for extensive information on zebrafish husbandry and breeding and gene expression methodology).

The results showed that anthracene exposure in zebrafish larvae did not induce *cyp1A* expression, however, anthracene exposed under UVA can induce *cyp1A* (6-fold induction). In the presence of TiO₂ NPs *cyp1A* remained at low levels, reducing the effect of photo-excited anthracene on *cyp1A* expression (Figure 1.2). The results indicate that anthracene under UVA irradiation altered chemical structure and metabolism of photo-excited anthracene induced *cyp1A* gene expression. The presence of TiO₂ NPs reduced the bioavailable anthracene by either providing enhanced surface area for anthracene to sorb leaving less/no amount of anthracene available to larvae or by degrading anthracene into by products that do not involve aryl hydrocarbon pathway biodegradation.

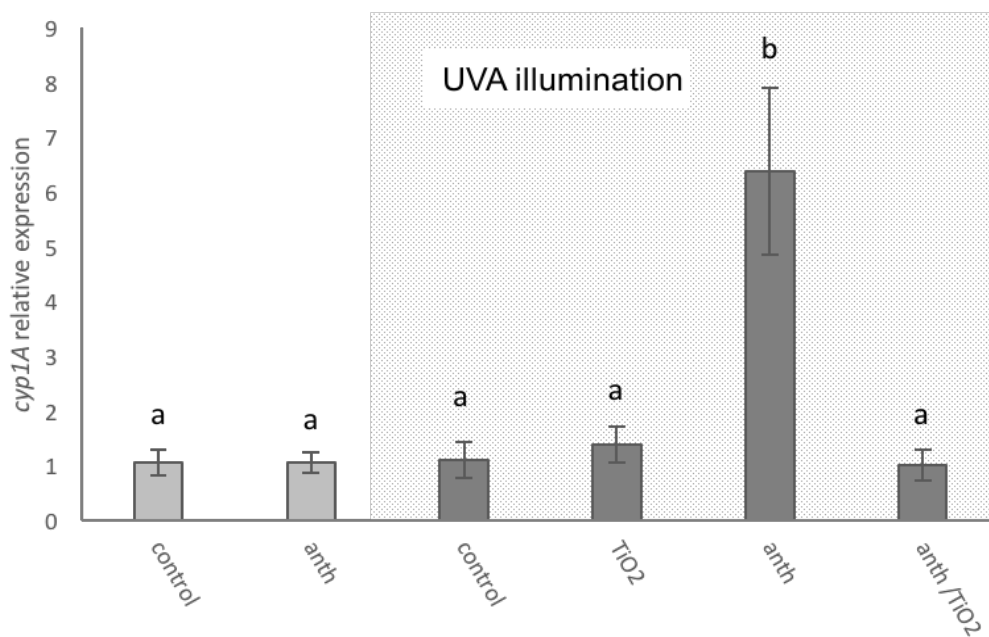


Figure 1.2: Relative expression of *cyp1A* in zebrafish larvae (72 hpf), after normalization to β -actin. When larvae (20 per sample) were exposed to 15 $\mu\text{g/L}$ of anthracene (anth) (n=3) no induction of *cyp1A* was observed. On the contrary, larvae exposed to anthracene under UVA illumination (5 W/m^2) (n=6) led to a 6.3-fold induction of *cyp1A*, suggesting that anthracene after UVA exposure creates photo-activated compound that is biodegraded by *cyp1A* enzyme. Exposure of TiO_2 NPs (2 mg/L) under UVA (n=3), do not induce *cyp1A* expression. The mixture of anthracene and TiO_2 NPs under UVA do not induce *cyp1A* expression, indicating that photo-activated anthracene is not bioavailable to the larvae (main study presented in Chapter 2). MEAN \pm SE, ANOVA, $p < 0.05$.

1.6 Thesis Objectives

To summarize, the present review indicates the urgent need to investigate NP environmental fate and the several implications of the sorption of organic contaminants onto a most abundant NP in the aquatic environment (i.e. TiO₂ NPs and agglomerates). It has been evident that the identification of the relationship of NP physicochemistry and NP toxicity in the aqueous phase is a fundamental issue to allow proper risk assessment. The indirect toxicity of NPs in the aquatic environment (e.g. ion release, sorption of existing environmental contaminants, etc) is a TiO₂ NPs are likely to interact with organic contaminants present in the aquatic environment during and after NP release. After manufacturing and during use and release in the aquatic environment, TiO₂ NPs can go through changes in their physicochemistry. Interactions between NPs or with ionic compounds, and solar irradiation can change the properties of the NP surface, making laboratory-based experiments more complicated to assess and interpret. Sorption of organic contaminants onto TiO₂ NPs can occur and promote transport of sorbent to aquatic organisms but can be influenced by changes in the physicochemistry of the surface of NPs and sorbent in the aqueous phase. TiO₂ NPs can facilitate photo-degradation of organic compounds with potential for use in environmental remediation; however, there is also potential that biologically active decomposition products are generated after interaction with UV light and organic substances adsorbed onto TiO₂ NPs. Evaluation of adsorbed substance bioavailability to investigate the sorption/desorption processes onto NPs is an environmentally relevant and sensitive approach that contributes important new information towards understanding sorption phenomena.

The experiments conducted in the present thesis were designed to investigate the aforementioned issues that occur with the presence of NP in the aquatic environment. All starting materials had all three dimensions in the nanoscale and have been referred to as NPs and NP agglomerates. While bioavailability measurements can change with changes of environmental factors, the bioavailability assessment of a model organism with well characterised and known responses (i.e. zebrafish) can be a very useful analytical tool. Zebrafish, *Danio rerio*, and the green microalga, *Chlorella vulgaris* were used as model organisms in the present study. Zebrafish is a fish with widely studied responses, standardised guidelines for conducting toxicity tests and completely sequenced genome. It is also an organism that develops fast and is easy to breed and keep in aquaria. *Chlorella vulgaris* has been chosen as second model organism with different biology compared to zebrafish, affected

potentially differently after exposure to the same toxicants, thus informing on and completing the knowledge acquired from zebrafish on NP behaviour and toxicity in the aqueous phase.

Specifically, the thesis objectives included the following:

1) Investigation of PAHs sorption on TiO₂ and Si NPs under UVA radiation by examining the PAH and by-products bioavailability in zebrafish larvae. The sorption of two representative, with distinct differences, photo-labile PAH compounds [anthracene and benzo(a)pyrene] was studied under laboratory and UVA light to identify effects of UVA radiation on sorption processes. Sorption was indicated by assessing bioavailability of PAHs and photo-by-products using expression of PAH metabolism genes. The study on sorption of PAHs onto NPs is presented in Chapter 2.

2) Investigation of copper sorption onto a wide range of NPs with different physicochemical properties in aqueous phase in the context of attributing co-contaminant sorption to NP physicochemistry. The positively charged copper ion sorption onto negatively charged NPs was studied by evaluation of copper bioavailability in *C. vulgaris* (growth inhibition) and zebrafish larvae (mortality and biomarker gene expression) in the presence of NPs. The study on copper sorption onto NPs is presented in Chapter 3.

4) Evaluation effects of lead-halide perovskites NPs (a new generation photovoltaic material) in the aquatic environment and whether perovskite toxicity can be attributed to Pb release. The perovskite toxicity was conducted by assessing perovskite NP toxicity in *C. vulgaris* and zebrafish larvae in the aqueous phase and via dietary exposure on adult zebrafish evaluating Pb bioavailability, tissue toxicity, and changes in zebrafish gut microbiota. The metal ion dissolution is an indirect effect of metallic NPs and respiration and dietary exposure are the major exposure routes of NPs in fish (Jang et al., 2014; Lu et al., 2017). Metal ion dissolution from metallic NPs significantly increases with low pH values (Bian et al., 2011), therefore, a dietary exposure can enhance metal dissolution after digestion of NP-spiked food and ion release in the gastro-intestinal (GI) tract. The exposure of perovskite NPs in algae and zebrafish is presented in Chapter 4.

5) Evaluation of relation between NP physicochemistry and acute toxicity of aqueous phase NPs in *C. vulgaris* and early life stage zebrafish with development of enhanced exposure methods. One major limitation of testing toxicity of aqueous-phase NM exposure is the lack of homogeneity of NM suspensions and toxicity of NPs has been reported to be related to the

dispersion state of NPs in the aqueous phase (Boyle et al., 2015). In Chapter 5 The issue of sedimentation of NP agglomerates has been addressed using an exposure chamber that allows exposure of zebrafish larvae to continuously dispersed NPs without damaging the larvae. The exposure chamber toxicity test has been compared to traditional static exposure methods and NP toxicity was also assessed in *C. vulgaris*, a standardised toxicity test that offers limited sedimentation of NPs.

Chapter 2 - Toxicity of PAHs in the Presence of NPs Depends on Sorption Capacity and Potential Photocatalytic Properties of NPs.

2.1 Abstract

Engineered NPs have unique physicochemistry that includes high surface area, surface reactivity, and photo-activity. In the aqueous phase, NPs can sorb substances and subsequently undergo complex chemical reactions that alter the chemistry of adsorbed substances. The present study evaluates sorption of two polycyclic aromatic hydrocarbons (PAHs) onto TiO₂ and Si NPs which have photo-activity and have been shown to sorb various substances in the aqueous phase. Sorption was evaluated by investigation of bioavailability of benzo(a)pyrene (BaP) and anthracene (ANT) through cytochrome P4501A (*cyp1A*) gene expression in larval zebrafish. The results support sorption of BaP under fluorescent light on both types of NPs (TiO₂ and Si NPs) as indicated by less bioavailability of BaP in the presence of NPs. Under ultraviolet radiation ANT and BaP were photo-lysed to by-products that significantly changed the gene expression of *cyp1A*, superoxide dismutase 1 and DNA damage protein 2. The presence of NPs and UVA promoted catalysis of both PAHs and ANT sorption onto NPs under UVA led to significantly reduced bioavailability of by-products compared to ANT alone under UVA suggesting a protective role of NPs. On the contrary, BaP toxicity under UVA was strongly related to sorption onto NPs and the surface are available. Specifically, at low concentrations of BaP, sorption and photo-catalysis were efficient that led to higher relative concentration and bioavailability of toxic photo-by-products. At high concentrations of BaP, the limited surface area of NPs present in the suspensions led to partial photo-catalysis of BaP therefore, showing relative lower toxicity when compared to BaP exposures under UVA alone. The present study suggested that sorption of PAHs onto NPs is closely related to surface area as well as the physicochemistry of the PAH. Finally, the photo-activity of the NPs can change the reactivity of the surface area, changing in turn the sorption processes. Understanding NP-substance sorption is an important consideration for managing the environmental risks of NPs.

2.2 Introduction

The unique physicochemical properties of NPs can have important implications on their interactions with other substances including toxicants in the aqueous phase. Both small size (high surface to volume ratio) and surface reactivity of NPs influence sorption capacity by increasing sorption sites on the surface of the NPs. Although some NPs can be of low toxicity, sorption/desorption of toxicants to NPs presents an important factor to consider for environmental risk assessments of NPs. Numerous reports of toxic substance sorption/desorption to NPs include nC₆₀ (Baun et al., 2008a; Henry et al., 2013; Park et al., 2011; Wang et al., 2009), carbon nanotubes (CNT) (Glomstad et al., 2016; Li et al., 2014; Pan et al., 2008), TiO₂ and SiO₂ NPs (Boran et al., 2016; Fang et al., 2015; Tian et al., 2014). These results suggest that NPs can act as a vehicle for the delivery of toxicants to organisms. Polycyclic aromatic hydrocarbons (PAHs) are a group of organic contaminants reported to associate with NPs in the aqueous phase (Baun et al., 2008b; Wang et al., 2009; Yang et al., 2006). Among the issues of toxicological importance regarding sorption/desorption of substances onto NPs are enhanced bioavailability of toxicants that are sorbed to NPs, interactions between NPs and toxicants that enhance toxicity (e.g., photo-activation of toxicants), and effects of toxicant sorption on NP physicochemistry.

Ultraviolet radiation of engineered NPs can cause photoexcitation and lead to photocatalytic decomposition of environmental organic contaminants. Photo-activation of NPs (e.g., TiO₂, ZnO, NiO NPs) can generate reactive oxygen species (ROS) (i.e. $\cdot\text{O}_2$, H₂O₂, $\cdot\text{OH}$) (Augugliaro et al., 2012) that have potential to react with organic substances including PAHs in aerated systems, with primary reaction initiated with the presence of the hydroxyl radical ($\cdot\text{OH}$) (Brubaker and Hites, 1998). Due to the different crystalline structures, the two most common in industry crystal types of TiO₂, anatase and rutile, exhibit functional differences, being commercially available in smaller size and having excitation range that corresponds to UVA wavelengths (388 nm). Rutile is thermodynamically stable and found commercially in larger sizes (200 nm particle diameter) and photo-excitation can occur in visible light wavelength (410nm) (Hurum et al., 2003). The outermost conduction band electrons of photo-activated TiO₂, can get caught by O₂ in aerated systems and create superoxide radical ions (O₂⁻) (Chen et al., 2004). Specifically, when TiO₂ P25 NPs were exposed under UVA, high levels of hydroxyl radicals ($\cdot\text{OH}$) were observed by electron pragmatic resonance spectroscopy (Pigeot-Remy et al., 2017). Additionally, Brame et al. (Brame et al., 2013) showed degradation of 4-

chlorophenol by food-grade TiO₂ NPs under sunlight, and degradation significantly decreased in the presence of the hydroxyl radical scavenger, isopropanol. Yang et al. (Yang et al., 2008) observed photo-degradation of half the amount of paracetamol within 300 min when TiO₂ P25 NPs were added in the aqueous solution and preparations were exposed under UVA while UVA or TiO₂ NPs alone caused minimal degradation of paracetamol.

PAHs are a group of hydrophobic organic compounds that can absorb energy from UV radiation and sorb to NPs in the aqueous phase. PAHs absorb light in the UVA region and create activated oxygen species that can pass the energy through the cell membrane and potentially lead to lipid peroxidation (Fu et al., 2012; Yu, 2002). Photo-toxicity of anthracene under UV radiation in fish was attributed to production of ROS (Oris and Giesy, 1990). Fluoranthene exposure under UVA led to developmental abnormalities, due to disorganised cell proliferation at the blastula stage and embryonic axis was not clearly visible, in Japanese medaka embryos (Diamond et al., 2006). PAHs have high molecular weight and low water solubility and have been reported to accumulate in organic material (Oris et al., 1990) and NPs in the aqueous phase (Baun et al., 2008). The sorption of phenanthrene to CNT was lower when CNTs with smaller number of potential adsorption sites were present, indicating that sorption is dependent on physicochemical properties of the NPs, such as surface area and functional groups (i.e. hydroxyl or carboxyl) (Glomstad et al., 2016). More phenanthrene molecules sorbed to multi-wall CNT compared to naphthalene molecules, a PAH with lower K_{ow} value and less hydrophobic than phenanthrene was observed (Wang et al., 2009), indicating the importance of the physicochemical properties of the adsorbate in the sorption processes.

Bioavailability of PAHs to model organisms has been used in the investigation of PAHs sorption to NPs. Bioavailability is defined as the amount of a compound that enters the target tissue and can have an active effect on a model organism (Semple et al., 2004). The NPs can act as a vehicle and transfer sorbed PAHs to exposed organisms, increasing the bioavailability or bioaccumulation of the compound after adsorbate desorption as indicated by mortality in *Daphnia magna* after ingestion of nC₆₀ aggregates and adsorbed phenanthrene by the organism (Baun et al., 2008), the adsorbate/NPs uptake by ark shell and amount of the desorbed compound measured inside the organism's tissues by analytical chemistry (Tian et al., 2014), or activity of well-known biomarkers for bioavailability of the adsorbate (i.e. ROS generation and GST activity for PAHs bioavailability) (Ferreira et al., 2014); no effects or direct toxicity of the specific NPs when exposed alone were observed, suggesting no bioavailability of NPs

(Ferreira et al., 2014; Tian et al., 2014). Hence, bioavailability indicates sorption of adsorbate onto NPs directly at the organism level and offers an environmentally relevant evaluation of impact of NPs in the aquatic environment. The presence of NPs, such as nC₆₀ agglomerates, reduced fluoranthrene photo-toxicity to *D. magna* after a short-term exposure (Yang et al., 2010). To our knowledge, although the photo-enhanced toxicity of PAHs is well reported, there is no information about how UVA can affect the sorption processes of PAHs on NPs with potential photo-activity and in turn the bioavailability of photo-excited PAHs in aquatic organisms.

The objective of this study was to further investigate sorption of PAHs onto commercially important engineered NPs adding the potential effect of UVA illumination in the aqueous phase. The selected NPs included semi-conductor materials belong to the energy value chain with potential photo-activity, specifically, two TiO₂ NPs with different properties (anatase : rutile ratios, and particle size) and Si NPs. Anthracene and BaP were selected as representative PAHs, that possess different physicochemical properties mainly are attributed to the differences in the molecular weight. Anthracene is a photo-labile and photo-toxic compound, with higher water solubility while BaP is a genotoxic compound and less water-soluble. The aim of the study was to investigate whether sorption of ANT and BaP can differ between NPs not only due to different physicochemical properties of both PAHs and NPs but also light excitation (after UVA illumination) of the tested compounds. The sorption of PAHs to NPs was evaluated by studying bioavailability as biomarker activity and specifically, gene expression, using well-documented and specific pathways (i.e. PAH metabolism) after PAHs exposure in larval zebrafish.

2.3 Materials and Methods

2.3.1 Chemicals

The NPs used for the sorption studies were: TiO₂ JRCNM01005a previously listed as NM105, Aeroxide P25 (Evonik Degussa) with a 25-30 nm particle diameter, anatase:rutile ratio of 85:15 and -6.45 mV z-potential when 10 mg/L were suspended in Milli-Q water, anatase TiO₂ NPs with primary particle diameter of 4-8 nm and z-potential of 46.8 mV in Milli-Q water and a Si NP provided by the Institute of Energy and Environmental Technology, Duisburg, Germany, with 100 nm particle diameter and -17.3 mV z-potential when 100 mg/L were suspended in

Milli-Q water. The PAHs used for this study were: anthracene (ANT) (Sigma-Aldrich, Lot#MKBN3282V) with 0.044 mg/L water solubility at 25 °C and benzo(a)pyrene (BaP) (Sigma-Aldrich, Lot#SLBM2972V) with 0.00162 mg/L water solubility at 25 °C. Dimethyl sulfoxide (DMSO) (Sigma Aldrich, Lot#: SHBF7881V) was used as solvent for ANT and BaP.

2.3.2 Experimental Organism

Zebrafish (*Danio rerio*) were obtained from the zebrafish research facility, Heriot Watt University. Husbandry, spawning and experiments using zebrafish were conducted following animal welfare regulations of the UK Home Office. Breeder fish were fed *ad libitum*, three times per day, with newly hatched *Artemia salina* or dry pellet food (ZM systems, Winchester, UK). Tap water was filtered through a reverse osmosis filter and fresh water was synthesised for husbandry and experiments in agreement with the OECD guidelines for fish early life-stage toxicity tests (OECD 210). The fresh water medium consisted of: 79, 38, 12, 17 and 2 mg/L of Ca²⁺, Mg²⁺, Na⁺ and K⁺, respectively with pH of 7.7. The temperature was maintained between 28-30 °C, and a 12-h photoperiod was kept in the zebrafish facility. More than 30 one-year-old zebrafish were used for each spawning event with a ratio of 3:2 females to males. Hatching occurred between 48 and 72 hours post fertilization (hpf) and fish of age 72 hpf were used for the experiments.

2.3.3 Experimental Design

Sorption of ANT and BaP on NPs was assessed by bioavailability assessments. The first experiment (experiment 1) investigated the gene expression of three biomarkers (cytochrome P450 1A (*cyp1A*), superoxide dismutase 1 (*sod1*), DNA damage protein 2 (*ddb2*)) for the evaluation of ANT bioavailability in larval zebrafish with and without UVA exposure. The following three experiments (numbers: 2, 3 and 4) were conducted for the investigation of sorption of PAHs on NPs under UVA using bioavailability of PAHs in larval zebrafish as the analytical tool (Figure 2.1).

2.3.4 Experiment 1: Anthracene toxicity under UVA exposure

Preliminary acute toxicity tests were conducted in zebrafish larvae (72-168 hpf) in a range of concentrations of ANT, 0 to 100 $\mu\text{g/L}$, and up to 45 $\mu\text{g/L}$ to BaP solved in DMSO, with final concentrations of DMSO in test solutions being less than 0.01%. Acute toxicity tests were conducted in 96-well plates in a total volume of 200 μl to assess mortality caused by exposure to ANT after 96-h exposure period. Three genes were investigated as indicators of ANT bioavailability in larval zebrafish. Zebrafish larvae 72 hpf were exposed to two parallel ANT dilution series (0-30 $\mu\text{g/L}$). Cytochrome P4501A (*cyp1A*), superoxide dismutase 1 (*sod1*) and DNA damage binding protein 2 (*ddb2*) were examined as potential biomarkers for studying ANT bioavailability. One dilution series was sampled after 24 h and the second dilution series was exposed to UVA (5 W/m^2). Preliminary time-point experiment (larvae exposed to 6 $\mu\text{g/L}$ ANT and samples selected at 0, 2, 4 and 6 h after the end of UVA exposure) indicated that *cyp1A* induced 3-fold 2 h after the end of the UVA exposure and the expression dropped at 4-h time-point. The *sod1* gene expression increased a 1.6-fold at 2 h after the end of the UVA exposure and a 1.9-fold at the 4 h time-point. The 3-h time-point was selected for further experimentation as both *cyp1A* and *sod1* were induced 3 h after the end of UVA exposure (Appendix A).

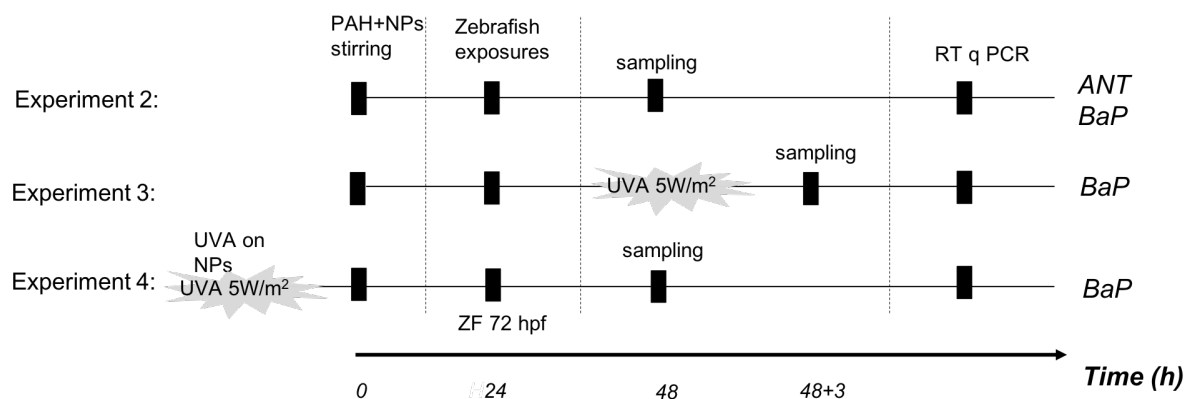


Figure 2.1: Experimental design of the present study featuring the experiments 2-4 that were designed to assess the effect of PAH sorption onto NPs under UVA illumination. Time (0h) starts with PAHs and NPs mixtures stirring (for 24 h) and then zebrafish larvae (72 hpf) are added and exposure starts. The sampling occurred at 24 h except experiment 3, where at 24 h the UVA exposure started, and sampling occurred 3 h after the end of the exposure.

2.3.5 Experiment 2: Sorption of BaP to NPs

Gene expression was used to assess bioavailability of BaP and indicate sorption of BaP onto NPs. For the sorption studies, two parallel dilution series of BaP were set up (0-3 µg/L) and in one dilution series 2 mg/L of each of NPs (NM105, TiO₂ 4-8 nm or Si NPs) were added. The BaP and NPs mixtures were prepared in fresh water medium (total volume of 20 ml) and stirred for 24 h prior to the start of the exposure. Zebrafish larvae at the developmental stage of 72 hpf were added in the preparations and exposed for 24 h. The exposures were conducted in 100-ml glass beakers and 15-20 larvae were exposed per beaker. After the end of exposure, the larvae were collected and stored at -80 °C until further analyses. ANT was not used as a co-contaminant in this set of experiments as no induction of any biomarker was observed in zebrafish larvae after a 24-h aqueous exposure.

3.3.5 Experiment 3: Sorption of PAHs to NPs under UVA

Both BaP and ANT were used for the following set of experiments. The concentration range used for BaP was 0-30 µg/L and for ANT, 0-27 µg/L. Two different experimental designs were followed using BaP as co-contaminant. The first included two BaP serial dilutions up to 1 µg/L and the second two serial dilutions up to 30 µg/L. The amount of NPs (NM105, TiO₂ 4-8 nm or Si NPs) added in one dilution series was 2 mg/L. The preparations with both PAH and NPs were stirred for 24 h prior the exposure. Zebrafish larvae 72 hpf were exposed to PAH and PAH/NPs mixtures. At the end of the 24-h exposure period, the preparations were exposed under UVA irradiation. The final volume of solutions was 20 ml and shallow enough for the UVA irradiation to be able to penetrate throughout. In the experiments with low BaP concentration range and ANT, larvae were collected 3 h after the end of UVA irradiation and stored at -80 °C until further gene expression analysis. At the higher BaP concentration range (0-30 µg/L), 3 h after the end of the UVA irradiation, the mortality of the larvae was recorded. The larvae were collected 3 h after the UVA irradiation for gene expression analyses. During the UVA treatment, preparations were placed in UV Crosslinker CL-1000, longwave emission of 365 nm. The energy the preparations were exposed to was 5 W/m². The light intensity inside the oven was measured by LI-COR LI-250A light meter and found to be 52.64 ± 2.17 µmol (mean ± SE, n=8) in different areas across the interior of the oven and 50.61 ± 1.18 µmol underwater.

2.3.6 Experiment 4: Sorption of PAHs to photo-excited NPs

Preparations of 2 mg/L of NM105, TiO₂ 4-8 nm and Si NPs in fresh water medium were exposed under UVA irradiation of 5 W/m². At the end of exposure, BaP was added in the preparations (0-3 µg/L) and which then were stirred for 24 h. Larvae at 72hpf were exposed for 24 h, collected, sacrificed and stored at -80 °C for gene expression analyses. The larvae exposed to BaP and NP mixtures were compared to the parallel exposure of larvae exposed to BaP alone.

2.3.7 Gene expression

Extraction of RNA was conducted, using RNeasy MiniKit for animal tissue, Qiagen, West Crawley, UK as described by (Boran et al., 2016). Zebrafish larvae 96 hpf (15-20 larvae per replicate) were homogenized with a pestle, treated with DNase (Qiagen) to prevent sample contamination from DNA, and eluted in 30 µL of sterile RNase/DNase free water. The concentration of the total RNA was measured using NanoDrop Spectrophotometer (ND-2000) and all samples with good quality RNA (280/260 ratio between 2.0-2.2) were diluted to a final concentration of 100 ng/µL. Reverse transcription was performed using Precision nanoScript2 Primer design kit with the following conditions: annealing at 65 °C for 5 minutes, extension at 42 °C for 20 minutes and inactivation of the reaction for 10 minutes at 75 °C. The cDNA was stored at -20 °C until gene expression analysis.

Primers designed for zebrafish from Primer BLAST (NCBI) for the following genes: cytochrome P4501A (*cyp1A*), β -actin, superoxide dismutase 1 (*sod1*) and DNA damage binding protein 2 (*ddb2*) as shown in Table 2.1. Precision PLUS Mastermix with SYBRGreen, Primer Design, was used for the quantitative PCR. Fluorescence was detected after 40 two-step cycles (denaturing temperature at 95 °C, primer specific annealing temperature and extension step 60 °C) by OneStep Real Time System (Applied Biosystems, Warrington, UK).

The efficiency of the qPCR was calculated ($e = 10^{(-\frac{1}{slope})} - 1$) based on a 4-point standard curve. Efficiencies between 0.9 and 1.1 were accepted for further analyses. The relative expression was calculated using the $\Delta\Delta C_t$ method (Henry et al., 2013).

2.3.8 Statistical analyses

Data followed normal distribution (as tested by the Shapiro Wilks test of normality, $p > 0.05$) and homogeneity of variance was assessed by the Bartlett's test ($p > 0.05$). Analysis of variance (ANOVA) was used to assess differences in gene expression with increasing concentration and UVA or gene expression (dependent variable) was modelled by general linear model according to the independent variables of PAH concentration, treatment (presence or absence of NPs), and concentration and treatment interaction (significance was considered at p-value of < 0.05). Mortality (dependent variable) of zebrafish larvae was modelled by logistic regression according to the independent variables PAH concentration, treatment (presence or absence of NP), and concentration x treatment interaction. The models were generated by iterative maximization of the likelihood function, and independent variables and their interactions were included if they significantly improved the model (likelihood ratio test, based on Wald χ^2 distribution). Differences in fish mortality among treatments (i.e., presence or absence of NPs) were determined by pair-wise contrast statements with a p-value of < 0.05 . All statistical analyses were conducted using *R statistics* (version 3.2.1, RStudio, Inc., 2015).

Table 2.1: Zebrafish gene specific primers for cytochrome P450 1A (*cyp1A*), superoxide dismutase 1 (*sod1*), DNA damage binding protein 2 (*ddb2*) and housekeeping gene (β -*actin*). Reference sequence numbers from NCBI, and product length in base pairs (bp).

Gene	Reference Sequence Number	Forward (5'-3')	Reverse (5'-3')	Product Length (bp)	Annealing Temperature (°C)
<i>cyp1A</i>	NM_131879.1	AGGACAACATCAGAG ACATCACCG	GATAGACAACCGCCCA GGACAGAG	174	60
<i>Ddb2</i>	NM_001083061.1	CATGCCGAATTCAAC CCTCG	GCTGTCAGCATTGACT GGTT	147	58
<i>sod1</i>	NM_131294.1	ACCGGCACCGTCTAT TTCAA	AGCATGGACGTGGAAA CCAT	105	55
β - <i>actin</i>	NM_131031.1	ACACAGCCATGGATG AGGAAATCG	TCACTCCCTGATGTCTG GGTCGT	138	60

2.4 Results and Discussion

2.4.1 Anthracene toxicity under UVA exposure

Significant increase in *sod1* and *ddb2* expression were observed in zebrafish larvae after exposure to ANT and UVA radiation. Specifically, after zebrafish larvae were exposed to 15 µg/L of ANT for 24 h, inductions of 0.8 and 1.2-fold were observed for *sod1* and *ddb2* respectively. On the contrary, when ANT exposure was followed by UVA radiation, 1.7 and 4.1-fold inductions were observed for *sod1* and *ddb2*, respectively (Figure 2.2). Induction of *sod1* suggests presence of ROS and induction of *ddb2* suggests DNA damage caused by exposure to ANT photo-by-product. Under UVA, ANT becomes photo-excited and undergoes photo-modification with possible main by-product 9,10 anthraquinone (Lee, 2003; Mallakin et al., 2000; Perraudin et al., 2007). Specifically, Mallakin et al. (2000) observed anthraquinone as the main photo-by-product 2 h after the light stimulation. PAHs quinones are electrophilic and they tend to bind to cellular nucleophiles such as proteins and nucleic acids (Kim et al., 2000). BaP quinones induced oxidative damage of lipid and protein in erythrocytes in rats (Kim et al., 2000). The epoxide metabolites of BaP can form DNA adducts with N² position of guanine (Miller and Ramos, 2001) and have been reported to induce *ddb2* gene expression along with other DNA damage related genes such as xeroderma pigmentosum, complementation groups C and F (*xpc* and *xpf*) in human cell lines (Christmann et al., 2016).

Significant changes in *cyp1A* expression were observed in zebrafish larvae after exposure to ANT and UVA. No induction of *cyp1A* expression was observed in this study after exposure to ANT without UVA radiation and a 45-fold induction was observed when preparations were exposed under UVA. No significant induction of the genes investigated in the present study was observed after exposure to UVA or NPs and UVA alone. The relationship between 3-ring PAHs such as ANT and the aryl hydrocarbon receptor pathway is not clear, and ANT has been characterised as non-reactive and not an aryl hydrocarbon agonist in fish (Barron et al., 2004). No activity of 7-Ethoxyresorufin O-Dealkylase (EROD), the catalytic measurement of *cyp1A* enzyme, was observed after exposure of ANT to rat hepatoma cell lines (Bosveld et al., 2002). In the present study, photo-excited ANT induced *cyp1A* in a bell-shape manner, indicating that the metabolism of ANT photo-by-product could involve the aryl hydrocarbon pathway. The bell-shape expression with increasing concentration could be explained by increasing *cyp1A*

gene expression and then reduction in expression levels when sufficient levels of *cyp1A* protein are present or the organism is not able to cope with the increasing concentrations of ANT photo-by-product that would eventually lead to larvae mortality. *Cyp1A* was selected for further experimentation of ANT exposures as it displayed high induction after the UVA radiation. The present study supports the existing literature on the photo-toxicity of ANT and provides an insight on gene expression profiles after exposure *in vivo* to ANT under UVA in larval zebrafish.

2.4.2 Sorption of BaP to NPs

Sorption of BaP onto all NPs tested in the present study, was indicated by reduced *cyp1A* gene expression in zebrafish larvae in the presence of the NPs. *Cyp1A* was positively induced following a linear pattern with increasing BaP concentration under laboratory light, and the presence of each NP significantly decreased *cyp1A* expression. At high concentration range of BaP (0-30 $\mu\text{g/L}$), reduction in gene expression was observed only in the presence of the smallest TiO_2 NPs (4-8 nm diameter) indicating sorption (Figure 2.3), while no changes in *cyp1A* gene expression in the presence of NM105 or Si NPs suggesting minimal sorption on the specific NPs. On the contrary, at low concentration range of BaP (0-2 $\mu\text{g/L}$), a significant decrease in *cyp1A* expression was observed when each one of the NPs tested were present in the exposure, suggesting that low concentration of BaP sorbed to surface area provided and consequently became less bioavailable in the presence of all NPs, independently of diameter size. Specifically, when zebrafish larvae were exposed to 1 $\mu\text{g/L}$ BaP, *cyp1A* was induced 5.13-fold (± 1.44 SE, $n=3$) and induction was observed up to 2.66, 1.32 and 2.69-fold when 2 mg/L of NM105, TiO_2 4-8 nm and Si NPs respectively, were present (Figure 2.4). The above support that sorption depends on the physicochemical properties of the NPs (i.e. surface area) and on the experimental conditions that the sorption processes are tested (i.e. concentration of adsorbent and adsorbate). Recent research has confirmed the importance of surface area in sorption of metals on the surface area of TiO_2 NPs. Specifically, more Hg^{2+} was bioavailable to zebrafish larvae (*mt2* gene expression was used as a biomarker of bioavailability of adsorbent) when bulk TiO_2 where added in aqueous Hg^{2+} solution compared to TiO_2 NM105 (Boran et al., 2016). Additionally, less copper was bioavailable to zebrafish larvae when TiO_2 4-8 nm (that is the same NP used in the present study) was added in solution when compared to larger TiO_2 NPs (such as NM105) (see Chapter 3). Della Torre et al. (Della Torre et al.,

2017) investigated sorption of BaP to carbon nanotubes (CNT) and although fluorescence of accumulated BaP in the zebrafish larvae increased with concentration, the presence of CNTs kept BaP concentration in zebrafish larvae to a higher level than the lower BaP concentrations tested but lower than the higher BaP concentration alone, indicating that CNTs acted as a vehicle increasing the co-contaminant concentration up to the maximum sorption capacity according to the surface area available. The present study suggests that sorption of BaP on NPs occurs and depends on both physicochemistry of the adsorbent and sorption capacity of the NPs.

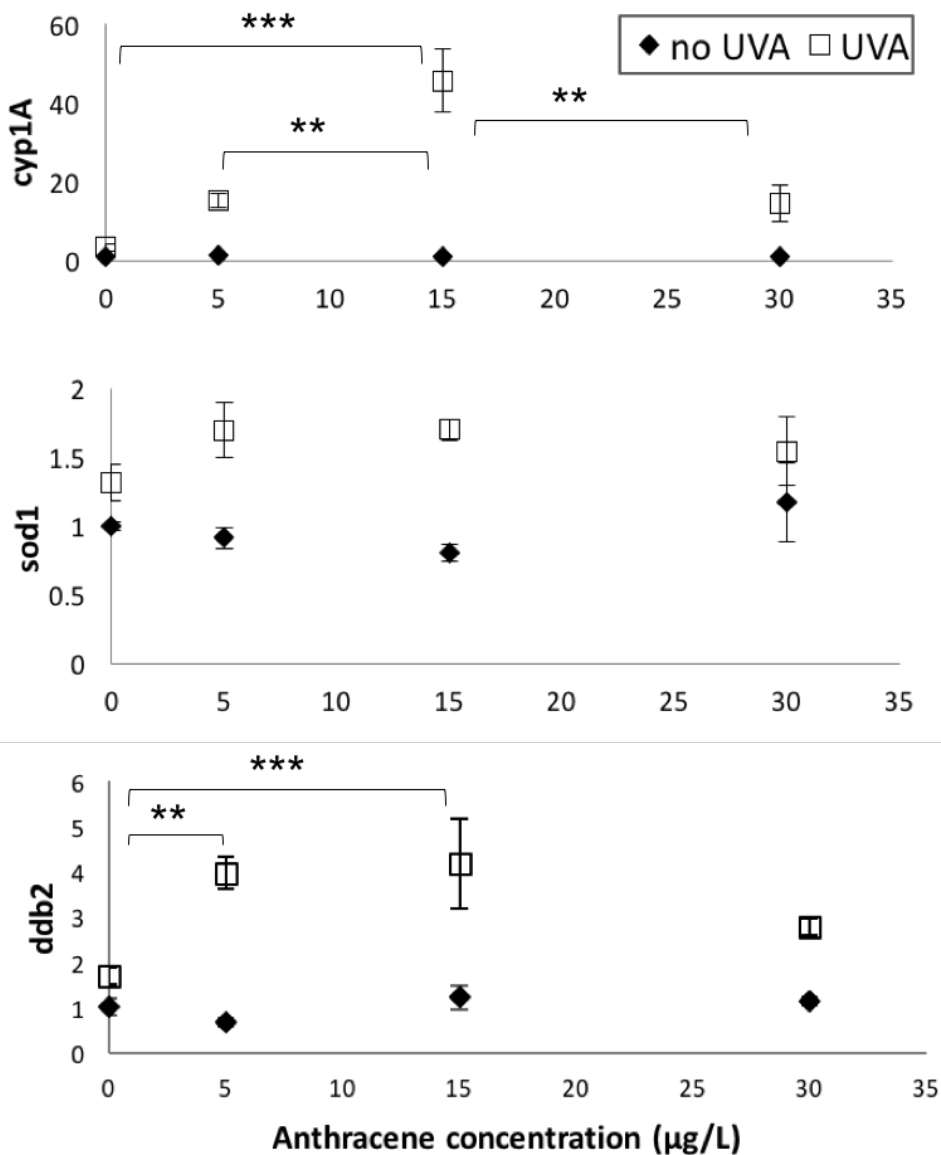


Figure 2.2: Q-PCR analysis of zebrafish stress gene expression after exposure to different anthracene concentrations and UVA radiation (5 W/m^2). *Cyp1A*, *sod1* and *ddb2* gene expression was normalised against β -actin. Significant differences in expression of all three genes was only observed under combined UVA and anthracene treatment (ANOVA, $p < 0.001$), data points show the mean \pm SE, $n=3$. Statistical differences were identified by two-way ANOVA, TukeyHSD, ***= $p < 0.001$, **= $p < 0.01$

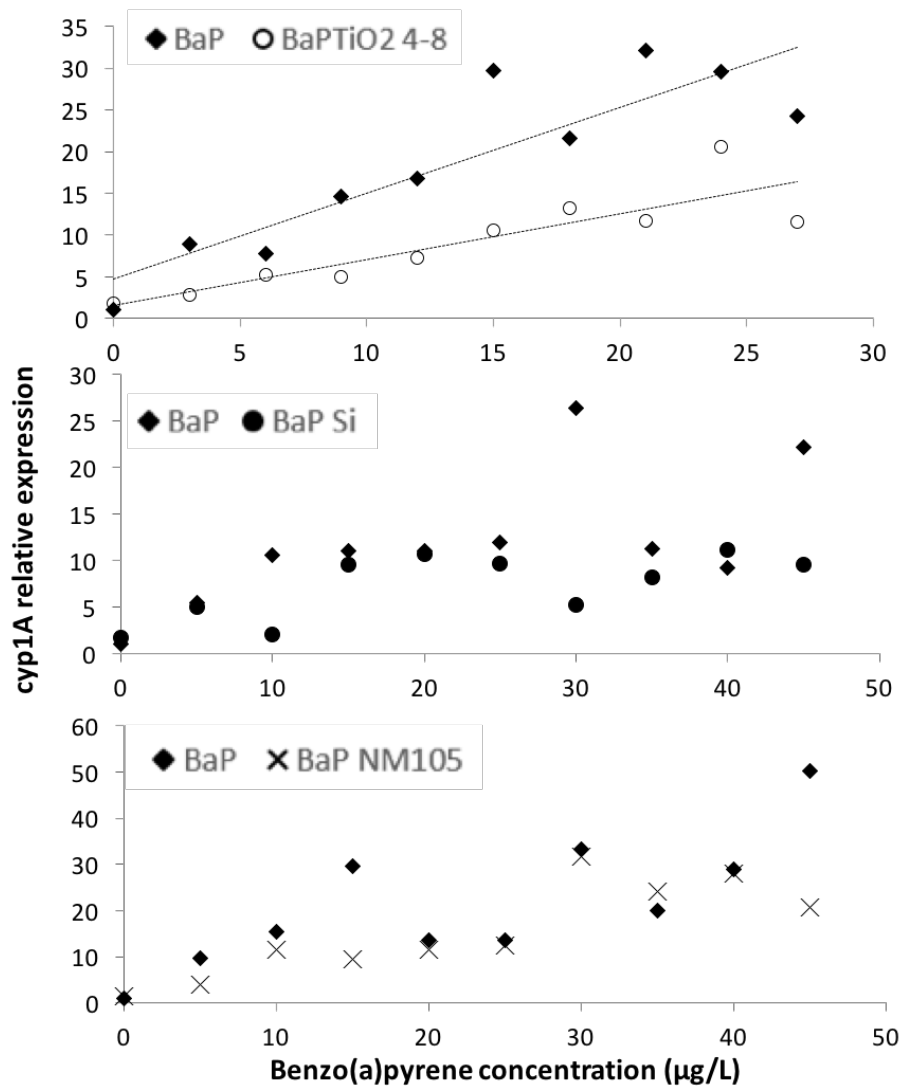


Figure 2.3: Q-PCR analysis of zebrafish *cyp1A* gene expression after exposure to different BaP concentrations alone (black diamonds) or in the presence of NPs (TiO₂ 4-8 nm, Si or NM105). *Cyp1A* gene expression was normalised against *β-actin*. Significant differences in expression with increasing BaP concentration were identified by general linear model ($p < 0.001$). Statistical differences between BaP alone and BaP in the presence of TiO₂ 4-8 nm NPs were identified by pair-wise contrast statements ($p < 0.001$). Data points show one replicate and a pool of 20 larvae.

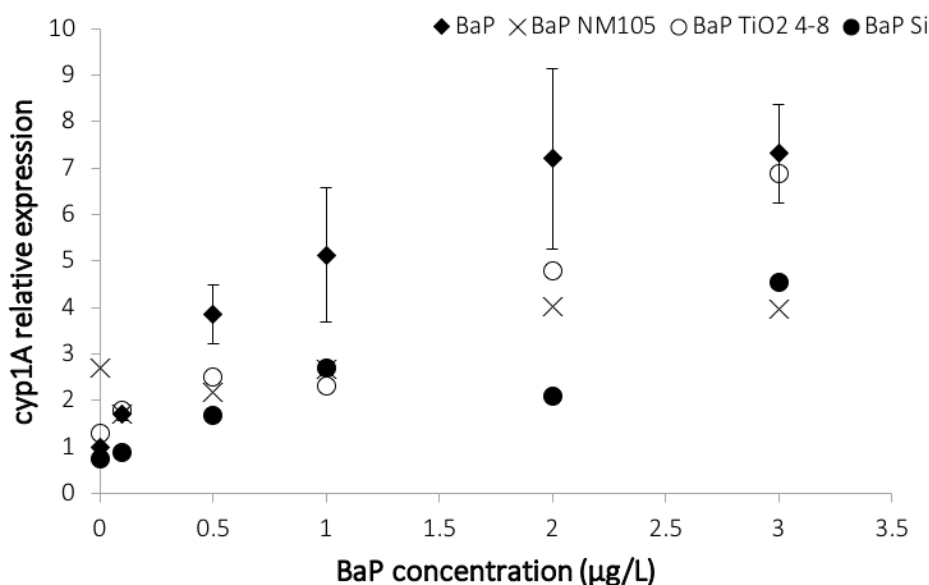


Figure 2.4: Q-PCR analysis of zebrafish *cyp1A* gene expression after exposure to different BaP concentrations alone (black diamonds) or in the presence of NPs (TiO₂ 4-8 nm, Si or NM105). *Cyp1A* gene expression was normalised against β -actin. Significant differences in expression with increasing BaP concentration were identified by general linear model ($p < 0.001$). Statistical differences between BaP alone and BaP in the presence of NPs were identified by pair-wise contrast statements ($p < 0.001$). BaP data points show MEAN \pm SE, $n=3$, the rest of data points show one replicate and a pool of 20 larvae.

2.4.3 Sorption of PAHs to NPs under UVA

The presence of 2 mg/L NM105, TiO₂ 4-8 nm and Si NPs led to no expression of *cyp1A* after exposure to ANT, UVA and NPs (Figure 2.5). ANT and UVA induced *cyp1A* with increasing concentration and no induction of *cyp1A* was observed after NPs alone or NPs and UVA exposure. The reduction in *cyp1A* expression in the presence of NPs indicated sorption of ANT photo-by-products on the NPs and potential photo-catalysis of ANT that was independent of the surface area of the three NPs investigated. When lower concentration of NPs was added in ANT dilution series (0.2 mg/L TiO₂ 4-8 nm or Si NPs that is 1/10 of the original concentration) no induction of *cyp1A* was found suggesting that reducing the surface area available for sorption ten times was still enough for the given concentration of ANT and/or photo-by-products to sorb and be not bioavailable to zebrafish larvae (Appendix A). This outcome emphasizes the importance of the physicochemistry of the adsorbate in the sorption processes,

the sorption capacity of NPs for low molecular weight ANT (with likely photo-by-product the oxygenated PAH, 9,10 anthraquinone, although chemical analysis of the by-products did not occur in the present study) when compared to a larger compound such as BaP (without UVA exposure).

The presence of NPs significantly reduced toxicity of BaP under UVA in high concentrations and induced bioavailability of BaP photo-by-product(s) in lower BaP concentration range. Mortality of zebrafish larvae was observed in high range of BaP concentrations (5-30 $\mu\text{g/L}$), 3 h after the end of UVA irradiation in a concentration-response manner, and the presence of each NP added in the BaP dilution series significantly lowered BaP photo-toxicity. All larvae died when exposed to 5 $\mu\text{g/L}$ BaP or higher under UVA (Figure 2.6) but in the presence of all NPs the mortality was reduced significantly (logistic regression, $p < 0.001$) as the concentration-response curve was shifted to the right. In lower BaP concentration range (0-2 $\mu\text{g/L}$), no mortality was observed, and the larvae were analyzed for *cyp1A* expression levels. BaP after UVA induced *cyp1A* 3.8-fold at 0.1 $\mu\text{g/L}$ and lower expression was observed at higher concentrations (0.5-1 $\mu\text{g/L}$) following a bell-shape pattern. The presence TiO_2 NPs, NM105 and TiO_2 4-8 nm, in the 0.1 $\mu\text{g/L}$ BaP solution, led to a higher expression of *cyp1A* (8.8-fold and 7.6-fold, respectively) than BaP alone, however, high variation was observed. The presence of Si NPs in BaP preparations kept the *cyp1A* expression at the same levels as the photo-activated BaP alone at 0.1 $\mu\text{g/L}$, however, at 0.5 $\mu\text{g/L}$ of BaP, the *cyp1A* expression was induced significantly higher when Si NPs were present in preparations (ANOVA, TukeyHSD, $p < 0.05$) (Figure 2.7). In the specific experiment, *cyp1A* induction can be explained as a combination effect of surface area and a critical amount of BaP/BaP photo-by-products adsorbed that led to higher bioavailability of the adsorbate. When NPs were exposed alone to UVA just before sorption to BaP was initiated, sorption of BaP was observed on the surface area of TiO_2 and Si NPs previously exposed to UVA as was suggested by the reduction in *cyp1A* expression in the presence of NPs (Figure 2.8).

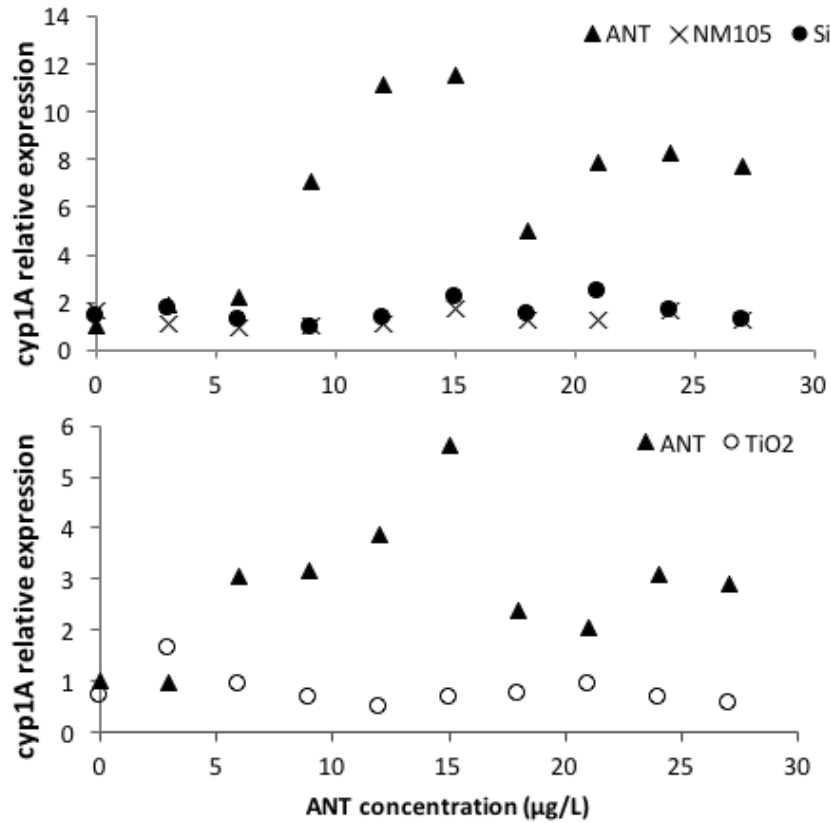


Figure 2.5: Q-PCR analysis of zebrafish *cyp1A* gene expression after exposure to different ANT concentrations alone (black triangles) or in the presence of NPs (TiO₂ 4-8 nm, Si or NM105). *Cyp1A* gene expression was normalised against *β-actin*. Significant differences in expression with increasing ANT concentration were identified by general linear model ($p < 0.001$). Statistical differences between ANT alone and ANT in the presence of NPs were identified by pair-wise contrast statements ($p < 0.001$). Data points show one replicate and a pool of 20 larvae.

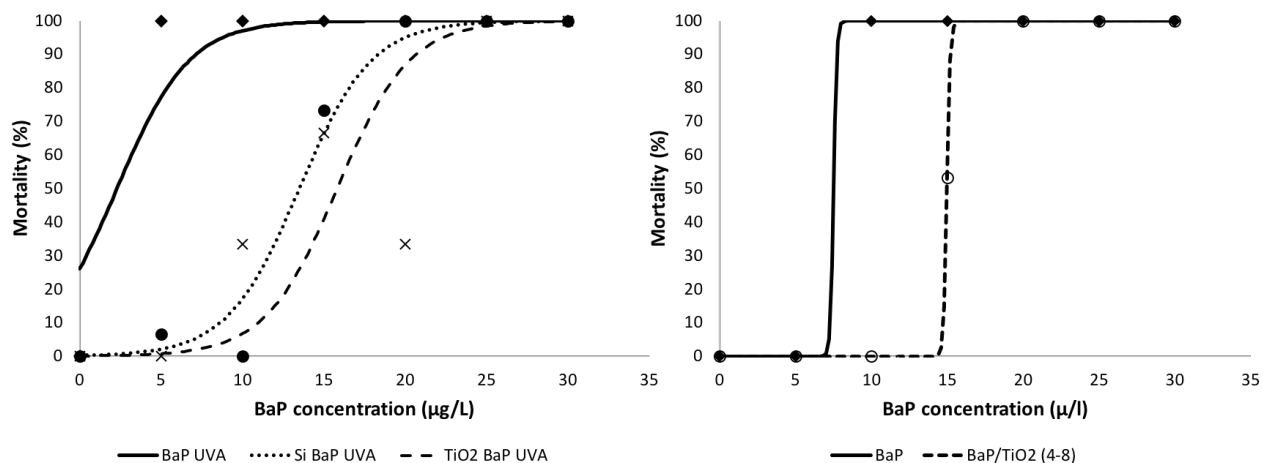


Figure 2.6: Zebrafish larvae mortality with BaP increasing concentration (black line) and BaP in the presence of NPs: on the left, NM105 (x), and Si NPs (black circles) and on the right TiO₂ 4-8 nm (empty circles), under UVA 5 W/m². Logistic regression was used to model the mortality according to concentration and treatment (independent variables), $p < 0.001$. The predicted mortality was obtained by the following exponential equation: $(e^{a+\beta x}) / (1 + e^{a+\beta x}) - 1$. Statistical differences between BaP alone and BaP in the presence of NPs were identified by pair-wise contrast statements ($p < 0.001$). Data points show one replicate and a pool of 20 larvae.

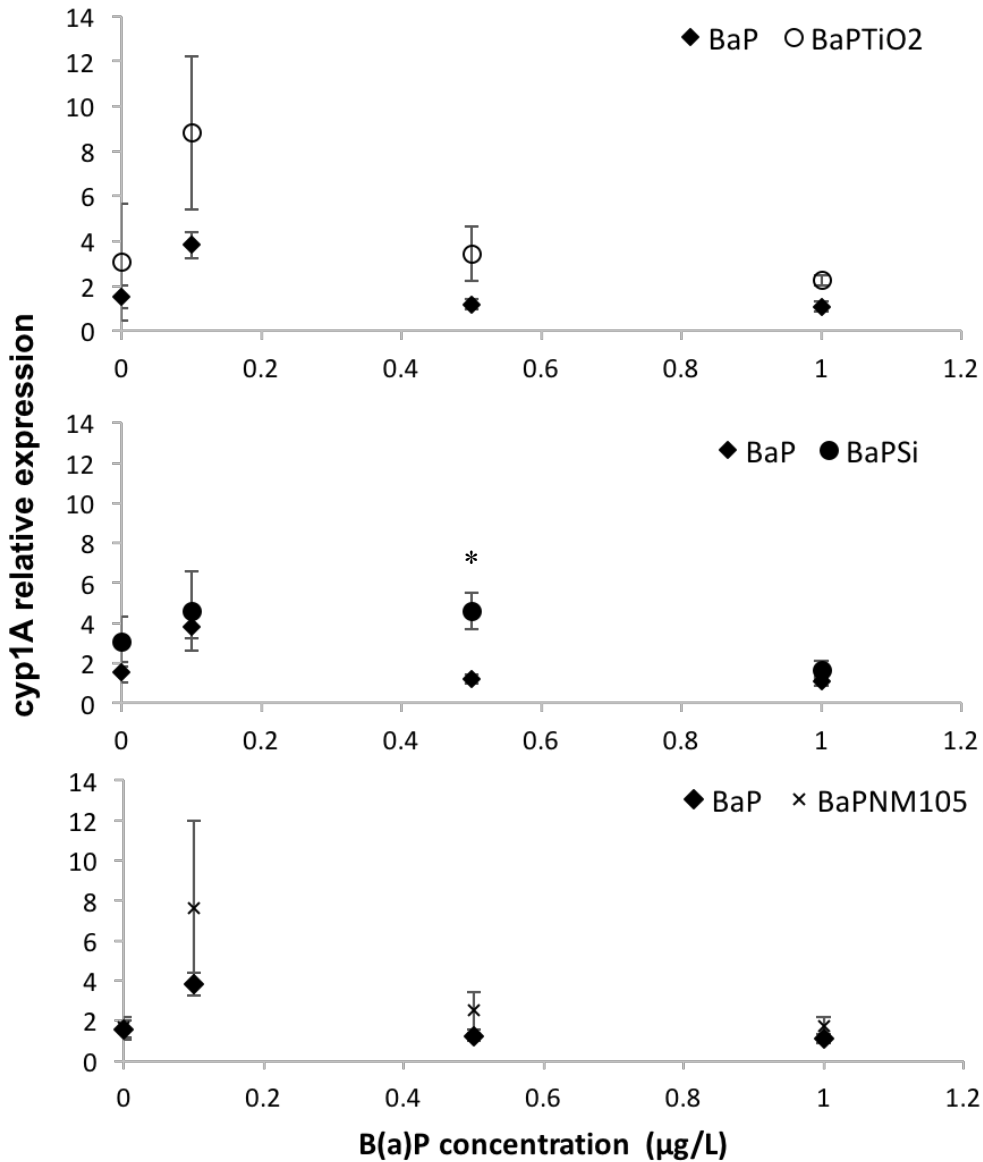


Figure 2.7: Q-PCR analysis of zebrafish stress gene expression after exposure to different BaP concentrations and UVA radiation (5 W/m^2). *Cyp1A* gene expression was normalised against β -actin. Significant differences in expression of all three genes was only observed under combined UVA and anthracene treatment (ANOVA, $p < 0.001$), data points show the mean \pm SE, $n=3$ ($n=4$ for BaP data points). Statistical differences were identified by two-way ANOVA, TukeyHSD, $*=p < 0.05$.

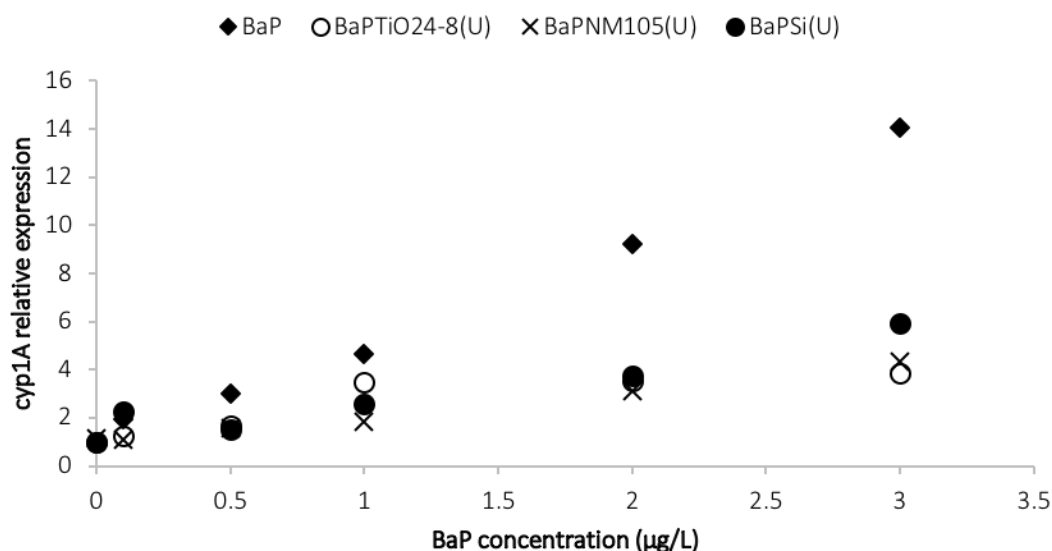


Figure 2.8: Q-PCR analysis of zebrafish *cyp1A* gene expression after exposure to different BaP concentrations alone (black diamonds) or in the presence of NPs (TiO₂ 4-8 nm, Si or NM105). *Cyp1A* gene expression was normalised against β -actin. Significant differences in expression with increasing BaP concentration were identified by general linear model ($p < 0.001$). Statistical differences between BaP alone and BaP in the presence of NPs were identified by pair-wise contrast statements ($p < 0.001$). Data points show one replicate and a pool of 20 larvae.

A number of studies report sorption of organic contaminants on NPs in the aqueous (see Chapter 1) and the importance of UVA radiation has been previously studied in analytical chemistry studies regarding photo-degradation abilities of TiO₂ material, but little is known about the effect of UVA in sorption and the impact on the aquatic organisms. The present study provided a fine example of the biological effect of the “Sabatier principle” where a volcano plot describes the efficiency of photo-catalysis that depends on the concentration of the catalyst and the adsorbate (Rothenberg, 2008). In the present study, the concentrations of NPs and BaP were not right to initiate efficient photo-catalysis and the differences found between high and low BaP concentration ranges can be explained as follows: At low BaP concentration range the photo-catalysis is more efficient compared to higher concentration range because of the limited sorption capacity of the NPs, therefore, at low concentration range, relatively more BaP photo-by-products are bioavailable and in turn, increased *cyp1A* expression. It can be concluded that the BaP photo-by-products are bioavailable, due to the differences in *cyp1A*

expression after zebrafish exposure to BaP or BaP and UVA. On the contrary, at higher BaP concentration range, NP sorption sites are all engaged, photo-degradation occurs at the adsorbed BaP, the NP concentration is limited and so are the sorption sites, therefore, less BaP photo-by-products are bioavailable, and the presence of NPs is reducing photo-toxicity of BaP. In the case of ANT, it can be concluded that under UVA irradiation the TiO₂ NPs catalyzed ANT degradation, however the photo-degraded substances either were sorbed on the surface area of the NPs, thus less bioavailable to the larvae, or they did not induce mortality or expression of the biomarkers used in the present study.

According to existing literature, the sorption on TiO₂ NPs accelerates photo-degradation of BaP under UVA but no investigation of the toxicity of photo-by-products was conducted in the study (Zhang et al., 2008). Toxicity of ciprofloxacin (CIP) has been reported to decrease in the presence of catalyst NPs (ZnO or TiO₂) under UVA, but with the increasing concentration of CIP photo-by-products, toxicity was increased again in *Vibrio fisheri* (Silva et al., 2016). The same study found toxicity of the NPs alone in *V. fisheri* under UVA radiation. On the contrary, TiO₂ catalyzed photolysis of ibuprofen with ibuprofen photo-by-products showing less toxicity in *Artemia salina* (Silva et al., 2014). UV radiation changes the surface chemistry of NPs such as TiO₂ with resulting ability for photo-catalysis of adsorbed organic substances. Organic environmental contaminants such as methylene blue (Xu et al., 1999), estrone and 17 β -estradiol (Zhang et al., 2007), ofloxacin (Paul et al., 2007) have been reported to degrade in the presence of TiO₂ NPs under UVA or visible light condition, however, degradation is still happening at a very slower rate just in the presence of TiO₂ NPs in the dark (Peterson et al., 2015). This study is the first to investigate the complications of sorption of two different PAHs on TiO₂ NPs under UVA radiation and analyze sorption by bioavailability of adsorbates in zebrafish. Si NPs are semiconductors of lower band gap (1.12 eV) than TiO₂ NPs (3.1-3.3 eV) (Strümpel et al., 2007), but the relationship between band gap energy and degradation of organic compounds is not clear. In the present study, all three NPs tested reduced ANT photo-by-product bioavailability and high concentrations of BaP photo-by-product mortality in larval zebrafish. However, at low BaP concentrations the amount of NP present photo-catalyzed BaP inducing bioavailability of photo-by-products and increasing indirectly BaP toxicity to zebrafish larvae under UVA.

2.4.4 Conclusions

In conclusion, the present study suggests that sorption of PAHs on NPs occurs and toxicity of PAHs and/or photo-by-products depends on the sorption capacity of NPs. Results here obtained indicate that sorption capacity depends on the quantity and physicochemistry of both adsorbent and adsorbate. The sorption of PAHs under UVA promoted photo-catalysis of PAHs to photo-by-products and the presence of the semiconductor NPs (TiO_2 and Si NPs) play key role as in low concentration of BaP, the photo-catalysis is efficient leading to higher bioavailability of toxic photo-by-products, while in higher BaP concentrations, photo-catalysis is less efficient due to limited sorption sites on the surface of NPs leading to less amount of photo-by-products, thus lower photo-toxicity of BaP. The current research used bioavailability to investigate the sorption processes of photo-labile compounds on photo-sensitive NPs with high potential of occurrence in the aquatic environment and under UVA exposure. As a result, the data presented here provide an insight on the broad interactions that can take place in the aquatic environment, the complicated sorption processes and the indirect effects of the presence of engineered NPs in the aquatic environment.

Chapter 3 - Differences in Engineered Nanoparticle (NP) Physicochemistry Revealed by Investigation of Changes in Copper Bioavailability during Sorption to NPs in the Aqueous Phase.

3.1 Abstract

The physicochemistry of engineered nanoparticles (NPs) in the aqueous phase influences their fate, behaviour, and environmental implications. Investigations of sorption of chemical substances to NPs in the aqueous phase can inform on these complex interactions and provide insight on environmental fate of NPs. The objective of this study was to use differences in sorption of copper (Cu) to investigate aqueous-phase physicochemistry of NPs (Si, perovskite and TiO₂ NPs). Along with analytical chemistry, sorption of Cu to NPs was evaluated by assessment of changes in copper bioavailability in the alga *Chlorella vulgaris*, and larval zebrafish. The presence of TiO₂ NPs reduced total Cu in the water column and Cu bioavailability (measured by growth inhibition, mortality, and metallothionein 2 (*mt2*) gene expression) suggesting Cu sorption to TiO₂ NPs. Less Cu was bioavailable when smaller TiO₂ NPs were present, indicating higher sorption capacity with increasing surface area. This is supported by a lower total Cu in the water column, less inhibition of *C. vulgaris* growth, less mortality and lower levels of *mt2* gene expression in zebrafish larvae making the surface area the most important factor affecting sorption demonstrated in the present study. Copper concentration in medium significantly decreased with increased Si NPs concentration measured by analytical chemistry, but no significant sorption was indicated on perovskite NPs. The results of this study strengthen the relevance of bioavailability as an analytical tool to assess the sorption of chemical substances on NPs in the aquatic environment.

3.2 Introduction

The low cost and increasing applications of nanotechnology leads to greater production and release of engineered nanoparticles (NPs) into the aquatic environment. The term engineered NPs is used to identify materials that have all three dimensions in the nanoscale (ISO, 2008), which frequently confers unique physicochemical properties that are attributed to their nanoscale size. A consequence of the increased use of NPs has been increased release of NPs into the environment, and estimated concentrations of NPs (e.g., Ag-NPs) are at part per billion

range in some surface waters (Gottschalk et al., 2013; Sun et al., 2014). Within the aqueous phase, some of the unique properties of NPs persist and these properties influence NP environmental fate, interactions with other substances, and potential toxicity. Changes in NP physicochemistry can occur in the aqueous phase, including release of ions, sorption of chemical substances to NPs, agglomeration of NPs with other substances and/or particles, and/or changes in NP surface chemistry (e.g., oxidation or changes of coating) (Petersen et al., 2014).

Chemical substances can adsorb to the surface of NPs or absorb within the NP matrix and sorption is dependent on the physicochemistry of both substance and NP. In the aqueous phase, sorption [defined as the taking up and holding of one substance by another (Dabrowski, 2001)] can be related to NP surface charge, surface area, the NP matrix, and characteristics of NP agglomerates, among other factors. Based on chemical analyses of NPs, copper, lead and zinc were found to have high affinity for SiO₂ NPs, and sorption was strongly affected by the ionic strength of the solution (Liang et al., 2011). In the aqueous phase, sorption of copper to TiO₂ NPs reduced the total copper concentration in the water column after centrifugation of mixtures (Fan et al., 2016) and the amount of copper adsorbed increased with percentage of anatase within TiO₂ NPs (Kim et al., 2003). Both anatase and rutile crystalline NP structures adsorbed copper, but the sorption of copper to rutile TiO₂ was four times lower than to anatase TiO₂ NPs (Rosenfeldt et al., 2015).

A challenge for research on NP sorption is that analytical methods applied can disturb the processes under investigation and innovative techniques are required to obtain results that are useful for interpretation. Upon sorption of toxicants (termed here “co-contaminants”) to NPs, bioavailability of the co-contaminants can be enhanced (Henry et al., 2013; Schwab et al., 2013) or reduced (Li et al., 2016b; Park et al., 2010), and changes in bioavailability can inform on NP physicochemistry in the aqueous phase. One definition of bioavailability is the proportion of a substance that enters an organism to react with biological molecules (Semple et al., 2004), and the molecular response of the organism can indicate changes in substance bioavailability that occur upon sorption with NPs. Aqueous-phase sorption to (C₆₀)*n* agglomerates decreased 17 α -ethinyl estradiol (EE2) bioavailability in zebrafish larvae, which was detected by reduction in vitellogenin gene (an EE2 responsive gene) expression (Park et al., 2010). On the contrary, sorption of Hg²⁺ to (C₆₀)*n* agglomerates led to increased bioavailability of Hg²⁺ in zebrafish larvae (Henry et al., 2013). The EE2 was presumed to be

absorbed within the (C₆₀)_n agglomerate matrix, whereas more labile sorption of Hg²⁺ to (C₆₀)_n agglomerate surfaces was postulated based on the different co-contaminant physicochemistries. The presence of TiO₂ NPs and sorbed As (V) enhanced the As (V) uptake in *Daphnia magna* compared to exposure to As (V) alone. Specifically, double the amount of As (V) was measured by mass spectrometry mainly in *D. magna* gut in the presence of 2 mg Ti /L (equivalent to 3.35 mg/L TiO₂ NPs) and five-times the amount of As was measured in the presence of increased TiO₂ NPs concentration (20 mg Ti /L or 33.5 mg/L TiO₂) (Li et al., 2016a). Rosenfeldt et al., (Rosenfeldt et al., 2014) observed a 2-fold increase in Ag body burden and 6-fold increase in As body burden in *D. magna* in the presence of 2 mg/L TiO₂ NPs, when compared to exposures to each heavy metal alone. These results with *Daphnia* suggest that TiO₂ NPs acted as a vehicle and increased bioavailability of Ag and As; however, in the same study, the presence of TiO₂ NPs reduced Cu body burden in *Daphnia*, indicating differences in sorption among adsorbates.

The potential of organism-based bioavailability tests to contribute to understanding of NP sorption processes in the aqueous phase should be applied to comparative studies with different NPs to clarify differences in NP physicochemistry. The objective of the present study was to use differences in copper sorption, detected by changes in copper bioavailability, to inform on differences in NP physicochemistry in the aqueous phase. Nanoparticles selected were TiO₂ NPs (4-30 nm diameter), spherical silicon (Si) NPs, and organo-metal perovskite cell NPs. Two organisms with different exposure conditions, (i.e. direct exposure of green alga *Chlorella vulgaris* to constantly agitated NP solution compared to indirect static exposure of larval zebrafish to NPs) were used to identify changes in copper bioavailability. Copper bioavailability was based on examination of the effect of copper on *C. vulgaris* growth and on survival and metallothionein 2 (*mt2*) gene expression in larval zebrafish.

3.3 Materials and Methods

3.3.1 Chemicals

The TiO₂ particles were used for the following experiments: TiO₂ bulk (NM100) of a primary size 200-220 nm and anatase crystal structure, TiO₂ NM105 (JRCNM01005a) with a manufactured size of 30 nm diameter and an anatase : rutile ratio of 85:15; TiO₂ NPs with manufactured size of 18 nm anatase and TiO₂ NPs with manufactured size of 4-8 nm anatase

provided by PlasmaChem, Germany (Table 3.1). The silicon (Si) NPs were synthesised composed of monosilane (SiH₄) with different percentages of diborane (1, 1.5, 2 or 2.5 %) and a primary size of 100 nm; they were provided by the Institute of Energy and Environmental Technology, Duisburg, Germany. Lead iodide perovskite NPs (CH₃NH₃PbI₃) were provided by the École Polytechnique Federal de Lausanne, Switzerland. Aqueous stock suspensions of powdered NPs were prepared in Milli-Q water (grade 18.2 MΩ cm; Millipore, Livingstone, UK) at concentrations of 1-5 g/L. Stock preparations of TiO₂ NPs were sonicated twice for 8 minutes (Jacobsen et al., 2010) and the Si and perovskite NPs were sonicated for 1 min according to recommendations provided by the manufacturers. Determination of average size (hydrodynamic diameter) and surface-related charge (ζ-potential) of NPs in suspension (milli-Q water) was conducted by Dynamic Light Scattering (DLS) at a concentration of 100 mg/L. The co-contaminant used was CuSO₄·5H₂O and purchased from Sigma-Aldrich (lot#: SLB4752V) with purity >98.0%.

Table 3.1: The list of nanoparticles (silicon, boron doped silicon, Perovskites, TiO₂) that have been employed for Cu sorption to NPs experiments. The average size and charge (ζ-potential) of the NPs suspended in Milli-Q H₂O, measured by Dynamic Light Scattering (DLS).

Sample Label	Material	Shape	Size (d. nm) ± SD	ζ -potential (mV)
SiB2.5%	B (2.5%) doped Si	Nano-sphere	303±125.8	-28.8
SiB2%	B (2%) doped Si	Nano-sphere	337.9±141	-28.7
SiB1.5%	B (1.5%) doped Si	Nano-sphere	384±197.4	-30.3
SiB1%	B (1%) doped Si	Nano-sphere	388±174.1	-27.3
Si	Si	Nano-sphere	447±155.6	-17.3
Perovskite	CH ₃ NH ₃ PbI ₃	Nano-cube	141.6±30.85	-13.1
TiO ₂ bulk	anatase		404.2 ± 11.9	-51
TiO ₂	JRCNM01005a	Nano-sphere	267.3	-6.45
	anatase/rutile			
TiO ₂	anatase	Nano-sphere	514	-20
TiO ₂	anatase	Nano-rods	467.05 ± 221	17.73

3.3.2 Analytical chemistry

Aqueous phase copper concentrations were determined by inductively coupled plasma mass spectrometry (ICP-MS, Agilent 7500ce, School of Chemistry, University of Edinburgh) to investigate sorption of Cu to NPs and the effect of NP surface area. A single nominal concentration of Cu salt (250 µg/L) was added to different concentrations (0, 2, 4, 8 and 16 mg/L) of Si NPs, NM105, TiO₂ (18 nm) or TiO₂ (4-8 nm) NPs. The preparations (20 ml) were stirred with a magnetic bar for 24 h for the sorption equilibrium to occur and then centrifuged at 24,000 rpm for 1 h. The supernatant (10 ml) was collected and acidified with 15% nitric acid (trace metal grade) for measurement of total Cu in the water column. From the remaining portion (10 ml) of each preparation, 9 ml were carefully removed and the remainder (1 ml, containing the pellet) was mixed by pipetting, allowed to dry, and used to investigate presence of Cu on the surface of NPs. Analyses on the pellet samples was conducted by X-ray photoelectron spectroscopy (XPS), Nexus, Newcastle University.

3.3.3 Test organisms

Chlorella vulgaris (Culture Collection of Algae and Protozoa 211/12, originally obtained from Scottish Marine Institute, Oban, UK) culture was grown in OECD TG 201 medium (and and Development), 1981) in 250-mL Erlenmeyer flasks (Scientific Laboratory Supplies, Coatbridge, UK) under constant rotary agitation (225 rpm), illumination (120 µmol /m² s) and temperature (23 °C) based on our established methods (Kalman et al., 2015). When the cell density reached ~10⁶ cells /mL, the stock culture was maintained under static conditions (illumination of 50 µmol /m² s) in a 16:8 h light : dark photoperiod at 20 °C. Cultures were maintained by transferring a small aliquot into fresh sterile medium and were checked every two months for bacterial contamination by plating on nutrient agar (Oxoid Ltd, Basingstoke, UK).

Zebrafish (*Danio rerio*) were obtained from the zebrafish research facility (Heriot-Watt University), and husbandry, spawning and experimentation were conducted with complete approval and according to animal welfare regulations of the UK Home Office. Water for experiments was synthesised fresh water with characteristics consistent with the OECD guidelines for fish embryo toxicity tests (OECD, 2013). Characteristics of water chemistry were 79, 38, 12, 17 and 2 mg/L of Ca²⁺, Mg²⁺, Na⁺ and K⁺, respectively; pH of 7.7; temperature

was maintained between 28-30°C, and a 12-h photoperiod. Hatching occurred between 48 and 72 hpf, and fish of age 72-168 hpf were used for the experiments.

3.3.4 Concentration-response assays

Preliminary experiments were performed to establish dose-response (growth inhibition) relationships for *C. vulgaris* to aqueous Cu (as CuSO₄). The toxicities of Si NPs, perovskite NPs and TiO₂ NPs, and bulk TiO₂ to algae were individually tested up to concentration of 100 mg/L (no toxic effects observed). The NPs selected for the following study were dispersed in milli-Q water (as described in section 3.3.1), bath sonicated and the solutions were vortexed before the preparation of each treatment to ensure homogeneous solutions.

Algal growth inhibition assays were performed in 250-ml Erlenmeyer flasks (Pyrex) according to the OECD test guideline (OECD 201) or in plastic 24-well plates using *C. vulgaris* in the exponential growth phase. Temperature and light conditions for toxicity tests were identical to those used for culture growth. Experiments were carried out in triplicate using five concentrations (0 to 40 µg/L) of Cu or (0 to 100 mg/L) of NPs. The initial concentration of the inoculum was 10⁴ cells per ml, which was required to ensure that cultures were at exponential growth. Cell density was determined after 24, 48 and 72 hours of exposure by measuring *in vitro* fluorescence of acetone-extracted chlorophyll *a* (Kalman et al., 2015) in experiments carried out in Erlenmeyer flasks (Cu, nano and bulk TiO₂). In the case of Si and perovskite NPs acute toxicity tests, 1.5 ml of each test solution was added in triplicate to wells of 24-well plates due to limited amount of Si and perovskite NPs available. Plates were sealed with parafilm to avoid evaporation. *In vivo* chlorophyll *a* was measured by fluorescent plate reader (Molecular Devices SpectraMax M5) using excitation wavelength at 435 nm and emission wavelength at 685 nm at the same time points. The NP exposure concentrations ranged between 1 and 100 mg/L for Si and perovskite NPs, and the TiO₂ NPs and bulk TiO₂.

Copper sorption on NPs was assessed by investigating changes in Cu bioavailability by exposing the test organisms to various concentrations of Cu in absence and presence of NPs. Two parallel Cu concentrations in a range of 0 to 60 µg/L were prepared in Erlenmeyer flasks. In one Cu dilution series, 2 mg/L of NPs were added. The parallel dilutions experiment was conducted once for each NP type. Algal growth inhibition, as chlorophyll fluorescence, was determined after 72 h of exposure.

Zebrafish larvae age 72-hours post fertilization (hpf) were exposed to Cu to establish the LC₅₀ and sub-lethal concentrations over 96-h exposure period. Two parallel Cu dilution series (0-360 µg/L) were prepared in glass beakers containing 50 ml of exposure solution, and 20-30 larvae were exposed in each beaker. In one dilution series, 2 mg/L of NPs were added, and the two concentration-response curves were compared. For each experiment, control beakers were included (one of fish water and one of fish water and NPs). Two Cu dilution curves were prepared for each NP type. Acute (96 h) toxicity tests were conducted to determine lethal effects of NPs in larvae aged 72-168 hpf. Larvae were exposed to NP concentrations between 0 and 200 mg/L, and 10 larvae were individually exposed to each concentration in 96-well plates with an exposure volume of 200 µL.

For the zebrafish co-contaminant experiments, two parallel dilutions of Cu were prepared (0-360 µg/L) and 2 mg/L of NPs were added to one dilution series. The Cu dilution series with added NPs were stirred with a magnetic stir bar at medium speed for 24 h prior to fish exposure. Every experiment had 20-30 larvae per preparation with a final volume of 50 ml in glass beakers. The parallel dilutions experiment was conducted once for each NP type and four times for NM105 using four different NP concentrations added in copper dilution series (1, 2, 3 and 4 mg/L). The mortality of the larvae was recorded daily and the dead larvae were removed from the preparations.

3.3.5 *mt2* gene expression

To evaluate the concentration-response relationship between Cu concentration and *mt2* gene expression, fish were exposed (24 h) to Cu (0, 120, 240 and 360 µg/L) or Cu and 2 mg/L of NPs (Si NPs, TiO₂ 18 nm or TiO₂ 4-8 nm). Three replicates were investigated for each condition. Larvae of 96hpf were sampled and stored at -80 °C until further analysis. Total RNA was extracted from larvae 96 hpf (30 larvae per replicate) after a 24-h exposure period, using RNeasy MiniKit for animal tissue, Qiagen, West Crawley, UK as previously described (Boran et al., 2016). Briefly, zebrafish larvae were homogenized with a pestle, a DNase treatment (Qiagen) was included as a step during the extraction to prevent sample contamination from DNA, and the RNA was eluted in 30 µL of sterile RNase/DNase free water. The concentration of the total RNA was measured using NanoDrop Spectrophotometer (ND-2000). All samples with 280/260 ratio between 2.0-2.2 were used for further analysis and diluted to a final concentration of 100 ng/µL. cDNA was synthesised using Precision nanoScript2 Primer design

kit with the following conditions: annealing at 65 °C for 5 minutes, extension at 42 °C for 20 minutes and inactivation of the reaction for 10 minutes at 75 °C. The cDNA was stored at -20 °C until gene expression analysis.

Primers designed for zebrafish from Primer BLAST (NCBI) for the following genes: *mt2* (NCBI Reference Sequence: NM_001131053.2, Forward (5'-3'): TGTTCTCAATCTTGTCTGTTTAATG, Reverse (5'-3'): TGTAGAGCACTATCAGAATAAACG, with product length of 108 bp and annealing temperature at 60°C) and *β-actin* (NCBI Reference Sequence: NM_131031.1, Forward (5'-3'): ACACAGCCATGGATGAGGAAATCG, Reverse (5'-3'): TCACTCCCTGATGTCTGGGTCGT, with product length of 138 bp and annealing temperature at 60°C) (Boran et al., 2016). Precision PLUS Mastermix with SYBRGreen, PrimerDesign, Eastleigh, UK, was used for the quantitative PCR. Fluorescence was detected after 40 two-step cycles (denaturing temperature at 95 °C, primer specific annealing temperature and extension step 60 °C) by StepOne Real Time System (Applied Biosystems, Warrington, UK). The efficiency of the qPCR was calculated ($e = 10^{(-\frac{1}{slope})} - 1$) based on a 4-point standard curve, and an efficiency of between 0.9 and 1.1 was required for further analyses. The threshold cycle C_T measured by the RT qPCR determined the expression levels of the housekeeping gene (*β-actin*) and *mt2*. The *mt2* levels were then normalised after the *β-actin* levels (ΔC_T) and the differences between the experimental control group and the exposed larvae were obtained by the $\Delta\Delta C_T$ method. The fold changes ($2^{\Delta\Delta C_T}$) of *mt2* levels in exposed samples were compared to the average $\Delta\Delta C_T$ of the control larvae (Henry et al., 2013).

3.3.6 Statistical analyses

All statistical analyses were conducted using *R statistics* (Team, 2015). The algal growth inhibition and Cu concentration relationship, in absence or presence of NPs, were modelled using the four-parameter log-logistic function and compared using *anova* in 'drc' package in R. Zebrafish mortality was modelled by logistic regression with the independent variables copper concentration, treatment (presence or absence of NP), and concentration and treatment interaction. The logistic regression models were generated by iterative maximization of the likelihood function, and independent variables and their interaction were included if they significantly improved the model (likelihood ratio test, based on Wald χ^2 distribution). The

median lethal concentration (LC_{50}) was calculated by the logistic regression model and the 95% confidence interval (CI) was calculated using the *logit* model in R statistics. For the gene expression analyses, the relative fold change was modelled by general linear model according to the independent variable of Cu concentration (p-value of <0.05). Differences in fish mortality among treatments (i.e., presence or absence of NPs) were determined by pair-wise contrast statements with a p-value of <0.05 .

3.4 Results and Discussion

All NPs tested tended to agglomerate in milli-Q water with average agglomerate diameter between 314 and 637 nm (NP concentrations 2mg/L), which was a higher average size than reported by manufacturers (Table 3.1). The average agglomerate size of Si NPs ranged between 324 and 627 nm diameter, with higher average agglomerate size observed in Si NPs with B coating of 1.5% and the size decreased in Si NPs with B 2% and B 2.5% coating, indicating that the differences observed among hydrodynamic diameters of agglomerates of Si NPs can be attributed to the boron coating percentage. In the present study, no measurements of the hydrodynamic diameter were conducted in fresh water media; however, all NPs tested formed visible agglomerates that settled on the bottom of the static exposure beakers within 24 h of the start of zebrafish larvae exposures. Agglomeration of TiO_2 NPs, with average hydrodynamic diameter between 1024 to 1792 nm, has been reported previously to occur within 10 minutes after the introduction of NPs in fresh water media such as algae medium (OECD, 2011), hard-water medium and *Lumbriculus variegatus* medium (OECD, 2007) (Nur et al., 2015). For all TiO_2 NPs measured in the present study, ζ -potentials were between -30 and 30 mV, a measurement that is consistent with other studies and has been attributed to the lack of sufficient repulsive forces between NPs to keep them in suspension in the aqueous phase (Honary and Zahir, 2013; Nur et al., 2015). The smallest TiO_2 NPs (4-8 nm) showed ζ -potential very close to zero (-2 mV), which is in agreement with the higher agglomerate sizes observed among TiO_2 NPs and indicates higher reactivity of the smaller NP (greater relative surface area) in the present study. A negative ζ -potential and high agglomeration was observed in perovskite NPs and the Si NPs were found more stable with higher absolute value of ζ -potential.

Sorption of copper to NPs was indicated by changes aqueous copper concentration and detection of copper in pelleted NPs. Specifically, copper decreased by 4.7 %, 1 % and 59 % when 2 mg/L of Si NPs, NM105 and TiO₂ 4-8 nm NPs were present, respectively. Total copper reduced further with increasing concentration of all NPs (Figure 3.1A); however, at the same NP concentration, more copper was removed by the smallest TiO₂ NPs (4-8 nm) likely because of greater surface area available for copper sorption. Copper was detected in the NP pellets in all preparations after XPS analyses (Appendix B). If the 2 mg/L TiO₂ 4-8 nm NPs with aqueous copper is at equilibrium regarding copper sorption to the NPs, then we can hypothesize that a doubling of the NP concentration would lead to double amount of copper adsorbed on NPs provided that agglomeration of NPs did not occur (e.g., as a consequence of the increased NP concentration). The results show that adsorption capacity of the NPs did not increase with higher NP concentrations and subsequent increased surface area as we would expect (Figure 3.1B). If the assumption of copper sorption equilibrium onto 2 mg/L NPs having been achieved after 24-h mechanical stirring is correct, then the observed reduction in copper sorption with increased concentration of NPs can be attributed to agglomeration of NPs that could affect their sorption capacity. The DLS analyses reported agglomeration of all NPs in the aqueous phase, however, the average agglomerate size (Table 3.1) cannot inform on the most abundant particle size in solution. Therefore, surface area in Figure 3.1 B was calculated by the reported manufactured particles dimensions. Agglomeration has been reported to affect the sorption capacity of TiO₂ NPs at high concentrations, such as 150 mg/L (Li et al., 2010), but no effect was observed in concentrations of lower range (0.2-2 mg/L) (Farkas et al., 2015). The results of the present study further support that sorption capacity of NPs depends on the different physicochemical properties of the NPs (i.e. different material or surface area), while agglomeration of NPs can decrease sorption capacity of NPs.

There was no effect of NP exposure (without copper) on *C. vulgaris* growth or zebrafish survival. No larval zebrafish died after exposure to 2 mg/L of TiO₂ NPs or bulk TiO₂, which is consistent with previous studies of TiO₂ NPs toxicology (Boran et al., 2016; Boyle et al., 2015). Exposure to TiO₂ NPs or bulk TiO₂ at tested concentrations (2 mg/L) did not affect growth of algae compared to unexposed controls, which is consistent with previous research (Hartmann et al., 2010). No larval mortality was observed after 2 mg/L exposures of perovskite, Si and Si-boron NPs and no growth inhibition was found in *C. vulgaris* after exposure to Si and Si-boron NPs (data not shown). It has been observed that the organo-metal halide cells in the aqueous

phase can release the metal halide (e.g. PbI_2) and the latter can cause mortality in zebrafish larvae at high concentrations (Babayigit et al., 2016; Benmessaoud et al., 2016), however, the low perovskite concentrations tested in the present study did not cause toxicity to *C. vulgaris* or zebrafish larvae. This is the first study to assess sorption of aqueous copper to Si and perovskite NPs as well as evaluate toxicities of Si, boron coated Si NPs and lead iodide perovskite NPs to *C. vulgaris* and zebrafish larvae.

No differences in the inhibition of *C. vulgaris* growth or in larval zebrafish mortality were observed after copper exposure in the presence of Si or perovskite NPs. Both growth inhibition of *C. vulgaris* after 72 h and zebrafish mortality (96-h exposure) increased significantly with copper concentration ($p < 0.001$) as expected. The presence of Si NPs or Perovskite NPs did not significantly affect copper toxicity in algae or zebrafish larvae (Appendix B), suggesting no observable interactions between copper and Si or perovskite NPs that did not alter copper bioavailability (and therefore toxicity) in algae or zebrafish. The 96-h zebrafish concentration-response curves suggest that not enough copper was adsorbed on Si NPs to reduce copper bioavailability, while the actual measurement of copper in the presence of NPs suggests that sorption of copper does occur on the surface of 2 mg/L Si NPs after 24 h of mechanical stirring. Si NPs were the largest NPs investigated (100 nm diam. primary size) and the lower amount of copper adsorbed onto Si NPs compared to smaller TiO_2 NPs used in the present study, can be attributed to the limited surface area available, however, the Si NP experiments demonstrate the differences in levels of detection of copper sorption among the techniques employed in the present study.

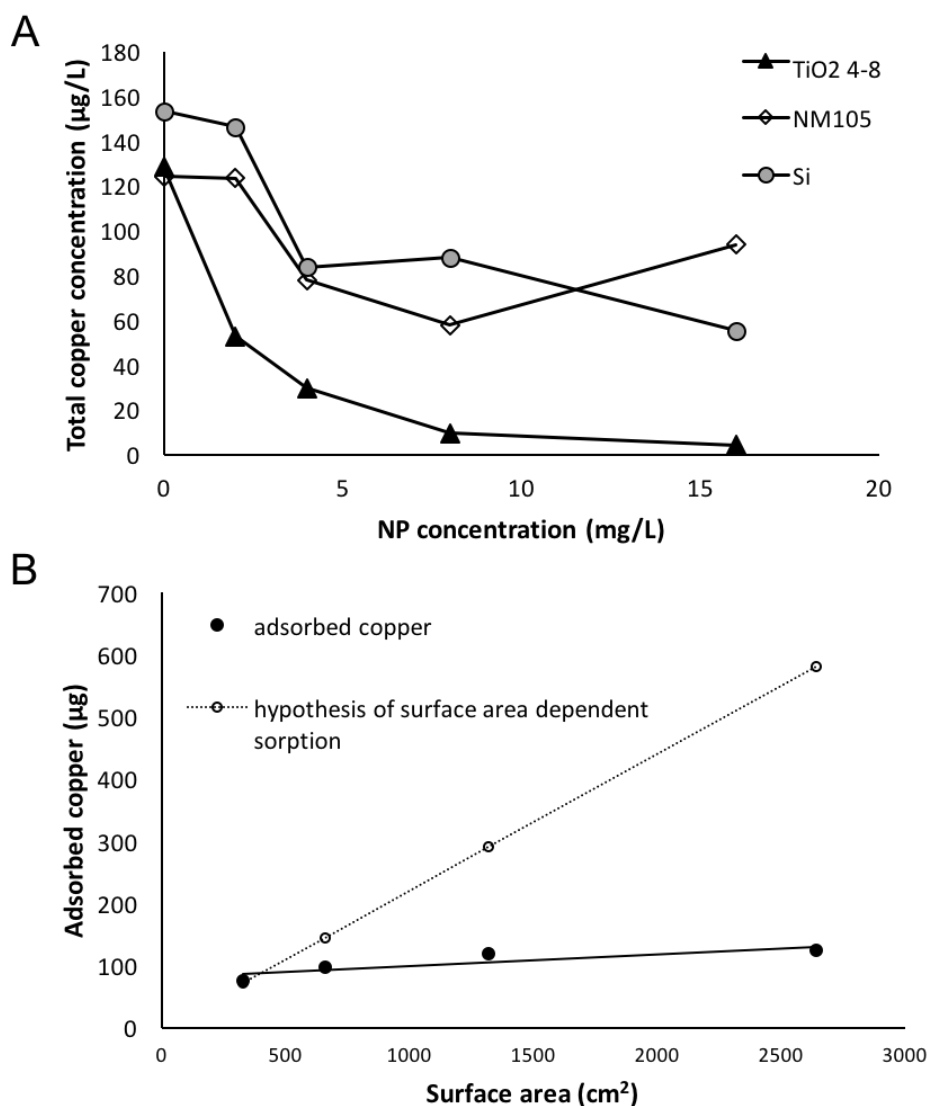


Figure 3.1. A) Total Cu concentration ($\mu\text{g/L}$) measured by ICP-MS in the presence of NM105 (diamonds), Si NPs (circles) and TiO_2 4-8 nm (triangles). Each point in the graph represents a single measurement. B) a correlation between copper sorption and surface area of TiO_2 (4-8) NPs if double sorption occurred when double the amount of the NPs were present in solution (dotted predicted line) compared to the actual total copper measured by ICP-MS (black line). The reduction of copper sorption can be attributed to agglomeration of the NPs leading to smaller surface area for sorption. Surface area was calculated by the reported manufactured diameter of sphere-shaped Si NPs and NM105 and the reported manufactured dimensions of rod-shaped TiO_2 4-8 nm NPs.

Sorption of copper on the surface of TiO₂ NPs and bulk TiO₂ was indicated by the reduced bioavailability of copper in both algae and zebrafish larvae in the presence of the TiO₂ NPs. Significant reduction in algal growth inhibition and larval mortality were observed in the presence of TiO₂ NPs ($p < 0.001$) (Figures 3.2 and 3.3). Reduced inhibition of algal growth and reduced larval mortality were most evident in the case of TiO₂ NPs with smallest particle size. Increased sorption occurred with higher concentration of NPs present in the copper dilution series. Specifically, NM105 increasing concentration, decreased copper toxicity in larval zebrafish, as was indicated by the difference in 96-h LC₅₀ (Δ LC₅₀) between copper alone and copper/NM105 mixtures concentration – response curves (Figure 3.4). The smaller diameter of TiO₂ NPs indicates greater surface area and reactive sites for sorption by the NPs (Zhang et al., 1998); however, agglomeration of TiO₂ NPs, that can occur at higher concentration ranges (i.e. 4-16 mg/L of TiO₂ NPs) as demonstrated in Figure 3.1 B or higher pH levels (i.e. the fresh water media used in the present study), can strongly change the reactivity of the particles by decreasing the capacity of aqueous ion adsorption (Gilbert et al., 2009; Suttiponparnit et al., 2011).

The importance of NP surface area on copper sorption was supported by the gene expression analysis. Induction of *mt2* occurred with increased copper concentration (GLM, $p < 0.001$) in zebrafish larvae, and *mt2* expression increased up to 8-fold after 24-h exposure to 360 μ g/L of copper relative to unexposed control fish. The presence of Si and TiO₂ 18nm NPs did not reduce the expression of *mt2*, however *mt2* expression decreased significantly when zebrafish larvae were exposed to copper in the presence of the TiO₂ 4-8 nm, the smallest particle tested (GLM, $p < 0.01$, $R^2 = 0.79$) (Figure 3.5). Exposure of zebrafish to TiO₂ for 24 h did not cause any induction of *mt2*, which is in accordance with previous investigation of *mt2* gene expression in zebrafish after exposure to TiO₂ NPs (Boran et al., 2016; Park and Yeo, 2013; Tan and Wang, 2014). Boran et al. (2016) indicated the importance of surface area in sorption processes when Hg²⁺ became less bioavailable to zebrafish larvae in the presence of TiO₂ NM105 compared to TiO₂ bulk. *Mt2* induction in the present study can be indicated as a fast and direct measurement of copper bioavailability and effectively demonstrated copper sorption on the smallest TiO₂ NPs.

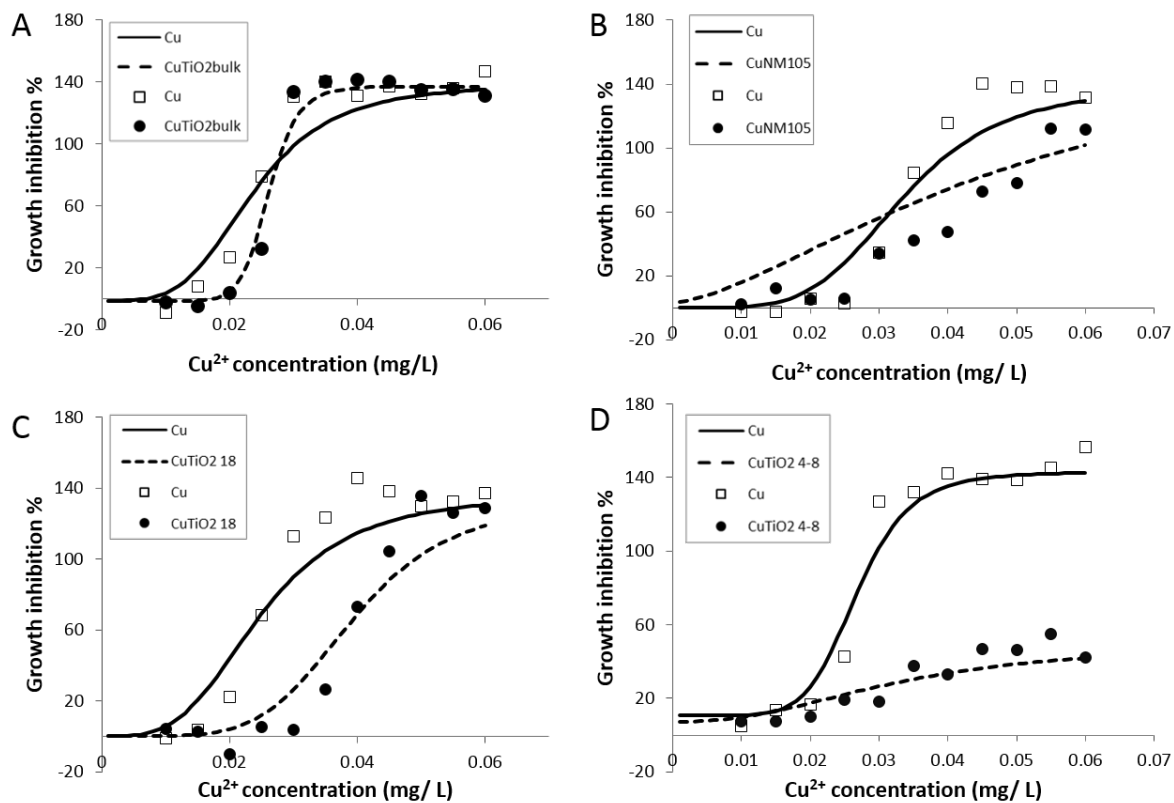


Figure 3.2: The growth inhibition (%) of the *C. vulgaris* over the range of Cu concentrations (solid lines) in association with 2 mg/L (dashed line) A) TiO₂ bulk, B) TiO₂ NM105, C) TiO₂ 18 nm NP and D) TiO₂ 4-8 nm NPs for 72 h, compared to the growth inhibition caused by Cu alone. Growth inhibition curves were obtained by a four-parameter log-logistic function. There was a significant difference in the concentration response curves between Cu and Cu with TiO₂ NP (B, C and D) indicating that the presence of TiO₂ NPs reduced the bioavailability of Cu (ANOVA, $p < 0.001$). No differences were observed in the presence of TiO₂ bulk.

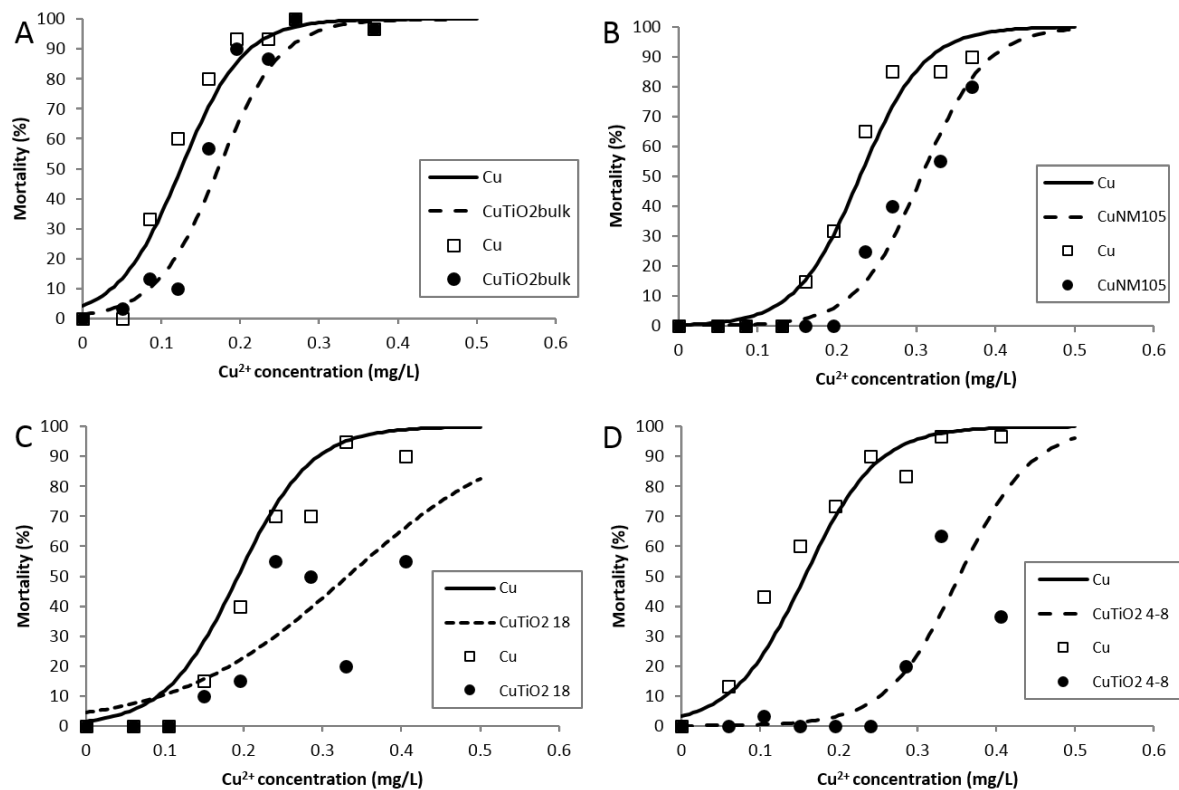


Figure 3.3: The mortality (%) of the zebrafish larvae over the range of Cu concentrations (solid line) in association with 2 mg/L (dashed line) A) TiO₂ bulk, B) TiO₂ NM105, C) TiO₂ 18 nm NP and D) TiO₂ 4-8 nm for 96 h, compared to the larvae mortality caused by Cu alone. The predicted mortality was obtained by the following exponential equation: $(e^{a+\beta x}) / (1 + e^{a+\beta x})$. There was a significant difference in the concentration response curves between Cu and Cu with TiO₂ NPs and bulk (A, B, C and D) indicating that the presence of TiO₂ NPs reduced mortality caused by Cu²⁺ (pair-wise contrast statements, $p < 0.001$).

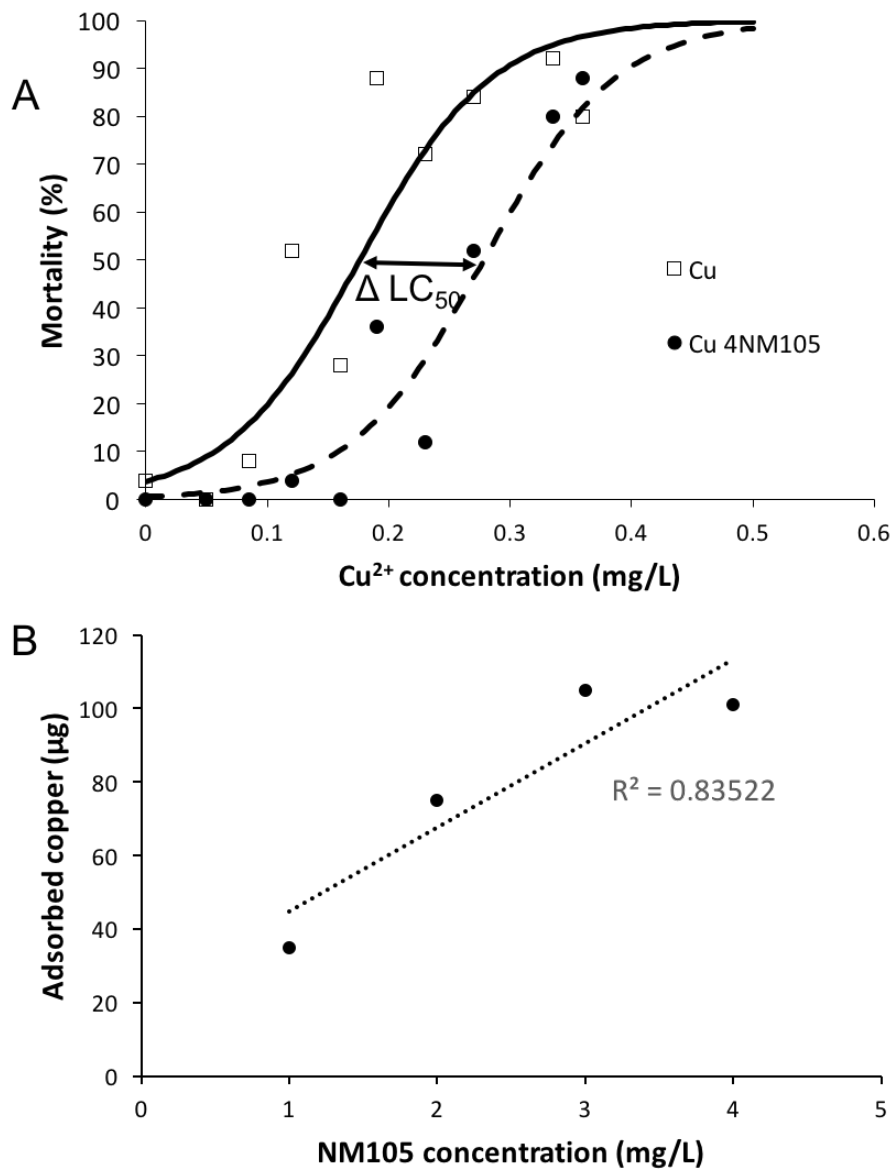


Figure 3.4: A) Copper concentration-response curve (solid line) and copper with 4 mg/L of NM105 concentration-response curve after 96-h exposure to zebrafish larvae. The difference between LC_{50} value of copper/NM105 mixture and copper alone is presented as ΔLC_{50} . The predicted mortality was obtained by the following exponential equation: $(e^{-a+\beta x}) (1 + e^{-a+\beta x})^{-1}$. B) Increase in the ΔLC_{50} with increased NM105 concentration. The NM105 added in the copper dilution series ranged between 1 and 4 mg/L. The difference between 96-h LC_{50} of copper alone and 96-h LC_{50} of copper with NM105 is increasing significantly with concentration of NM105 added in the dilution series.

Copper sorption to TiO₂ NPs reduced concentration of bioavailable copper to a level low enough to significantly decrease copper-induced growth inhibition, mortality and *mt2* expression in *C. vulgaris* and zebrafish larvae, respectively. Several studies have supported sorption of aqueous metals such as cadmium (Hartmann et al., 2010; Yang et al., 2012) and chromium (IV) (Dalai et al., 2014) on TiO₂ NPs. Fan et al (Fan et al., 2012) reported an increased activity of superoxide dismutase after sorption of Cu onto TiO₂ NPs and a positive correlation between the enzyme activity and mortality in *D. magna* in the presence of 2 mg/L TiO₂ NPs after Cu sorption onto TiO₂ NPs, however, reduced toxicity of copper presumably as a consequence of aqueous-phase copper sorption to TiO₂ NM105 has been reported using the same organism (Rosenfeldt et al., 2014; Rosenfeldt et al., 2015). Specifically, Rosenfeldt and colleagues observed that TiO₂ NPs agglomerates were actively ingested by *D. magna* but no release of adsorbed copper in the gastrointestinal tract was observed. In the present study, although *C. vulgaris* came in direct contact with NP agglomerates with sorbed copper (constant agitation), the free-swimming zebrafish larvae (static test) were less likely to have physical contact or actively ingest the settled TiO₂ agglomerates with adsorbed Cu at the early developmental stage of 96 hpf. The inability of 96-hpf zebrafish larvae to actively ingest micro-scale NP agglomerates (visible with naked eye at the bottom of glass beakers), may have lessened the likelihood of NPs to act as a delivery vehicle for copper to the organism and therefore, led to decreased bioavailability of co-contaminant. Although assessing bioavailability of an adsorbed co-contaminant does not inform on specific co-contaminant and NP surface interaction, it does inform directly on potential implications by the presence of NPs in the aquatic environment.

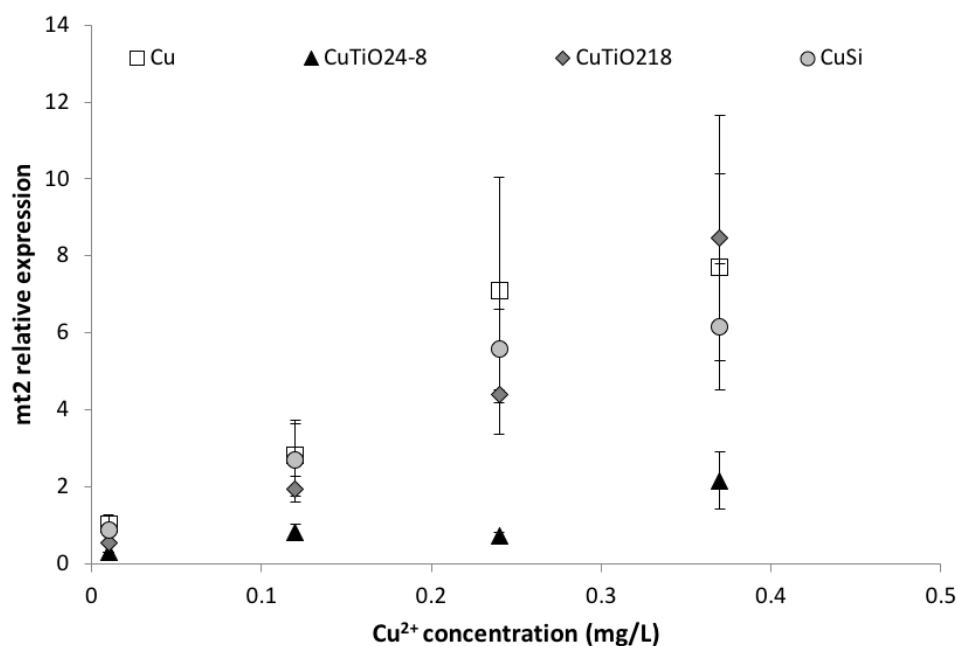


Figure 3.5: Induction of *mt2* gene in zebrafish larvae after a 24-h exposure to copper (Cu), copper and 2 mg/L TiO₂ 4-8 nm (CuTiO₂4-8), copper and 2 mg/L TiO₂ 18 nm diam. (CuTiO₂18), or copper and 2 mg/L Si NM (CuSi). No significant difference was observed between Cu and CuTiO₂ 18nm or CuSi ($p>0.05$) but Cu *mt2* expression was found significantly different from CuTiO₂ 4-8 nm, GLM, $p<0.001$. Data represent MEAN \pm SE, $n=3$.

The present study provided unique insight in the sorption of copper onto a wide range of NPs, how sorption indications can vary between experimental methods and how bioavailability can inform on environmentally relevant effects of co-contaminant sorption onto NPs. Analytical chemistry, algal growth inhibition, zebrafish larvae mortality and zebrafish gene expression identified a positive relationship between copper sorption and surface area of NPs, using a wide range of NPs of different physicochemical properties. The close similarity of the slopes of the sorption (%), as identified by each methodology, in relationship to NP surface area (Figure 3.6) suggest increasing sorption with surface area (calculated after the reported manufactured particle diameter), that can establish the surface area as the strongest factor affecting sorption in the present study. Accepting a linear relationship of sorption with surface area, the highest intercept potentially indicates highest copper sorption capacity of the NPs that is identified by each methodology or organism used. Therefore, the data provided by Cu bioavailability in the presence of NPs using two model organisms with different exposure approaches, the zebrafish

larvae mortality and growth inhibition of *C. vulgaris*, can inform effectively on sorption capacity of the NPs compared to sensitive gene expression and ICP-MS analyses after a 24-h exposure. Without having investigated the underlying mechanisms of metal ion sorption on NPs, taken together the findings of the present study indicate that sorption of copper can differ between different materials with the same surface charge (i.e. Si, perovskite and TiO₂ NPs) or between different physicochemical properties of the same material (e.g. TiO₂ NPs of different size). This study finally demonstrates the importance of bioavailability as a unique evaluation tool of the direct effect of sorption of copper on NPs contributing to an environmentally relevant assessment of the impact of NPs in the aquatic environment.

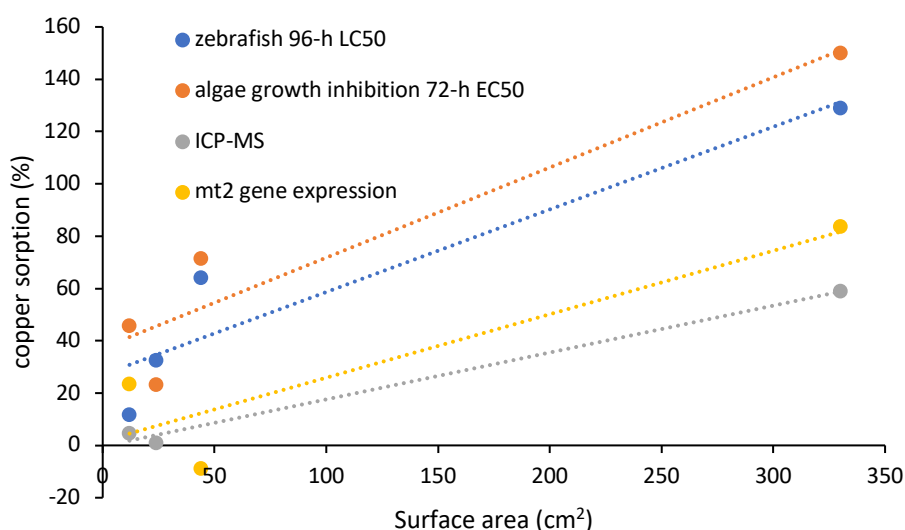


Figure 3.6: Representation of Cu sorption (%) as indicated by four independent analyses, conducted in the present study, show a positive correlation with the surface area (calculated by the reported manufactured particle diameter) of the NPs used in the present study (cm²). The differences in the 72-h EC₅₀ (Δ 72-h EC₅₀) of Cu exposure with and without NP using *C. vulgaris* tests, the Δ 96-h LC₅₀ of the zebrafish larvae Cu exposure with and without NPs, the differences in *mt2* gene expression and the analytical chemistry (ICP-MS) generated curves with R²: 0.90, 0.88, 0.81 and 0.99, respectively.

Chapter 4 - Investigation of Eco-Toxicity of Perovskite Nanomaterials in Aquatic Organisms.

4.1 Abstract

Lead-halide perovskite nanoparticles (NPs) is a new technology with high potential in photovoltaic industry. The investigation of ecotoxicity of lead-halide perovskite NPs is of great importance due to the potential of lead (Pb) dissolution in the aquatic environment. Parallel exposures of perovskite NPs and Pb ions to *Chlorella vulgaris* and zebrafish investigated the relationship of perovskite NP toxicity and Pb ion dissolution. Specifically, the aqueous perovskite NPs concentration – response curves of growth inhibition of *C. vulgaris*, mortality and metallothionein 2 (*mt2*) gene expression in zebrafish larvae did not differ from Pb ions concentration – response curves. Adult zebrafish were fed diets containing perovskite NPs or lead nitrate (500 µg Pb ions per gram of food) for 14 days. Induction of *mt2* expression in liver tissues showed Pb bioavailability after exposure to perovskite-spiked feeds. Changes in zebrafish gut microbiome were revealed by terminal restriction fragment length polymorphism (tRFLP) and sequencing of 16S rRNA of the gut bacteria after Pb exposure that can have an indirect effect in the organism health. The aqueous and dietary exposures demonstrated Pb toxicity in *C. vulgaris* and zebrafish after perovskite NP exposures and induction of *mt2* expression in zebrafish larvae and liver tissue but perovskite NP-spiked feeds did not affect the gut microbial community.

4.2 Introduction

Alkali metal halides (perovskites) technology is growing in the energy industry with promising potential and opportunities. Perovskites are coloured and three-dimensional materials, with a crystal structure ABX₃ whose optical and electronic properties have been discovered for thirty years (Grätzel, 2014; Hoefler et al., 2017). Perovskite technology is expected to exceed the currently well-established silicon-based one and perovskites are characterised as next generation solar cell materials due to their low cost and high-power conversion efficiency (Lee et al., 2012). Most suitable metal cation used for perovskites nanoparticles (NPs) that leads to the highest efficiency of the material, is lead (Pb), however, few studies have been investigating

the stability of the perovskite cell and its suitability for outdoor applications and their environmental risks have not yet been evaluated.

The release of metal ions from metal NPs is an issue that has been concerning the scientific community for the last decade. Nanoparticles possess a number of unique properties such as a high surface to volume ratio, that increases the surface interaction with the surrounding environment and, in turn, increases the potential of metal ion release (Petersen et al., 2014). For instance, in the case of silver (Ag) NPs, it is still unclear whether the toxicity of the particles can be attributed to the Ag⁺ release, the Ag NPs or a combination of both. In fish, evidence supports that the toxicity of Ag NPs is mainly caused by the silver ions (Griffitt et al., 2009; Jang et al., 2014) although this is not the case for all aquatic species and exposure conditions (Griffitt et al., 2009; Jang et al., 2014; Kalman et al., 2015).

The chemical reactions of perovskite materials in the aqueous phase can lead to release of the metals and cause subsequent toxicity in aquatic organisms. Stress factors such as UV radiation, oxygen or high temperatures, can initiate degradation processes of the metal halide perovskite materials (Aristidou et al., 2015; Han et al., 2015) and the use of lead as the metal component of the perovskite cells increases the awareness and risk from the toxicological and environmental point of view. An X-ray electron spectroscopy scan showed that PbI₂ and SnI₂ were the main by-products of full degradation of pristine perovskite particles containing Pb or tin (Sn) that were heated at 200 °C in air for 30 min, respectively (Babayigit et al., 2016). The same study investigated the acute toxicity of PbI₂ and SnI₂ in zebrafish embryos in a low hardness fresh water medium (E3 medium) and after dissolving the metal halides in dimethyl sulfoxide (DMSO). PbI₂ was found less toxic in zebrafish embryos (4 days post fertilization, dpf) with a median lethal concentration (LC₅₀) of 0.382 g / L compared to SnI₂ which toxicity was mainly attributed to reduction in media pH (Babayigit et al., 2016). No studies have been conducted up to date using Perovskite nanomaterials in zebrafish larvae.

The dietary exposure to metals is an important route of exposure and accumulation and toxicity of metals in fish (Meyer, 2005). Lead, a well-known environmental contaminant and neurotoxin, has been shown to be available to fish for uptake through dietary exposures. Specifically, physiological and morphological changes that have been noticed after Pb-spiked dietary exposure were damages in enterocytes (Crespo et al., 1986) and accumulation in body and intestinal tissues (Alves and Wood, 2006; Mount et al., 1994) with no effects on survival or growth. Heavy metals, and specifically Pb, can inhibit the activity of ALA-D (δ-

aminolevulinic acid dehydratase) or induce the activity of metallothionein (MT) proteins and both ALA-D and MT have been commonly used as biomarkers after Pb exposure (Johnson, 1998; Wang and Fowler, 2008).

The expected increasing application of the perovskite technology and the potential of ion leaching out of metal NPs leads to an urgent need to investigate perovskite NPs toxicity in the aquatic environment. The objective of this study was to assess the acute toxicity of five perovskite NPs, lead iodide and lead bromide-based materials, in the aqueous phase, using the green microalga *Chlorella vulgaris* and zebrafish larvae. The two model organisms were selected for the study as during exposure conditions algae are in direct contact with the NPs in contrast to zebrafish larvae that are in indirect contact due to NPs agglomerates settling at the bottom of the exposure vessel. Perovskite toxicity tests were held parallel to Pb ion exposures to evaluate whether toxicity of perovskite NPs can be attributed to Pb ions leaching. For the second part of the study, Pb bioavailability was evaluated after a 14-d dietary exposure to perovskite or Pb-spiked feeds to adult zebrafish to assess how ingestion can affect the function of the digestive system and the organism health by assessing hepatic gene expression of Pb-specific biomarkers, tissue morphology and disruption of zebrafish gut microbiome.

4.3 Materials & Methods

4.3.1 Perovskite NPs

The organometal perovskite NPs were manufactured at Ecole Polytechnique Federal de Lausanne, Switzerland. All five particles contain Pb and either Br or I, forming the chemical formula as the following: $\text{CH}_3\text{NH}_3\text{PbI}_3$ (MALI), $\text{CH}_3\text{NH}_3\text{PbBr}_3$ (MALB), $\text{CH}_3\text{NH}_3\text{CH}_2\text{NH}_3\text{PbI}_3$ (MAFA), $\text{CH}_3\text{NH}_3\text{CH}_2\text{NH}_3\text{PbBr}_3$ (MAFB), $\text{CH}_3\text{NH}_3\text{PbI}_3$ (FALI) (Table 4.1). Lead ions were used as a positive control ($\text{Pb}(\text{NO}_3)_2$, Sigma-Aldrich).

Table 4.1: The perovskite NPs used for the present study, the chemical type and molecular weight of each particle, along with the percentage of Pb that each NP contains.

Name	Chemical type	Molecular weight (g/mol)	Pb ²⁺ (%)	Experiments conducted
<i>MALI</i>	CH ₃ NH ₃ PbI ₃	619.9785	33.42	<i>C. vulgaris</i> and zebrafish acute toxicity tests, dietary exposure
<i>FALI</i>	CHNHNH ₃ PbI ₃	632.9772	32.73	<i>C. vulgaris</i> and zebrafish acute toxicity tests
<i>MALB</i>	CH ₃ NH ₃ PbBr ₃	478.9770	43.26	<i>C. vulgaris</i> and zebrafish acute toxicity tests, dietary exposure
<i>FALB</i>	CH ₃ NHNH ₃ PbBr ₃	491.9758	42.12	<i>C. vulgaris</i> and zebrafish acute toxicity tests, dietary exposure
<i>MAFA</i>	CH ₃ NH ₃ CHNHNH ₃ PbI ₃	665.0422	31.16	<i>C. vulgaris</i> and zebrafish acute toxicity tests

4.3.2 Aqueous acute toxicity tests

Algal growth inhibition assays were performed in glass 250-ml Erlenmeyer flasks according to the OECD test guideline (OECD 201) in the exponential growth phase. Temperature and light conditions for toxicity tests were identical to those used for culture growth. Experiments were carried out in triplicate. The initial concentration of the inoculum was 10⁴ cells per ml, which was required to ensure exponential growth. Cell density was determined at 0, 24, 48 and 72 h of exposure by measuring *in vitro* fluorescence of acetone-extracted chlorophyll *a* (Kalman et al., 2015). The exposure concentrations ranged between 5 and 200 mg/L for perovskites NPs. The detection of reactive oxygen species is based on the fluorescence of the probe 2, 7 dichlorofluorescein diacetate (H2-DCF-DA) and conducted by fluorescent plate reader (Molecular Devices SpectraMax M5) using excitation wavelength at 488 nm and emission wavelength at 525 nm at the same time points. For the reading, black 96-well plates were used, 250 µl of each flask were added per well in triplicates at 72 h after the start of the

exposure. DCF (10 μ l) diluted in ethanol (180 mg/L) was added per sample in the dark and the plate was kept in dark conditions for 1 h till the fluorescence measurement.

For the zebrafish acute toxicity tests, 72 hpf larvae were used. The duration of the exposure was 96 h and it was conducted in 96-well plates. One larva was placed per well and the well final volume was 200 μ l. Ten wells were used per treatment and six treatments per plate. The electrolyte composition of system water was: 79.38, 12, 17 and 2 mg/L of $[\text{Ca}^{2+}]$, $[\text{Mg}^{2+}]$, $[\text{Na}^+]$ and $[\text{K}^+]$, respectively. The larvae were observed under the dissection microscope daily and mortality was recorded. The plates were kept at 28 ± 1 °C throughout the exposure duration.

For the *mt2* gene expression study 15-20 larvae were exposed for a 24-h period in static solutions in glass beakers of total volume of 20 ml. The concentrations of particles ranged between 0 and 80 mg/L of the Pb the perovskite particles contain according to molecular weight (Table 4.1). Samples of the aqueous solutions at the end of the exposure were collected for Pb detection.

4.3.3 Dietary exposure

Wild type zebrafish were obtained from the zebrafish facility, Charles River laboratories (Tranent, UK), and fish were treated humanely in accordance with the regulations on animal use in UK. Adult fish (6-month old) were used for the dietary exposure experiment, of an average wet weight of 606 mg and fork length of 37.9 mm, were kept in recirculating biological systems with a 12:12 light:dark photoperiod. The electrolyte composition of system water was: 79.38, 12, 17 and 2 mg/L of $[\text{Ca}^{2+}]$, $[\text{Mg}^{2+}]$, $[\text{Na}^+]$ and $[\text{K}^+]$, respectively.

The zebrafish fish food was purchased from ZM systems, Winchester, UK, and it consists of 52% protein, 12% oil, 10.3% ash, 1% fibre, vit A: 25,000 I.U./Kg, vit D3: 2,500 I.U./Kg, vit E: 300 mg/Kg, vit C: 300 mg/Kg. For the preparation of experimental feeds, Milli-Q water was added on dry food pellets, enough to create a thick mixture with pellets be no longer distinguishable. For the food with Pb, the water used to prepare the mixture contained the appropriate amount of Pb dissolved from $\text{Pb}(\text{NO}_3)_2$. The pellets were formed using a steel mesh with a hole size of 0.915 mm and were put to dry at room temperature for 24 h and finally stored at -20 °C.

Treatment food was prepared as follows: control, and 500 $\mu\text{g/g}$ of Pb^{2+} that lead nitrate and the three perovskite particles contain according to molecular weight (0.8 mg $\text{Pb}(\text{NO}_3)_2$ per g of food; 1.496 mg perovskite MALI per g of food; 1.1872 mg perovskite FALB per g of food; 1.155 mg perovskite MALB per g of food). During the two days of acclimation period, all fish were fed control food. Measurements of pH and total ammonia were conducted daily (pH: 7.41-7.88 and unionised ammonia levels were at all times below 0.08 mg/L). The exposures were static with air supply, 50% of water was replaced twice daily and the average dissolved oxygen concentration was 8.24 mg/L. Fish were observed during feeding and all food was consumed. The exposure of experimental diets continued for 14 days. Before sampling the weight and fork length (from the tip of the snout to the middle of the caudal fin) of each fish were measured and the sex and condition of the gut (empty, half full or full) were recorded (Appendix C). Zebrafish were sacrificed with an overdose of tricaine methanesulfonate (MS-222) (Sigma Aldrich).

Liver samples were extracted at 0, 48 and 96 h of exposure from 2 fish per tank and stored at -80°C for RNA extraction. At 14 d after the start of the exposure the zebrafish liver and digestive tract was removed aseptically, placed immediately in liquid nitrogen and stored at -80°C for further analyses. A whole fish per tank was fixed in 10% neutral buffered formalin solution for histological analyses. Sampling occurred at all times before first feeding. Water samples were collected during the 14-d exposure period for Pb detection by ICP-MS/OES.

4.3.4 Measurements of Pb by analytical chemistry

Aqueous phase Pb concentrations were determined by inductively coupled plasma mass spectrometry (ICP-MS, Agilent 7500ce, School of Chemistry, University of Edinburgh) to investigate leaching of Pb from perovskite NPs and lead nitrate in the aqueous exposures of zebrafish larvae and leaching of Pb from perovskite and lead nitrate-spiked food pellets in the aquaria during the 14-d dietary exposure. Samples (10 ml) from the water column were collected during the zebrafish acute toxicity tests, without disturbing the bottom of the beakers and the settled NP agglomerates. Samples were then acidified with 15% nitric acid (trace metal grade) for measurement of total Pb in the water column.

Sub-samples ($n = 5$ of approximately 0.5 g) of each diet were accurately weighed into acid-washed glass beakers and 5 mL trace-analysis grade HNO_3 (Primar PlusTM, for Trace Metal

Analysis, Fisher, UK) added. The beakers were then covered with a watch glass and after incubation for 1 h to digest easily oxidised material, the acid was then heated to boiling and simmered for a further 1 h on a hot plate. Once cooled, digests were decanted through filter paper (Whatman, UK) into acid-washed volumetric flasks and made up to volume with 2% HNO₃ prepared in ultrapure water (ELGA). Samples (n = 3) of similar mass of a fish protein certified reference material (DORM-3, National Research Council of Canada) and procedural blanks (digests performed as described above but without solid material added to beakers) were also prepared as described above. Concentrations of total Pb in diets were then measured in digests using ICP-MS (low expected Pb concentrations, control, DORM-3 and procedural blanks; Thermo Electron Corporation X-Series II quadruple ICP-MS) and ICP-OES (Pb-spiked diets; Varian 725-ES, Agilent Technologies Inc.) and compared to matrix-matched elemental standards. The mean measured concentrations of Pb in the procedural blanks were < 1 µg/L. Measured Pb concentrations in DORM-3 were 0.33 ± 0.04 µg/g compared to certified values of 0.40 ± 0.05 µg/g.

4.3.5 Gene expression analysis

Total RNA was extracted from larvae 96 hpf (15-20 larvae per replicate) or liver samples using RNeasy MiniKit for animal tissue, Qiagen, West Crawley, UK as previously described (Boran et al., 2016). Briefly, zebrafish larvae were homogenized with a pestle, a DNase treatment (Qiagen) was included as a step during the extraction process remove DNA to prevent sample contamination from DNA, and the RNA was eluted in 30 µL of RNase/DNase free water. The concentration of the total RNA was measured using NanoDrop Spectrophotometer (ND-2000) and all samples were diluted to a final concentration of 100 ng/µL. cDNA was synthesised using Precision nanoScript2 Primer design kit with the following conditions: annealing at 65 °C for 5 minutes, extension at 42 °C for 20 minutes and inactivation of the reaction for 10 minutes at 75 °C. The cDNA was stored at -20 °C until the gene expression analysis.

Primers designed for zebrafish from Primer BLAST (NCBI) for the following genes: *mt2* (NCBI Reference Sequence: NM_001131053.2 Forward (5'-3'): TGTTCTCAATCTTGTCTGTTAATG, Reverse (5'-3'): TGTAGAGCACTATCAGAATAAACG), *ala-d* (NCBI Reference Sequence: NM_0007645, Forward (5'-3'): CACGTTCCCTGAGCTTGTGT and Reverse (5'-3')):

ACAGCTTGCGGCATTATCCA) and *β-actin* (NCBI Reference Sequence: NM_131031.1 Forward (5'-3'): ACACAGCCATGGATGAGGAAATCG, Reverse (5'-3'): TCACTCCCTGATGTCTGGGTCGT). Precision PLUS Mastermix with SYBRGreen, Primer Design, was used for the quantitative Polymerase Chain Reaction (q PCR). Fluorescence was detected after 40 two-step cycles of 95°C denaturing temperature, primer specific annealing temperature and extension step 60 °C by OneStep Real Time System (Applied Biosystems, Warrington, UK). The efficiency of the qPCR was calculated ($e = 10^{(-\frac{1}{slope})} - 1$) based on a 4-point standard curve. Efficiencies between 0.9 and 1.1 were accepted for further analyses.

4.3.6 Assessment of gut microbiota

The bacterial communities of the gut were identified by using a sequencing-based technique for rapid profiling, the terminal restriction fragment length polymorphism (tRFLP) analysis of 16S rRNA genes. The DNA of 64 samples was extracted from the whole GI tract using DNeasy blood and tissue kit (Qiagen), including treatment with proteinase K. Following that, the 16S rRNA gene was amplified using PCR with the primer pair: labelled (6FAM) 63f (Marchesiet al., 1998) and 530r (Lane, 1991). Amplification was conducted using 2 µl of template DNA and 0.5 µl bovine serum albumin (BSA; Ambion) in a 50 µl reaction mixture of Taq PCR mastermix kit (QIAGEN). The DNA used for PCR was 100-fold dilution of initial DNA to minimise effect of PCR inhibitors. The PCR conditions were as follows: initial denaturation for 90 s at 94 °C followed by 30 cycles of 15 s at 94 °C; annealing for 30 s at 56 °C; elongation for 30 s at 72 °C; and a final elongation step for 10 min at 72 °C. The PCR products were verified on a 1 % (w / v) agarose gel by electrophoresis. Purified PCR products were quantified using a Nanodrop spectrophotometer (NanoDrop 2000). ExoSAP-IT (Thermo Scientific) was used to purify the amplified samples, 5 µl of PCR samples were mixed with 2 µl of reagent, incubated for 15 min at 37 °C to activate the exonuclease and then 15 min at 80 °C to deactivate the enzyme. The digested product was analysed by GeneWiz, ML, USA, using Liz 500 size standard. The electropherograms were then analysed by the GENEMARKER software (SoftGenetics, PA, USA), using manually created bins. Peaks of less than 50 nucleotides length or having intensity of less than 50 units were not included in the analysis.

Nested PCR of DNA samples were prepared for MiSeq (Illumina) analysis. Amplification of 8F to 1492R region of 16S rDNA using HotStart PCR mastermix kit (ThermoFisher), were

carried out under the following PCR conditions: 96 °C for 1 min, 30 cycles of 96 °C for 30 sec, 50 °C for 30 sec, 72 °C for 30 sec, and 1 cycle of 72 °C for 3 min, prior to a secondary amplification of the V4 region with Golay barcoded 515F and 806R primers according to the Earth Microbiome protocol (Earth Microbiome Project, 2016). The PCR products were purified using GFX PCR DNA and Gel Band Purification kit (GE Healthcare). Concentration and quality of barcoded amplicons were evaluated using NanoDrop and 240 ng of each sample were pooled together and sent to Edinburgh Genomics (Edinburgh, UK) for next generation Illumina MiSeq sequencing. The operational taxonomic unit (OTU) identification was conducted using the Mothur pipeline (Schloss et al., 2011) and Silva ribosomal RNA database.

4.3.7 Histological analysis

One fish per aquarium was fixed in 10 % formalin and further dehydrated through ethanol, Histo-Clear II (National Diagnostics Inc., UK), and paraffin. The tissues were embedded in paraffin wax and then mounted on slides (8 mm sections). The transverse section selected were between the level of the heart and the end of the gastro-intestinal (GI) tract. The sections were stained with haematoxylin for 5 min and eosin for 5 min followed by thorough water washes.

4.3.8 Statistical analyses

The algal growth inhibition (dependent variable) and Pb concentration (independent variable) relationship, were modelled using a concentration-response model for algae, by 'drc' package in R. Mortality (dependent variable) of zebrafish larvae was modelled by logistic regression according to the independent variable of Pb concentration. The logistic regression models were generated by iterative maximization of the likelihood function. The median lethal concentration (LC₅₀) and effective concentration (EC₅₀) were calculated by the logistic regression model and the 95% confidence interval (CI) was calculated using the logit model in R statistics. For the gene expression analyses, the relative fold change (dependent variable) was modelled by general linear model according to the independent variable of Pb concentration (p-value of <0.05). Concentration-response statistical analyses were conducted using R statistics (version 3.2.1, RStudio, Inc., 2015).

The gut microbiota community composition within the 5 different treatments was analysed by non-metric multidimensional scaling (NMDS), based on Bray-Curtis similarities after square root transformation. Bacterial diversity was assessed using Shannon-Wiener's diversity Index (H-index) on the 13 tRFLP peaks and 396 bacterial phylla identified by illumine MiSeq analysis. Bray-Curtis similarities were plotted against food treatments to examine community treatment - response relationships. Permutational multivariate analysis of variance of sums of squares (PERMANOVA) was used to test for statistically significant differences between the bacterial communities of the control diets and Pb and NPs spiked diets. The numerical analyses for the gut microbiota data were conducted using PRIMER-E (v.7 PRIMER-E Ltd, Plymouth Marine Laboratory, Plymouth, UK).

4.4 Results and Discussion

A positive concentration – response relationship was observed after Pb or perovskite NPs exposure to *C. vulgaris*. Specifically, a 72-h EC₄₀ of 99 mg/L was observed after Pb ions exposure to *C. vulgaris*, MALB showed similar toxicity with Pb with a predicted 72-h EC₄₀ of 194 mg/L (equivalent to 84 mg/L Pb ions as seen in Figure 4.1). The rest of perovskite NPs, FALI, FALB, MAFA and MALI once converted to Pb ion concentration according to molecular weight, caused similar and less growth inhibition to *C. vulgaris* after 72-h exposure when compared to MALB NPs or lead nitrate (Figure 4.1), suggesting that the observed acute toxicity can be caused by Pb ion release. The MALI, FALB and MAFA NPs were found to cause less growth inhibition and the predicted 72-h EC₂₀ for FALI was found at 199 mg/L of FALI NPs that is equivalent to 65 mg/L of Pb ions. The outcome of the Pb toxicity in *C. vulgaris* is in agreement with previous research where significant reduction (66 %) in chlorophyll α (Chl α) levels was observed in *C. vulgaris* after 72-h exposure to 80 mg/L of Pb (Zhang et al., 2013) and in the present study a reduction of 45 and 82 % at Chl α levels was observed at 62 and 125 mg/L of Pb, respectively. The differences in perovskite NPs toxicity can be attributed to to different chemical type of perovskite NPs and different dissolution rates in the aqueous phase.

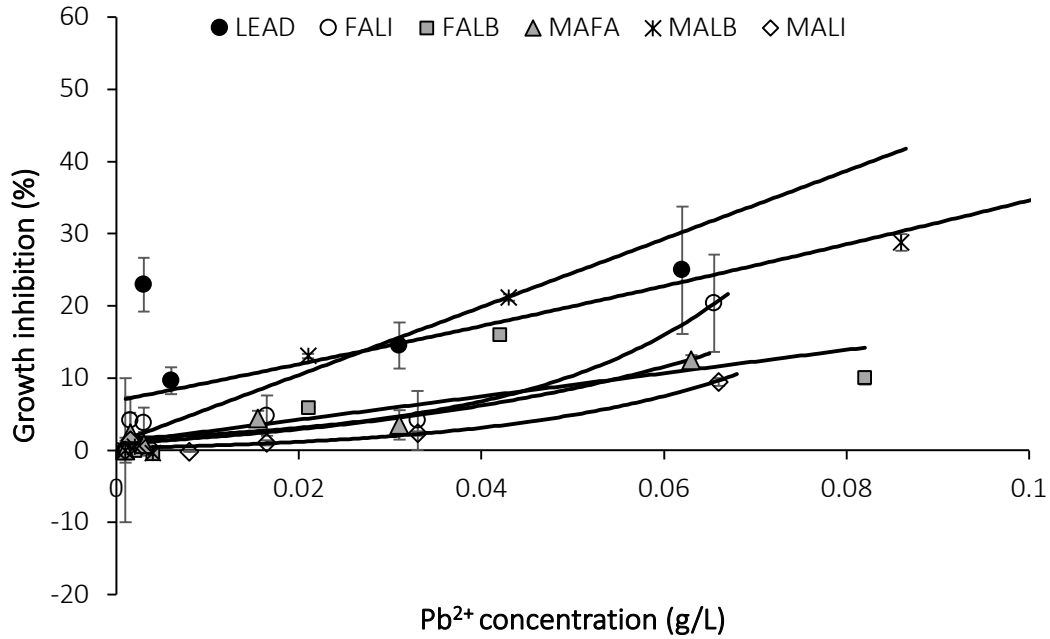


Figure 4.1: Growth inhibition of *C. vulgaris* with Pb^{2+} concentration after 72-h exposure (black circles). Plotted in the graph is the growth inhibition observed after MALI (diamonds), FALB (squares), MALB (*), MAFA (triangles) and FALI (empty circles) perovskite NPs transformed to Pb^{2+} , according to molecular weight.

The intracellular ROS activity increased significantly with increased concentration of all perovskite NPs. FALI and MAFA NPs reaching 2,300 and 1,652 relative fluorescence units at the higher concentration tested that was similar to the levels of fluorescence after lead nitrate exposure (1,685) while exposure to 200 mg/L of FALB perovskite NPs produced more than four-times higher fluorescence (19,896 fluorescent units, as shown in Figure 4.2). The high concentration of perovskite NPs (200 mg/L), up to which *C. vulgaris* was tested, is considerably lower than environmentally relevant concentrations for perovskite NPs. No environmental concentrations of perovskite NPs are reported in the literature, however, TiO_2 NPs that are the most commercially used NPs (as reported in Chapter 1) has been estimated at μg level in surface waters (Sun et al., 2014). This is the first study to conduct risk assessment of lead-halide perovskite particles and inform on acute toxicity in green micro-algae.

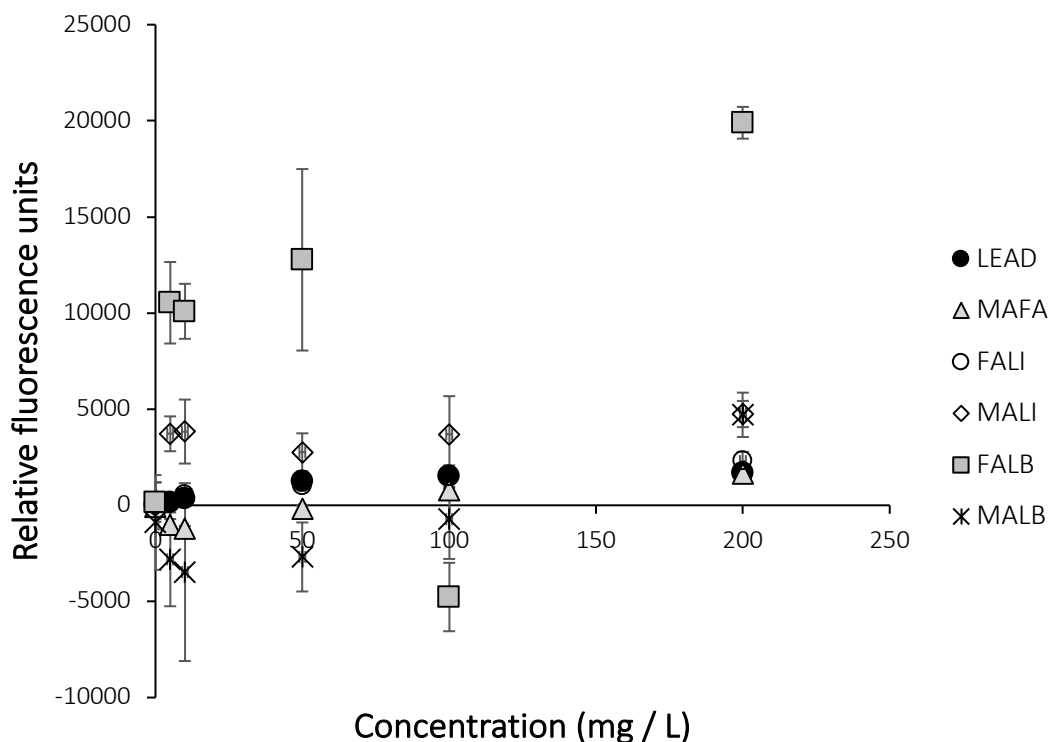


Figure 4.2: Relative fluorescence units of DCF after 72-h *C. vulgaris* exposure in perovskite NPs (MALI, MALB, FALB, MAFA and FALI) in parallel to lead nitrate exposure up to 200 mg / L. Data have been normalised to cell number of each sample, mean \pm SE, n=3, control n=6.

Zebrafish larvae mortality and *mt2* gene expression were significantly increased with Pb ions increasing concentration, while Pb concentration showed an inverse relationship to *ala-d* expression. The median lethal concentration (LC_{50}) for Pb was 67 mg/L (CI 95%= 23 – 209) for 96-h exposure of zebrafish larvae and when zebrafish larvae were exposed to a range of Pb for 24 h, *mt2* induced up to 50-fold after normalization to control exposure ($R^2= 0.91$, Figure 4.4A) and *ala-d* decreased down to 0.65 ($R^2= 0.92$, Figure 4.4C). Previous studies have evaluated Pb toxicity in zebrafish embryos and have reported 95 % mortality after 96-h exposure to 100 mg/L Pb ions (Peterson et al., 2011) and a 4-d LC_{50} of 382 mg/L for PbI_2 in zebrafish embryos (Babayigit et al., 2016). Lead ions water solubility and therefore Pb aqueous toxicity are strongly dependent on the ionic strength of the exposure medium (Alsop and Wood, 2011). Specifically, in soft water medium 71 % of total Pb was found in dissolved ionic form, while only 6.25 % of dissolved Pb ions were found in hard water medium (33 mg/L of Pb ions

nominal concentration). Peterson et al. (2011) also reported a 1.1-fold induction of *mt2* after 72-h exposure to 0.1 mg/L of Pb, while western blotting revealed a 600% induction of *mt2* protein levels. In the present study, the levels of *mt2* gene were assessed after a 24-h exposure and a 21-fold induction was observed after 24-h exposure of 10 mg/L Pb ion in 96-hpf larvae. The differences between the two studies can be attributed to the differences in concentration range, exposure period and developmental stage of zebrafish, however, these findings suggest that *mt2* is a relevant biomarker for Pb bioavailability in zebrafish. The loss of Pb ions in the water column can explain the high LC₅₀ values for zebrafish larvae and the variation in lead toxicity among studies can be attributed to differences in hardness of the water medium.

Perovskite NPs toxicity followed similar patterns of zebrafish mortality and *mt2* gene expression as Pb ions. The LC₅₀ for MALI and FALB NPs were estimated at 220 and 206 mg/L in zebrafish larvae after a 96-h exposure, respectively, and when the MALI and FALB NPs were converted to the equivalent amount of Pb (66.84 and 83.888 mg/L, respectively), a similar pattern to Pb concentration - response was observed (Figure 4.3) that can be attributed to lead dissolution of the perovskite NPs. Specifically, no differences were found between Pb(NO₃)₂ and MALI concentration-response curves, while FALB concentration did not cause higher mortality than Pb. No mortality was recorded when larvae were exposed to MALB, FALI or MAFA NPs up to 200 mg/L concentration which contain 86.5, 65.46 and 62.32 mg/L Pb, respectively. When zebrafish larvae were exposed to MALI, MALB and FALB NPs for 24 h, in parallel with Pb ions, *mt2* expression was positively induced with increasing concentration and no differences were observed among NPs or between NPs and Pb ions (GLM, p>0.05, Figure 4.4B). The parallel exposures and the lack of significant differences between the perovskite particles and the lead (II) nitrate *mt2* expression suggests that the toxicity of perovskite particles can be attributed to the presence of Pb in the perovskite particles. The *ala-d* expression after a 24-h Pb or perovskite NPs exposure to zebrafish larvae showed inhibition with increasing concentration and no significant differences were found among perovskite NPs or between NPs and lead nitrate, however, high variation in expression was observed (Figure 4.4D). This is the first study to investigate *mt2* and *ala-d* expression after lead-halide perovskite particles after aqueous exposure.

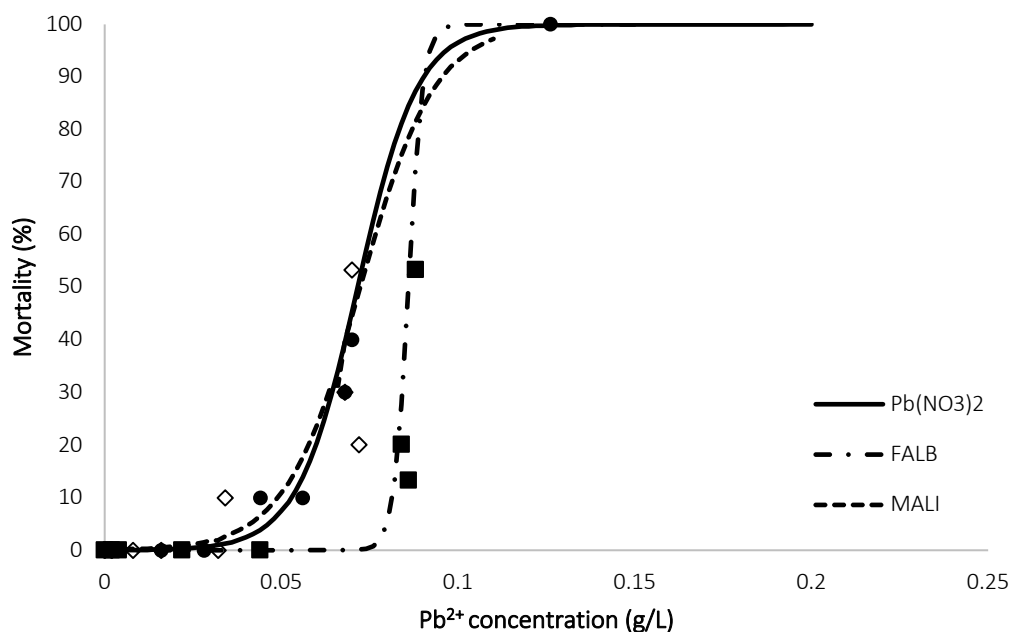


Figure 4.3: Mortality of zebrafish larvae with Pb^{2+} concentration after 96-h exposure (black circles and curve). Plotted in the graph is the mortality recorded after MALI (white diamonds) and FALB (black squares) perovskite NPs transformed to Pb^{2+} , according to molecular weight. The predicted mortality was obtained by the following exponential equation: $(e^{a+\beta x}) / (1 + e^{a+\beta x})^{-1}$. No mortality was observed after exposure to MALB, MAFA or FALI perovskite NPs up to 200 mg / L of NPs. Statistical differences between curves were obtained by pair-wise contrasts statements.

Hepatic *mt2* expression was induced and hepatic *ala-d* was inhibited after dietary exposure to both Pb and perovskite NP-spiked feeds. Both *mt2* and *ala-d* expression differed significantly between male and female fish (ANOVA, Tukey HSD, $p < 0.05$), therefore the data are presented in separated graphs. Both female and male liver *mt2* levels exhibited significant differences between 48-h exposure and 96-h or 14-d exposure, specifically, *mt2* levels after lead nitrate-spiked diet, induced an 8-fold in female liver at 48 h after the start of exposure (highest induction observed in the present study), while down-regulation was observed at 96 h and 14 d of 0.4 and 0.38-fold, respectively (Figure 4.5). The FALB-spiked diet led to significant induction of *mt2* in female liver after 48-h exposure compared to fish fed with non-spiked diet, while MALB and LEAD-spiked diets led to increased *mt2* expression with high variation between samples. No significant differences were observed in the male liver *mt2* levels,

however, the LEAD, MALI and FALB treatments resemble similar pattern to the female liver *mt2* (Figure 4.5). Additionally, low dissolution of Pb was observed in the water of the aquaria out of the Pb or perovskite-spiked feeds excluding the possibility of aqueous exposure to Pb ions during the 14-d period and a Pb recovery of higher than 81 % was revealed by ICP in the perovskite NP-spiked food pellets (Table 4.2). No differences were observed in hepatic *ala-d* expression after 48-h dietary exposure across treatments, however, all perovskite NPs and lead treatments showed inhibition of *ala-d* expression at the 96-h exposure period (Figure 4.5). At the end of the dietary exposure (14 d), *ala-d* expression increased. Restoration of normal *ala-d* values has been previously reported, specifically, in blood samples of Nile tilapia after a 9-d exposure of lead (Dos Santos et al., 2016). Dietary exposure is a relevant scenario of NP exposure to fish and other aquatic organisms and the present study is the first study to report on dietary exposure to perovskite NPs in fish as well as Pb bioavailability after dietary exposure in zebrafish. Lead has been reported to accumulate in liver tissue after one-day exposure (sub-lethal injection) (Vinodhini and Narayanan, 2008), high variation was observed in the present study after lead dietary exposure and gender-dependent *mt2* and *ala-d* expression, that can be attributed to the experimental design of the present study. Although all food was consumed, not all individuals consumed identical amount of food per aquarium, and the dominant behaviour of larger individuals may explain the high variation. The large size of zebrafish has been reported to lead to dominant behaviour independently of fish sex (Hamilton and Dill, 2002). The first sampling for *mt2* expression occurred 48 h after the start of exposure and it is possible that expression occurred swiftly and would have been more obvious after 24-h exposure. The down-regulation observed at 96-h and 14-d sampling support the hypothesis that *mt2* protein is in high levels in the exposed fish.

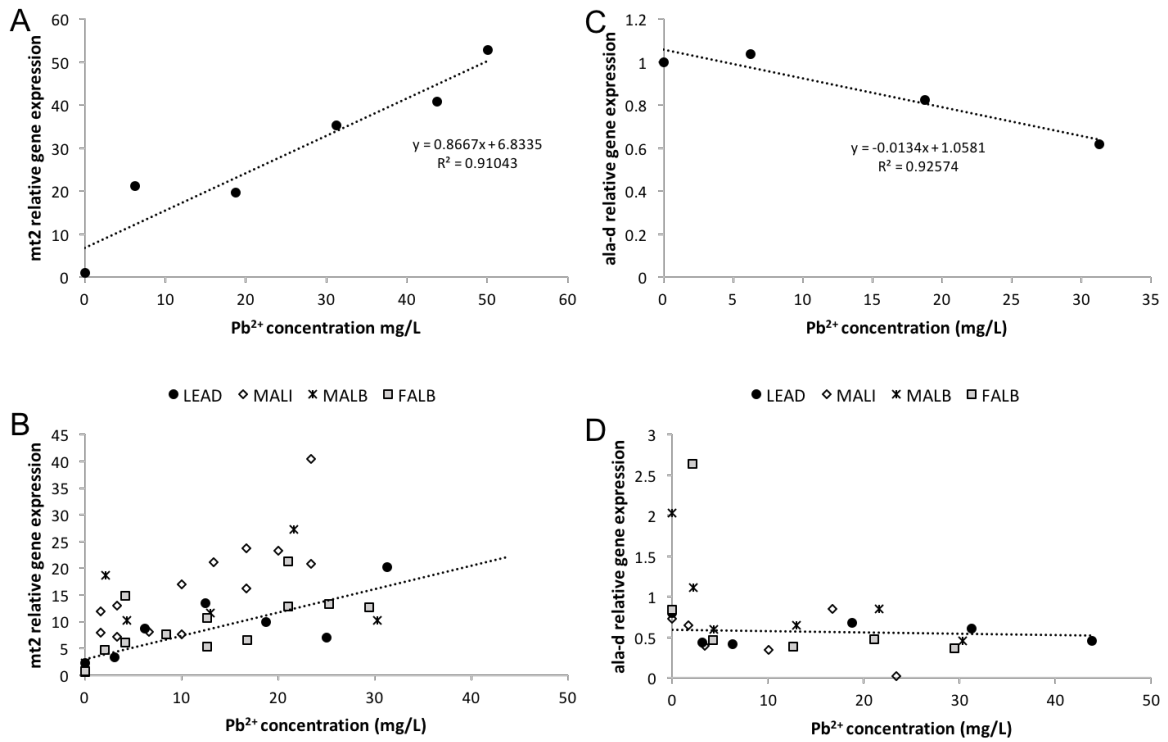


Figure 4.4: Relative expression of A) *mt2* and C) *ala-d* with Pb concentration after 24-h exposure in zebrafish larvae ($R^2 = 0.91$ and 0.92 , respectively). B) The *mt2* relative fold induction and D) the *ala-d* inhibition with Pb concentration after 24-h exposure to $\text{Pb}(\text{NO}_3)_2$ (black circles). Plotted in the graph is the *mt2* induction with the Pb concentration the particles MALI (diamonds), FALB (squares) and MALB (*) contain, according to molecular weight.

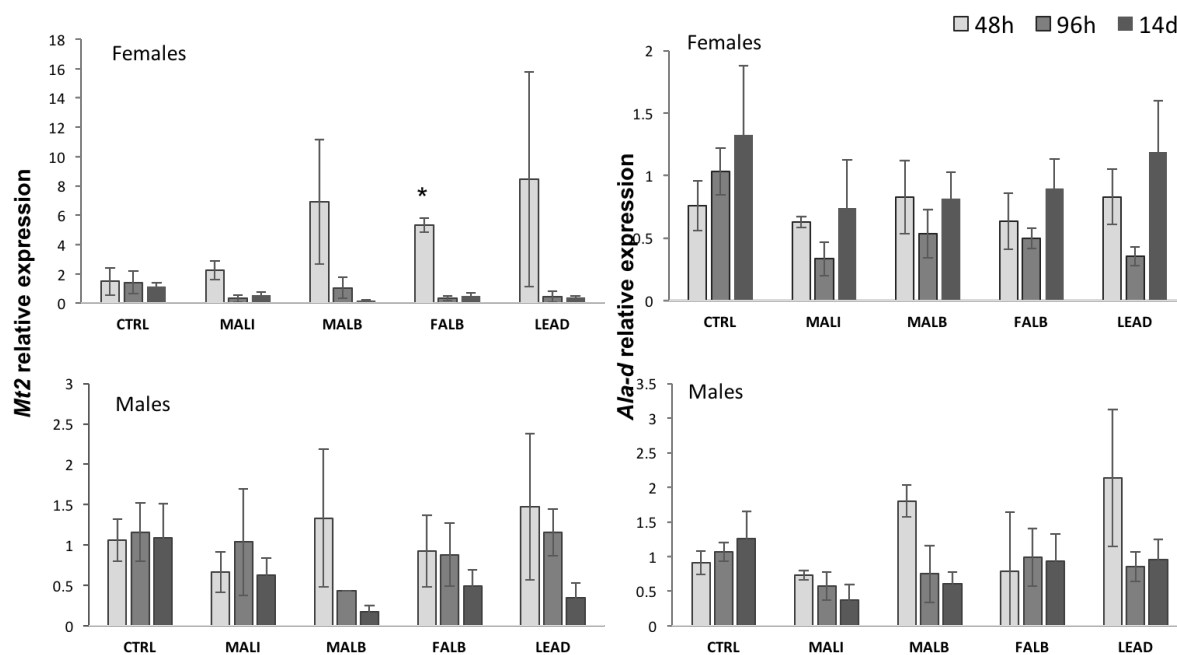


Figure 4.5: Response of *mt2* gene expression after dietary exposure to perovskite NMs or lead nitrate contaminated food with concentration of 500 $\mu\text{g/g}$ of Pb^{2+} . The *mt2* levels were assessed in liver tissues after normalization to β actin. The graph A presents the results from female zebrafish liver tissue and the graph B from male tissue. Data are MEAN \pm SEM, n=3, ANOVA, $p < 0.05$

The tRFLP analysis identified 15 different taxonomical units (OTUs) of zebrafish gut microbiome whose distribution were influenced by the treatment. Zebrafish fed with Pb-spiked food displayed significant changes in the gut microbiome community compared to fish fed control food (PERMANOVA, $p < 0.05$) while MALI-fed fish gut microbiome differed compare to Pb-fed fish with a $p = 0.06$ (PERMANOVA), showing no differences compared to control-fed fish. Non-metric MDS analysis of tRFLP data of different diet types is shown in Figure 4.7. Results from this analysis revealed multivariate patterns among observations, and specifically, a strong distinction between Pb and control treatments was observed, while the perovskite NPs treatments were placed between the range set by control and Pb treatments along the y axis. The Shannon-Wiener Index, a measure of species diversity in bacterial communities (Marrugan, 2004), was significantly reduced in the MALB treatment when compared to FALB or LEAD treatments, while none of the spiked-fed fish microbiomes differed significantly compared to control treatment (Figure 4.6). Lead-spiked food, which was

used as a positive control in the present study, led to significant changes in the zebrafish gut microbiome communities, while the perovskite-spiked feeds did not change significantly the structure of the zebrafish gut microbiome after a 14-d dietary exposure. The Illumina MiSeq analysis of the control, lead nitrate and perovskite FALB samples identified 396 16S rRNA sequences and bacterial phylla of control and lead nitrate samples were grouped separately as shown in Figure 4.8. The analysis of presence or absence of the identified phylla (Figure 4.9) led to no differentiation among treatments, that is in contrast with the Shannon-Weiner Index out of tRFLP analysis. The high bacterial phylla richness identified by miseq Illumina compared to the relatively few alleles identified by tRFLP suggests loss of information using the tRFLP analysis, however, both analyses led to the same result regarding abundance of gut microbiota; the lead-spiked feeds led to differences in bacterial distribution that, in the case of tRFLP obtained data, was found statistically important.

Table 4.2: Total lead concentration measured by ICP-MS and ICP-OES in the water column of aqueous exposures to perovskite NPs (MALI, MALB, FALB) and $\text{Pb}(\text{NO}_3)_2$ with nominal concentration of 60 mg / L; measurements of water of the aquaria after 14 d dietary exposure to NP or lead contaminated food; and measurements of total lead found in acid digested food pellets, mean \pm SE, n=5.

Samples from:	Water column of exposure vial (nominal concentration 60 mg / L, in mg / L)	Aquarium water following dietary exposure (in $\mu\text{g}/\text{L}$)	Contaminated food pellets (nominal concentration 500 $\mu\text{g}/\text{g}$, in $\mu\text{g}/\text{g}$)
MALI	0.212	<0.001	467.163 \pm 15.6
MALB	0.152	0.2973	406.917 \pm 5.5
FALB	0.223	0.31484	484.814 \pm 11.5
$\text{Pb}(\text{NO}_3)_2$	0.189	<0.001	286.753 \pm 5

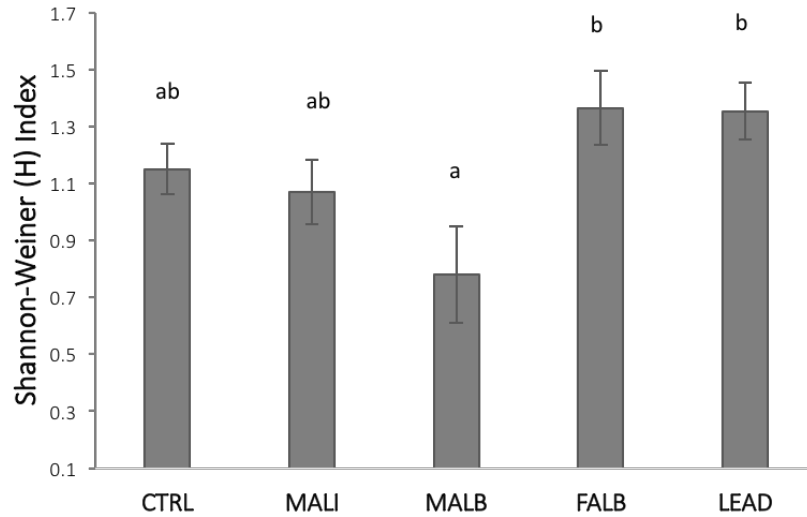


Figure 4.6: Shannon-Weiner Index that informs on species richness and proportion within the zebrafish gut community using data collected from tRFLP analysis of the gut microbiota. The microflora richness of fish fed with MALB-contaminated food was found significantly different from FALB-fed and LEAD-fed fish gut microflora. Data represent mean \pm SE, ANOVA, TukeyHSD, $p < 0.05$

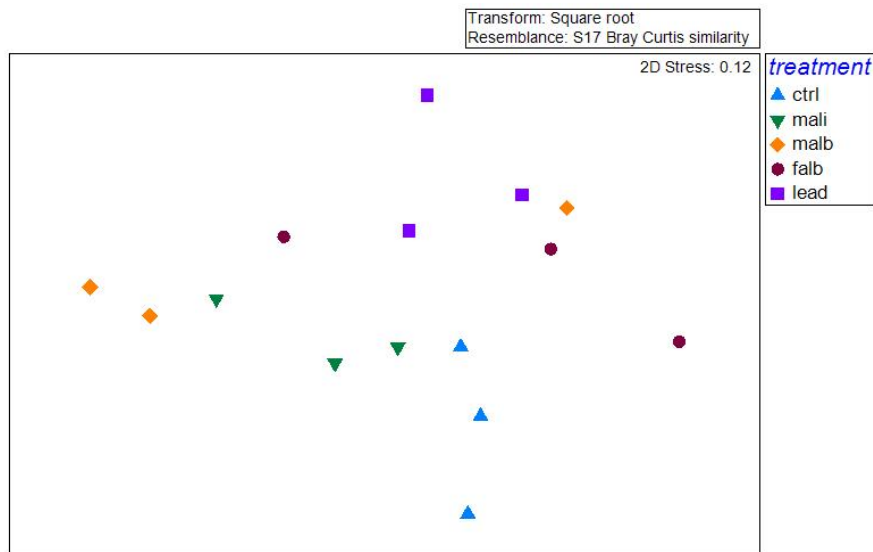


Figure 4.7: Nonmetric Multidimensional Scaling (NMDS) ordination displaying microbiome communities of gut microbiota of fish fed control, MALI, MALB, FALB, or lead-spiked feeds. Microbiomes were distinct between control and lead-spiked feeds along y axis, while microbiomes of perovskite-spiked feeds were placed between control and lead treatments. Each point in the graph, represents 1 aquarium and pooled allele data obtained from the fish sacrificed per aquarium.

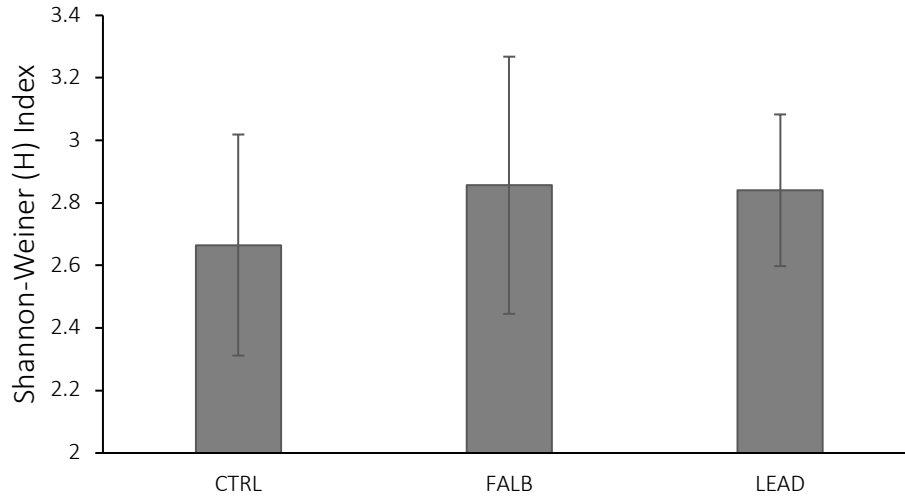


Figure 4.8: Shannon-Weiner Index that informs on species richness and proportion within the zebrafish gut community using data collected from illumine miSeq analysis of the gut microbiota. The microflora richness of fish fed with FALB or lead-contaminated food was found at similar levels with control diet-fed fish gut microflora. Data represent mean \pm SE, n=3 (n=2 for FALB treatment).

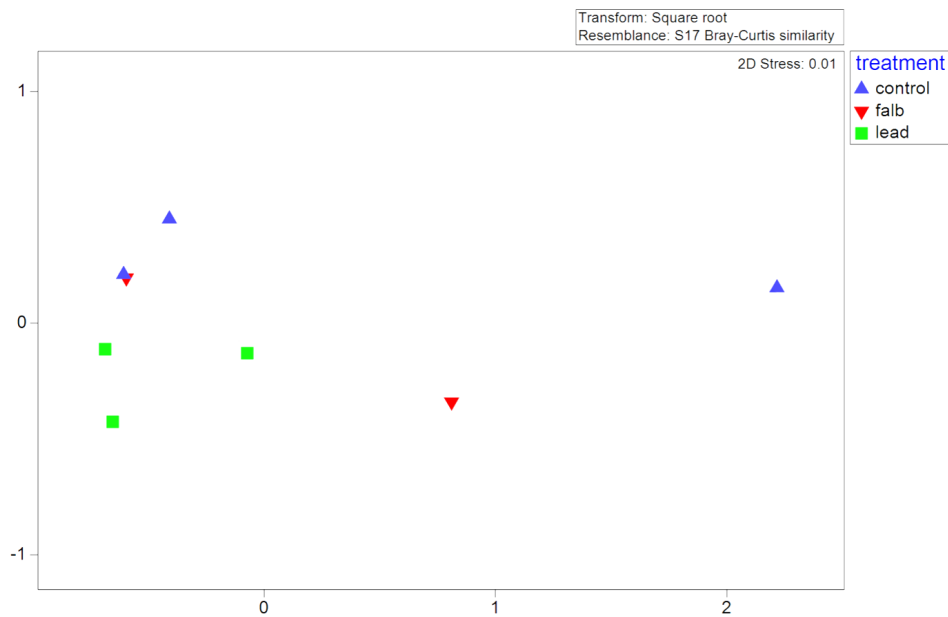


Figure 4.9: Nonmetric Multidimensional Scaling (NMDS) ordination displaying microbiome communities of gut microbiota of fish fed control (blue), FALB (red) or lead-spiked feeds (green). Microbiomes were distinct between control and lead-spiked feeds along y axis. Each point on the graph represents 1 aquarium and 5 pooled fish gut microbiome DNA.

The histological examination of zebrafish cross sections revealed no lesions associated with Pb or perovskite NPs exposure after 14-d dietary exposure (Appendix C). Specifically, no indication of inflammation or lesions were observed in liver and kidney tissues, and no lesions were found the intestinal mucosae when sections were compared to fish fed with control food (Figure 4.10). A low incidence of basophilic cytoplasm and nuclei pyknosis indicative of early stages of cellular necrosis have been reported in neotropical fish *Hoplias malabaricus* liver tissue, after injection of 8 or 14 doses of inorganic lead (4 µg per g of fish daily) (Rabitto et al., 2005). The observed differences between Rabitto et al. (2005) and the present study can be explained by the exposure methods that were employed by each investigation. Specifically, the injection is considered more potent exposure compared to dietary exposure, as during the latter the compound reaches the blood flow indirectly after absorption from the lumen of the gut (Boyle et al., 2013) indicating that although during an injection exposure all external factors are eliminated, a dietary exposure is an environmentally relevant way of assessing toxicity of NPs.

Taken together, the results of this study indicate that toxicity of perovskite NPs is attributed to Pb release in the aqueous phase, while less Pb ion bioavailability occurred through dietary exposure. The results of the present study revealed growth inhibition and ROS generation in *C. vulgaris* and mortality of zebrafish larvae in high concentration of lead-halide perovskite NPs, and this toxicity can be attributed to increased Pb bioavailability after dissolution, identified by induction in expression *mt2* and inhibition of *ala-d* expression. Lead became bioavailable after a dietary exposure with perovskite-spiked feeds in adult zebrafish. The data gathered by the DNA analyses suggest significant changes in gut microbiome community after a 14-d exposure to lead-spiked food, while the perovskite-spiked food did not affect the microbiome. The present study provides evidence of indirect toxicity of lead-halide perovskite NPs due to lead dissolution and shows potential direct and indirect roots of exposure of perovskite NPs in the aquatic environment.

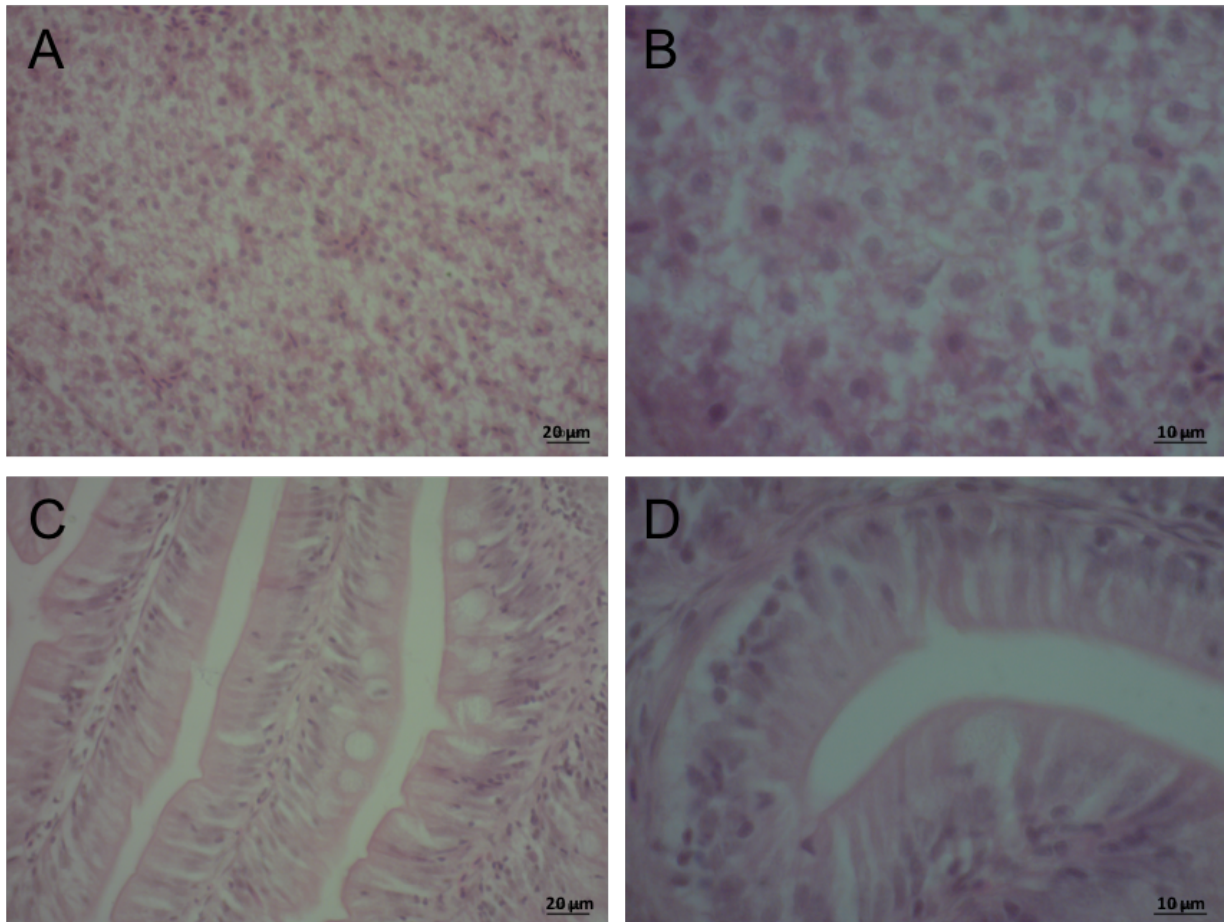


Figure 4.10: Representative image of liver (A and B) and intestine (C and D) tissue sections after H&E staining in x40 (A and C) and x100 (B and D) from fish fed with control food. The liver tissue sections (A and B) showed healthy hepatic cells with intact cell membrane, visible nucleus and nucleolus and no signs of haemorrhage. The lumen of the gut (C and D) showed no lesions or any epithelial cell defects.

Chapter 5 - A Comparison of Nanoparticle (NP) Acute Toxicity Tests in the Aqueous Phase: The Importance of Homogeneous NP Dispersions.

5.1 Abstract

The agglomeration and settling of NPs in the aqueous phase makes the conventional fish larva toxicity test inefficient to identify the relation between NPs unique physicochemistry and toxicity. The unique physicochemical properties (e.g., size, surface charge etc.) of aqueous-phase NPs and lack of reproducibility of NP eco-toxicity tests is a critical issue may be consequent on a variety of causes (e.g., different NPs, exposure media, etc.). Differences in toxicity of NPs have been reported for NPs tested in parallel under static versus controlled dynamic suspensions and toxicity has been found dependent on the consistency of exposure concentrations throughout the exposure. The aim of the present study was to further develop an exposure chamber with characteristics that allow routine testing and low amount of waste and to compare toxicity of zebrafish larvae in the exposure chamber, to traditional static toxicity tests (i.e. glass beakers and 96-well plates). Results indicated consistently higher toxicity of all NPs when toxicity tests were conducted in the exposure chamber compared to static exposures. The fish larvae NP toxicity tests were held in parallel to fresh algae NP toxicity tests, where no sedimentation of NPs occurs during the exposure period and NPs are in direct contact with the algal cells since the algae are constantly agitated. This study provided a pragmatic approach on NP toxicity testing, emphasizing the ineffectiveness of the current experimentation limiting the probability of toxicity artefacts and maximising the exposure for an efficient risk assessment.

5.2 Introduction

The physicochemistry (e.g., size, surface charge etc.) of aqueous-phase NPs are hypothesized to be related to their toxicity in aquatic organisms. The change in physicochemistry of NPs alters the exposure conditions, therefore testing this hypothesis requires careful characterization of NP physicochemistry in the aqueous phase, and consistent exposure conditions such that results of toxicity tests can be reproduced independently. Despite considerable effort over numerous years, mechanistic links between NP physicochemistry and toxicity in aquatic organisms have not been yet established (Holden et al., 2016; Selck et al., 2016). Research indicates that some aqueous-phase NPs can dissolve (dissolution of metal ions) or form agglomerates with consequent changes in NP physicochemistry (i.e. changes in particle size and active surface area) that can change during the exposure in the aqueous phase and add to the difficulties of attributing NP physicochemistry to toxicity (Petersen et al., 2014). In addition, concentrations of NPs that induce toxic responses can be below the concentrations in which NP physicochemistry can be effectively analysed (e.g., for some Ag-NPs), making difficult to identify the physicochemistry of the NPs at the exact exposure conditions.

The lack of consistency of NP ecotoxicity tests is a critical issue that must be resolved for a better understanding of NP ecotoxicology. Although differences in toxicity results among studies are expected and may be a consequence of the exposure (e.g., different size NPs, coatings, exposure media, differences between nominal and real concentrations, different sizes of exposure vessels etc.), the lack of reproducibility among tests (even within laboratories) suggest other factors that must be addressed. An example of inconsistent results among several studies on NP toxicity is evident for Ag NPs. Specifically, exposure conducted in petri dishes with Ag NPs stabilised with polyacrylate sodium acquired a 96-h LC_{50} of 1.18 mg/L in zebrafish embryos (Massarsky et al., 2013), polyvinyl alcohol Ag NPs tested in 6-well plates obtained a 72-h LC_{50} of approximately 75 mg/L using the same model organism (AshaRani et al., 2011). After a 4-d exposure to pure Ag NPs in petri dishes obtained an LC_{50} of 2 mg/L in zebrafish embryos (Kovriznych et al., 2013), a 48-h LC_{50} of 7.20 mg/L was observed when 24 hpf zebrafish embryos were exposed in 12-well plates mg/L (Griffitt et al., 2008) and an LC_{50} of 10 mg/L was obtained after exposure to 3 nm Ag NPs in 96-well plates (Bar-Ilan et al., 2009). The inconsistent results may be due to differences in the methods used for the exposure (e.g. 24-well plates, petri dishes, glass beakers, developmental stage of the organism). Disparity in NP toxicity is also evident in reports of TiO_2 NPs toxicity, with studies reporting 96-h LC_{50}

of TiO₂ NPs exposure to Japanese medaka embryo at 155 mg/L under laboratory light and daily solution changes (Ma et al., 2012), and no mortality in zebrafish embryos up to 1600 mg/L (Boyle et al., 2015; Griffitt et al., 2008; Harper et al., 2008; Kovriznych et al., 2013). The rapid sedimentation and agglomeration of TiO₂ NPs can lead to fish embryo toxicity artefacts and unrepresentative toxicity of zebrafish embryos that can be a consequent of suffocation of embryos due to clogged chorion pores. The fish embryos are settled at the bottom of the exposure vessel and the embryo chorion can be considered as a mechanical barrier, protecting the embryo from NP agglomerates larger than 200 nm diameter changing in a way the actual exposure condition.

Nanoparticles do not behave as traditional dissolved toxicants and the currently standardised methods of exposure to homogeneous aqueous dispersions do not apply to all model organisms used in eco-toxicological studies. With the exception of the microalgae toxicity test, that offers constant agitation of the algal cells and the NP agglomerates during the exposure, therefore, limited sedimentation of NPs, other aquatic organisms, including fish, are not exposed to nominal NP concentration due to sedimentation of agglomerates. The issue of sedimentation of NPs within aqueous exposure preparations has been addressed in an earlier study (Boyle et al., 2015), demonstrating that toxicity of NMs is dependent on the consistency of exposure concentrations throughout the exposure. Boyle et al., reported an 80 and 81.2 % of initial Ag and Cu NPs at the end of a 96-h exposure period, using an exposure chamber, that enabled homogeneous dispersions of the NPs in a 2-L beaker, while the zebrafish larvae were held in a semi-isolated chamber in the water column (Figure 5.1). On the contrary, 3.1 and 2.3 % of Ag and Cu NP, respectively, were found in the water column, in a static beaker after a 96-h exposure. Consequently, significantly lower 96-h LC₅₀ values and variability were found for both NPs using the exposure chamber when compared to static beaker exposures. Shaw and colleagues (2016) attempted a miniaturization of the exposure chamber and reported a 74 and 83 % of TiO₂ NM105 and Ag NM300K after 24 h dispersion. Assessment of NPs toxicity requires testing strategies that are reproducible and accessible under laboratory conditions, therefore, the step forward regarding the exposure chamber will be to improve its design using smaller volumes, that would in turn enable more replication of the toxicity tests and less waste production.

In contrast to the fish embryo toxicity tests, the microalgae NP toxicity test is considered to have limited issues with respect to sedimentation. The nature of the algal toxicity tests can

ensure true dosimetry (loses only to sorption to exposure vessel) and algal cells are continuously in direct contact with NPs through the incubation period. The diameter of the pores in the cell wall of algae can range between 5 and 20 nm (Navarro et al., 2008), suggesting internalization of NP agglomerates rather unlikely. Microalgae can be considered as a very sensitive aquatic toxicology model organisms as they are highly dependent on the chemical composition of the medium. Subsequently, several indirect effects of NP toxicity have been reported such as shading effects in high NP concentrations which inhibit photosynthesis (Aruoja et al., 2009) and mineral nutrient depletion, as essential nutrient adsorb on NPs and become less bioavailable to the microalgae (Van Hoecke et al., 2009). The algal toxicity test can be held in direct comparison with the zebrafish larvae toxicity test regarding the sedimentation of the NPs.

The objective of this study was twofold. First, the 2-L exposure chamber (Boyle et al., 2015) was further developed to allow routine toxicity testing using smaller volumes and advance towards standardization of the *in vivo* assessment of NP toxicity in the aqueous phase. A range of commercially important engineered NPs were tested using zebrafish larvae. Second, widely used traditional aqueous toxicity assays and their variability in the outcomes were compared to the exposure chamber assay. Specifically, the experimental comparison of NP acute toxicity included static test in glass beakers, polystyrene 96-well plates, and the modified exposure chamber toxicity test system. Toxicity tests in zebrafish larvae were held in parallel with fresh water algae toxicity test using *Chlorella vulgaris*, as the algal NP toxicity test is considered to have limited issues with respect to sedimentation and dosimetry during exposure in contrast to the fish embryo NP toxicity test.

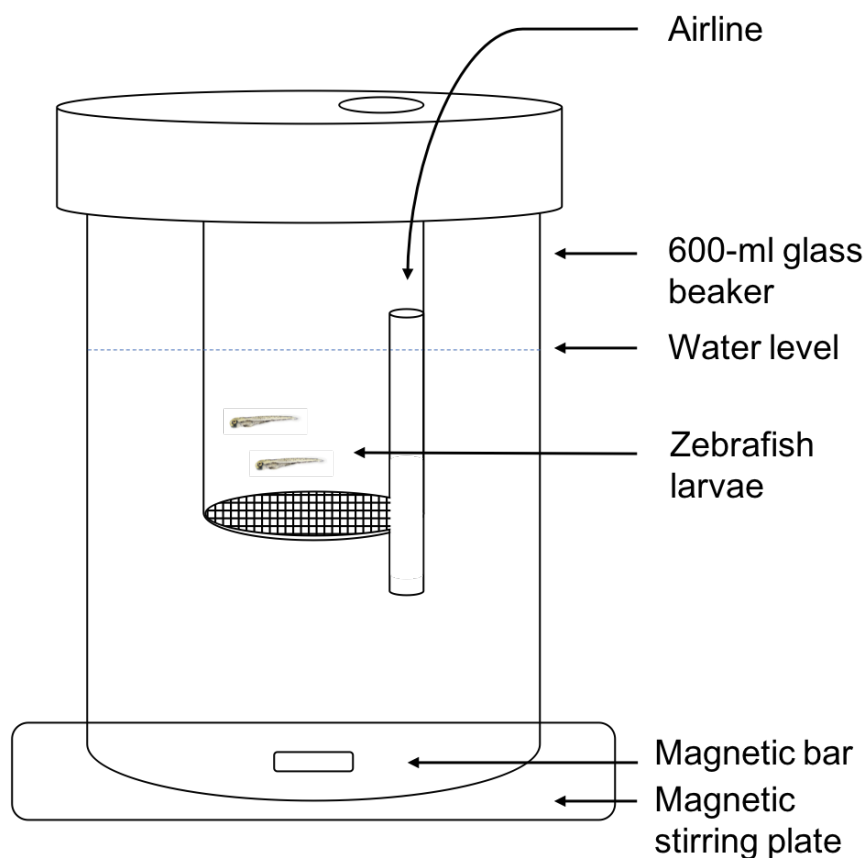


Figure 5.1: Schematic outlining of the major features of the exposure chamber used to assess the toxicity of NPs to zebrafish larvae in the present study. The exposure chamber has a bottom mesh that separates and protects the exposed zebrafish larvae from the magnetic stirring bar at the bottom of the 600-ml glass beakers while the NPs are kept in constant dispersion throughout the exposure duration. The water circulation is enhanced by the air supply through the thin tube inside the inner chamber.

5.3 Materials and Methods

5.3.1 Nanoparticles tested

For the present study, four NPs with different physicochemistry were selected (Table 5.1). Ag polyvinylpyrrolidone (PVP) coated nano-prisms, CeO_2 and TiO_2 NPs with hexamethylenetetramine (HMT) and tetramethylammonium hydroxide (TMAOH) stabilising agents, respectively, and CuO NPs, were suspended in Milli-Q water and the stocks were sonicated for 8x2 min before the preparation of the exposure solutions. Silver nitrate (AgNO_3)

was used as a control toxicant compound and was provided by FSA Laboratory Supplies. For NP characterization, 10 mg/L of each NP in milli-Q water was sonicated and the measurements of the average hydrodynamic size of NP agglomerate in the aqueous solution (z-average) and the surface charge of the NPs (ζ -potential) were conducted using Dynamic Light Scattering (DLS).

Table 5.1: The list of NPs used in the present study included Ag nanoprisms, CeO₂ and TiO₂ NP and CuO NPs. The table summarises the NP physicochemistry as in the shape, coating and size provided by manufacturer and the average agglomerate size in aqueous solution (z-average) and NP charge (ζ -potential) as measured by DLS at Heriot Watt University. Data are means \pm standard error, n=3.

NPs	Characterisation (manufacturer data)	z-average (diameter, nm \pm SE)	Z-potential (mV \pm SE)	NPs provided by
Ag	Nano-prisms coated with polyvinylpyrrolidone (PVP)	39.56 \pm 0.2	-18.26 \pm 0.6	Philipps Universitaet Marburg, Germany
CeO ₂	Stabilised with hexamethylenetetramine (HMT)	1185.13 \pm 199.4	4.9 \pm 0.5	Fundacio Privada Institut Catala de Tecnologia, Spain
TiO ₂	4 nm diam., nano-spheres, stabilised with tetramethylammonium hydroxide (TMAOH)	66.54 \pm 0.9	-24.56 \pm 0.9	Fundacio Privada Institut Catala de Tecnologia, Spain
CuO	12 nm diameter	343.13 \pm 28.3	-7.98 \pm 0.6	PlasmaCheam, Germany

5.3.2 Acute Toxicity Tests

Zebrafish (*Danio rerio*) were obtained from the zebrafish research facility (Heriot-Watt University), and husbandry, spawning and experimentation were conducted with complete approval and according to animal welfare regulations of the UK Home Office. Characteristics of water chemistry were 79, 38, 12, 17 and 2 mg/L of Ca^{2+} , Mg^{2+} , Na^+ and K^+ , respectively; pH of 7.7; temperature was maintained between 28-30 °C, and a 12-h photoperiod. Ammonia, nitrate, nitrite and chlorines were measured weekly and kept under 0.02, 5, 0.05 and 0.05 mg/L, respectively. Breeder fish were fed daily dry pellet food ZM systems, Winchester, and newly hatched *Artemia salina*.

Embryos (1-2 hpf) were collected, non-fertilised embryos and debris were removed and clean embryos were placed in petri dishes (~30 ml volume) in fresh water medium. Hatching occurred between 48 and 72 hpf, and fish of age 72-168 hpf were used for the experiments. The NPs used for toxicity tests were the TiO_2 , CeO_2 , Ag nanoprisms, CuO NPs. The model toxicant used in the study was Ag^+ (in the form of AgNO_3). The concentrations the larvae were exposed ranged between 0 and 200 mg/L and the medium used was consistent with the OECD guideline no.236 (OECD, 2006). Each zebrafish larvae exposure experiment included exposures using all three methodologies in parallel to allow comparison of results. The NP exposures were repeated twice, and the silver nitrate exposures were conducted once. The experimental preparations were kept at 28 °C throughout the exposure duration. The larvae survival was observed under a dissection microscope daily during the 96-h exposure period. Mortality was expressed as the total number of dead larvae at the end of 96-h exposure period according to total number of larvae exposed.

Larvae age 72 hpf were used for the static exposures in Corning® Costar® 96-well plates. One larva was placed per well, 200 µl exposure volume, 10 independent replicate wells per treatment, 6 treatments per plate, without using the outer well lines to reduce evaporation of water. Pyrex glass beakers of 100 ml volume were used for the static exposure experiments. The total volume of the exposure was 40 ml and 15 to 20 larvae were placed per beaker. Lids were placed on top of the beakers to reduce evaporation.

The design of the exposure chamber was based on the chamber described in Boyle et al. (2015) as the nano-SCAPE test system. The chamber was constructed to keep NPs in suspension throughout an acute fish larvae toxicity test. The larvae are held inside a PVC chamber where

the bottom end is closed with a fine mesh (mesh eye) and the upper end is open. At the wall of the chamber lays a vertical tube where an air tube fits to provide aeration and circulation of the NPs held in suspension without disturbing the larvae inside the chamber. The modification of the chamber included reducing the volume to a 600 ml-glass beaker compared to the initial 2-L beaker design (Boyle et al., 2015). Solutions of 450 ml final volume were prepared and 6 - 8 conditions were tested at a time for a 96-h exposure period. The beakers with a magnetic stir bar at the bottom were set on a multi position magnetic stirrer with speed set at 250 rpm, to stir the water and keep a homogeneous NP dispersion.

Algal growth inhibition assays were performed in pyrex 250-ml Erlenmeyer flasks according to the OECD test guideline (OECD 201) in the exponential growth phase. Temperature and light conditions for toxicity tests were identical to those used for culture growth. Experiments were carried out in triplicate. The initial concentration of the inoculum was 10^4 cells per ml, which was required to ensure exponential growth. Cell density was determined at 0, 24, 48 and 72 h of exposure by measuring *in vitro* fluorescence of acetone-extracted chlorophyll *a* (Kalman et al., 2015). The exposure concentrations ranged between 0.01 and 10 mg/l for Ag nano-prisms and between 5 and 200 mg/L for CeO₂ NPs.

5.3.3 Antioxidant Activity

The detection of reactive oxygen species is based on the fluorescence of the probe 2, 7 dichlorofluorescein diacetate (H₂-DCF-DA) and conducted by fluorescent plate reader (Molecular Devices SpectraMax M5) using excitation wavelength at 488 nm and emission wavelength at 525 nm at the same time points. For the reading, black polystyrene 96-well plates were used, 250 µl of each flask were added per well in triplicates at 72 h after the start of the exposure. DCF (10 µl) diluted in ethanol (180 mg/L) was added per sample in the dark and the plate was kept in dark conditions for 1 h till the fluorescence measurement.

5.3.4 Statistical analyses

Mortality (dependent variable) of zebrafish larvae was modelled by logistic regression according to the independent variables copper concentration, treatment (exposure methodology), and concentration x treatment interaction. The logistic regression models were generated by iterative maximization of the likelihood function, and independent variables and

their interaction were included if they significantly improved the model (likelihood ratio test, based on Wald χ^2 distribution). The median lethal concentration (LC_{50}) was calculated by the logistic regression model and the 95% confidence interval (CI) was calculated using the *logit* model in R statistics. Differences in fish mortality among treatments (i.e., presence or absence of NPs) were determined by pair-wise contrast statements with a p-value of <0.05. The algal growth inhibition (depended variable) and NP concentration (independent variable) relationship, and the median effective concentration (EC_{50}), were modelled using a concentration-response model for algae, by ‘drc’ package in R. All statistical analyses were conducted using *R statistics* (version 3.4.2, RStudio, Inc., 2015).

5.4 Results and Discussion

No differences were observed between the concentration-response curves of larvae inside the exposure chamber and the static glass beakers. Results obtained in this study indicated no additional mortality of the zebrafish larvae inside the exposure chamber that can be attributed to the exposure chamber. Significantly less mortality was observed if zebrafish larvae were exposed to $AgNO_3$ in 96-well plates (Figure 5.2, Logistic Regression, $p < 0.001$). In the present study, silver ions (as $AgNO_3$) were used as a model toxicant to evaluate whether the exposure chamber is causing additional mortality by design, and the results were compared to traditional static exposure methods. The toxicity of $AgNO_3$ was found higher using the exposure chambers, followed closely by the toxicity curve generated employing static glass beakers and $AgNO_3$ was significantly less toxic inside the 96-well plates compared to the two previous methodologies. This outcome is in agreement with the surface-to-volume ratio hypothesis, resulting to less toxicity when smaller exposure vessels are employed. The compound in assessment can sorb on the surface area of the exposure vessel, therefore the larger the surface area, the less compound can be available by the organism and silver ions are considered a highly-adsorbing substance (Baumann et al., 2014).

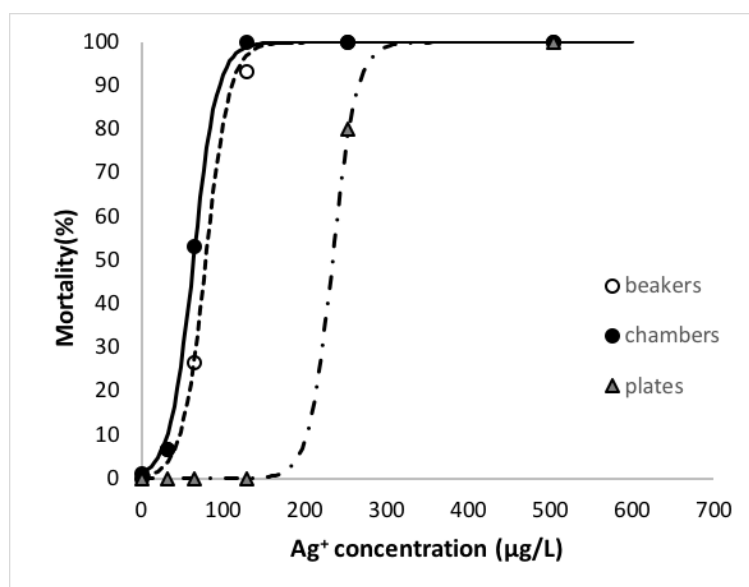


Figure 5.2: Concentration-mortality (%) curves after 96 h exposure of Ag⁺ (AgNO₃) to zebrafish larvae at 72 hpf developmental stage. The exposures were conducted in exposure chambers (black dots, black curve), glass static beakers (empty circles, dotted curve) and 96-well polystyrene plates (grey triangles, dotted curve). The predicted mortality was obtained by the following exponential equation: $(e^{-a+\beta x}) / (1 + e^{-a+\beta x})^{-1}$. The concentration-response curve generated mortality after exposure in chambers was found significantly different, from the concentration-response curves in static glass beakers or 96-well polystyrene plates by pair-wise contrast statements, $p < 0.001$. No differences in larvae mortality were observed between exposure in static glass beakers and 96-well plates.

Zebrafish mortality was significantly increased with NP concentration independent of the method of exposure used and NPs showed more potency when the exposure chamber was employed (Figure 5.3). Specifically, for Ag PVP-coated NPs the 96-h LC₅₀ using the exposure chambers was found 220 µg/L (CI 95% = 107-420) while the 96-h LC₅₀ in 96-well plates and glass beakers were found 13.5 (CI 95% = 3-23.5) and 15.5 mg/L, respectively. The mortality curve after chamber exposure was found significantly different compared to beakers or 96-well plates (Logistic regression, $p < 0.001$), while no differences were found between the curves generated in glass beakers and 96-well plates. Polyvinyl alcohol coated Ag NPs of lower diameter (25 nm) have been found less toxic to zebrafish embryos (72-h LC₅₀ of 85 mg/L) (Asharani et al., 2011) and PVP coated Ag NPs (20 nm diameter) caused increased incidence of mortality in concentration higher than 10 mg/L in 96-well plates (Kim et al., 2013). Kim et

al. (2013) also concluded that Ag PVP NP toxicity can be NP size dependent. For CuO NPs, the 96-h LC₅₀ of larvae exposed inside the chamber was found 8.2 mg/L (CI 95% = 3.6-18.7). No 96-h LC₅₀ was found for larvae exposed to CuO NPs in 96-well plates and no mortality was found for larvae exposed in static glass beakers up to 200 mg/L of CuO NPs. No significant changes in mortality has been found in zebrafish embryos exposed to CuO NPs (Vicario-Parés et al., 2014), survival rate dropped to 30% when zebrafish embryos (4 hpf) were exposed to concentrations higher than 25 mg/L and hatching rate dropped to less than 20% in concentrations higher than 6.25 mg/L of CuO NPs in well-plates (Sun et al., 2016), and no mortality was found in zebrafish larvae when exposed to 16 mg/L of CuO NPs (Thit et al., 2017). In the present study, the CeO₂ NPs were found significantly more toxic inside the exposure chambers compared to static exposures (Logistic Regression, $p < 0.001$). No zebrafish 96-h LC₅₀ was found after CeO₂ NP exposure in static glass beakers and no mortality was observed when larvae were exposed in 96-well plates up to 200 mg/L. No acute toxicity of CeO₂ NPs has been found in zebrafish embryos in previous study (van Hoecke et al., 2009), and the high number of CeO₂ NP agglomerates was observed to adsorb onto the chorion of zebrafish embryos. Finally, for TiO₂ NPs, no dead larvae were found in either 96-well plates or glass beakers at the end of the 96-h exposure period that is in agreement with previous studies using other kinds of TiO₂ NPs (Boyle et al., 2015; Griffitt et al., 2008). Mortality was observed for larvae exposed to TiO₂ NPs inside the exposure chamber in the present study, however, no significant mortality response was found with increasing concentration.

Employing the fish larva toxicity test for traditional dissolved environmental pollutants to assess NP toxicity may not be representative as the NPs are not in dispersion throughout the exposure duration and fish are not exposed to the nominal NP concentrations. The use of the exposure chamber in the present study prohibited the NP sedimentation, with zebrafish larvae being exposed to NPs in the water column throughout the exposure duration. The NPs concentration-response curves of zebrafish larvae exposed inside the chambers were significantly different from NP concentration-response curves generated when larvae were exposed in static vessels (Figure 5.3).

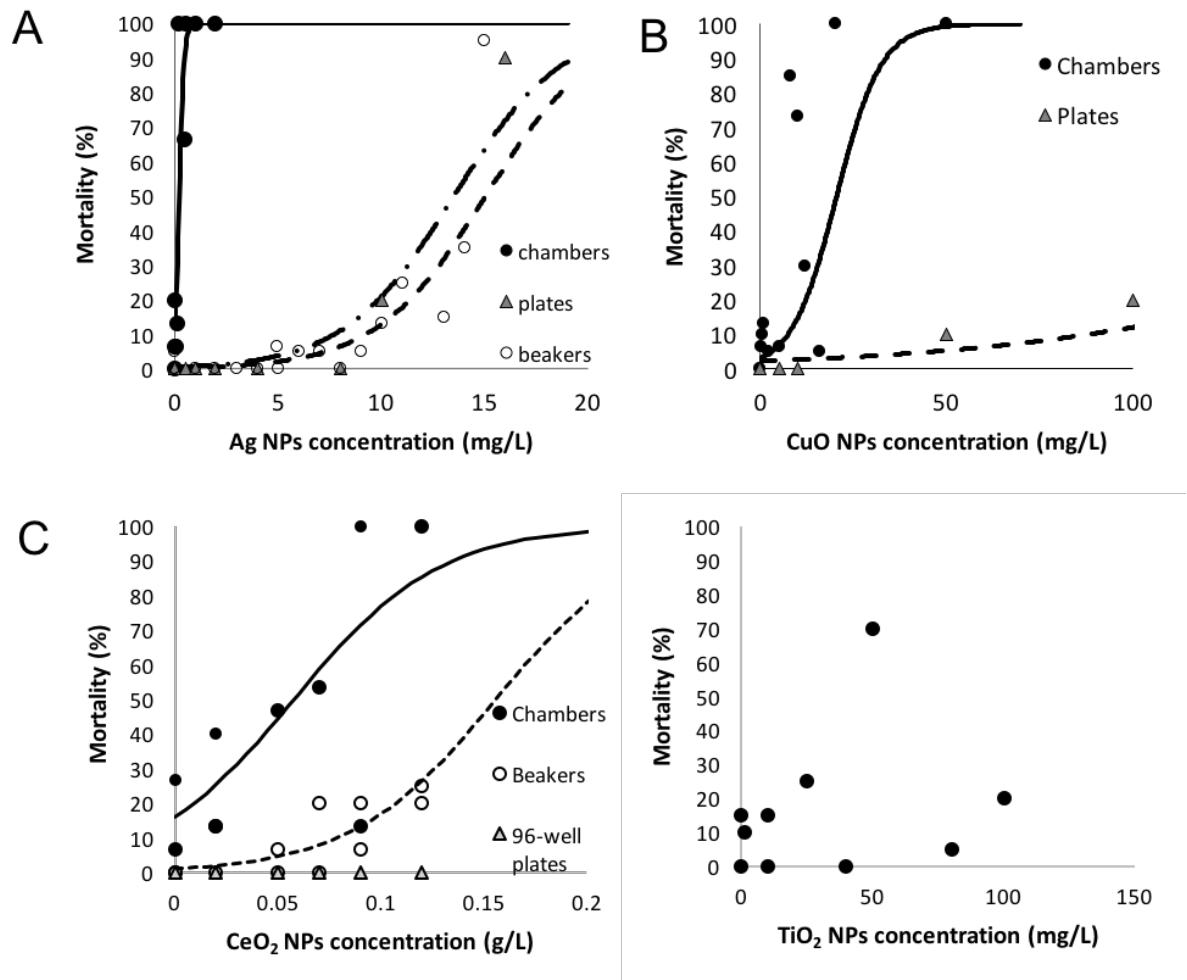


Figure 5.3: Concentration-mortality (%) curves after 96 h exposure of Ag-PVP, CuO, CeO₂ and TiO₂ NPs to zebrafish larvae at 72 hpf developmental stage. The exposures were conducted in exposure chambers (black dots, black curve), glass static beakers (empty circles, dotted curve) and 96-well polystyrene plates (grey triangles, dotted curve). The predicted mortality was obtained by the following exponential equation: $(e^{-a+\beta x}) / (1 + e^{-a+\beta x})^{-1}$. The mortality observed after exposure to TiO₂ NPs in exposure chamber was not related to NP concentration ($p > 0.05$).

Although, all NPs inside the exposure chamber were found more toxic, no clear pattern was observed between the static exposures (glass beakers compared to 96-well plates) that can be attributed to the different material, coating or shape of NPs. The Ag and CuO NPs, were more toxic in the 96-well plates compared to glass beakers, while the CeO₂ NPs were more toxic in glass beakers and no mortality was observed in 96-well plates. The CeO₂ NPs seem to follow

the surface-to-volume ratio (S:V) hypothesis that indicates how shallow or deep the exposure vessel is, how much toxicant can adsorb on the surface relative to the total volume of the exposure that, in turn, can change the quantity of toxicant that can be bioavailable. Toxicity and reactivity of NPs cannot be solely attributed to S:V ratio since toxicity is strongly affected by dissolution ratio, stabilizing agents, and other factors (Petersen et al., 2014). The miniaturization offers many advantages such as reduced number of animals used, reduced waste production, less space and the possibility of identifying effects in individuals (e.g. monitoring heart-beat, swimming behaviour), however, the high surface-to-volume ratio in small exposure vessels (i.e. 96-well plates) can result in considerably less toxicity that can depend on the toxicant tested (Figure 5.4). Silver ions are considered a highly-adsorbing substance (Baumann et al., 2014), and the lower mortality of zebrafish larvae in 96-well plates compared to glass beakers are in agreement with the S:V hypothesis (Figure 5.6C). On the contrary, the S:V hypothesis does not apply to the not-water-soluble NPs. The volume of NP solution that corresponds per larva is the highest inside the chamber (25 ml per larva) and, additionally, the NPs are in constant dispersion during the exposure chamber method, in contrast to the traditional static methodologies. The well of the 96-well plate has the lowest volume per larva (0.2 ml) and in the static beaker 2.2 ml of solution corresponds to each larva (Figure 5.4). Furthermore, the 96-well plate offers limited space for the larva to swim in the water column while the static beaker offers the opportunity of depuration as 96-hpf and older zebrafish larvae can freely swim in the water column and avoid the settled NP agglomerates at the bottom of the exposure vessel. It is important to consider also the possibility of the larvae been exposed to NPs via a dietary route as the 120-hpf zebrafish larvae have developed mouth and the yolk sac has been consumed. Taking all the above under consideration, the lack of pattern in the toxicity of the NPs of the present study using static exposure methods can be explained.

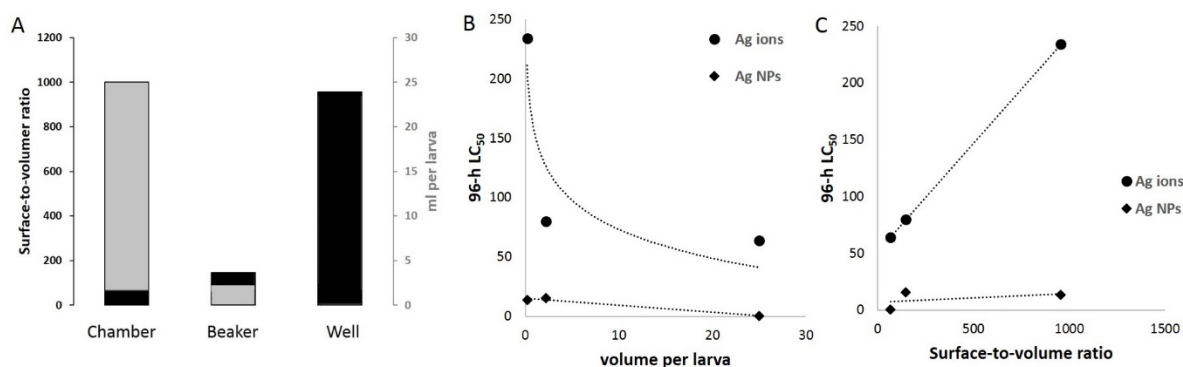


Figure 5.4: A) The surface-to-volume ratio (black bars) presented in the exposure vessels for zebrafish assays in the present study, along with the volume (ml) that each larva is exposed to in the different exposure regimes (grey bars); B) the toxicity (96-h LC₅₀) of zebrafish exposed to Ag ions and Ag NPs correlated with the volume each larva was exposed; C) the toxicity (96-h LC₅₀) of zebrafish exposed to Ag ions and Ag NPs correlated with the surface-to-volume ratio.

C. vulgaris growth was inhibited with increasing concentration of all NPs tested. In particular, the 72h-EC₅₀ was found 4.28 mg/L when *C. vulgaris* was exposed to Ag-PVP nano-prisms (Figure 5.5). Regarding the Ag PVP NPs, the PVP coating has been shown to reduce the toxicity caused by Ag NPs in microalgae (Tuominen et al., 2013), and the reduced toxicity can be explained by increased the size after the addition of the coating layer and reduced dissolution of Ag ions. No investigation of un-coated Ag NPs has been conducted by the present study, however, similar EC₅₀ have been found in other microalgae after Ag-PVP NPs exposure (3.7 mg/L in *Pseudokirchneriella subcapitata* (Moreno-Garrido et al., 2015)). CeO₂ 72h-EC₅₀ was found at 123 mg/L but no EC₅₀ was detected after exposure to TiO₂ NPs up to 200 mg/L. Van Hoecke and colleagues (Van Hoecke et al., 2009) reported a surface area dependent toxicity of CeO₂ toxicity in *P. subcapitata* with 72-h EC₅₀ values ranged between 7.6 and 28.8 mg/L. Rogers and colleagues (2010) reported with an 72-h EC₅₀ of 10 mg/L in *P. subcapitata*, and suggested indirect toxicity in the fresh water microalgae due to sorption of nutrients, such as phosphate, on the surface area of CeO₂ NPs thus less nutrients were available to the microalgae which led to inhibition of growth. In the present study, we reported less toxicity of CeO₂ NPs that can be attributed to less sorption of nutrients on the HMT coating. For TiO₂ NPs, an EC₅₀ of 120 mg/L was found after a 6-day exposure of 5-10 nm diam. anatase TiO₂ NPs in *C.*

vulgaris (Ji et al., 2011) but no growth inhibition was observed after a 5-day exposure to TiO₂ NM105 in the same microalgae species up to 300 mg/L (Cardinale et al., 2012). The *C. vulgaris* toxicity assays, demonstrated that the toxicity of the NPs tested in the present study lay in the same range as it has been previously reported by other studies using NPs of similar physicochemistry.

Exposure to Ag, CeO₂ and TiO₂ NPs at 72 h induced the intracellular production of ROS in a positive manner with increasing concentration. Specifically, at highest concentration of Ag NPs tested, the highest amount of fluorescence was recorded, at 3,000 fluorescent units (Figure 5.6). Increasing concentration of CeO₂ NPs led to increased fluorescence (5,000 fluorescence units) up to 100 mg/L and no further increase was recorded at 200 mg/L of CeO₂ NPs. The highest fluorescence with high variation was observed after TiO₂ NPs exposure reaching 11,500 fluorescence units at 50 mg/L and decreasing to 6,000 at 200 mg/L. Positive concentration-response relationship with Ag NPs has previously been reported in *C. vulgaris* (Oukarroum et al., 2012), with CeO₂ NPs in *P. subcapitata* (Rodea-Palomares et al., 2012) and TiO₂ NPs in *C. vulgaris* (Lin et al., 2012) and *Chlamydomonas reinhardtii* (Von Moos et al., 2016). The intracellular H₂O₂ production can be monitored by non-fluorescent dichlorofluorescein diacetate (H₂DCF-DA), that upon oxidation by H₂O₂ it is converted to its fluorescent form, dichlorofluorescein (DCF) (Lee et al., 1999). However, false positive results after TiO₂ NPs measurements have been reported as DCF fluorescence can be increased by solely TiO₂ NPs (Guadagnini et al., 2015). In the present study, the fluorescence of DCF/TiO₂ NPs alone need to be subtracted from the fluorescence generated when the algae were present to eliminate artefacts in the ROS production measurements.

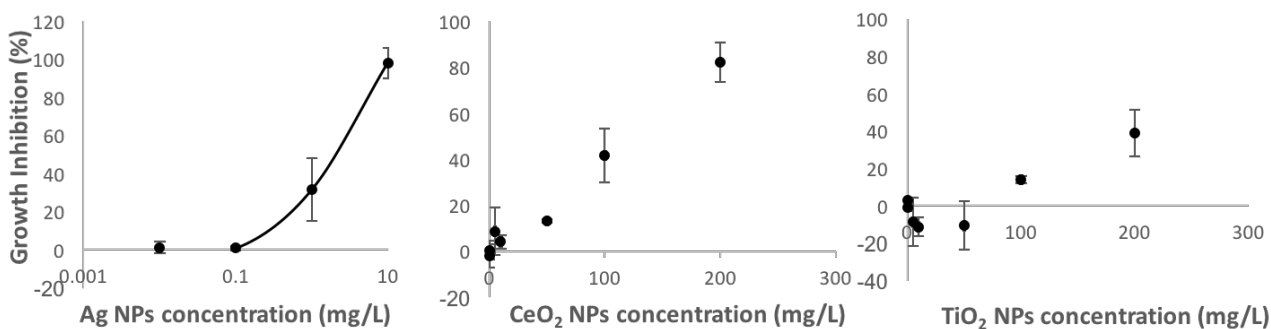


Figure 5.5: Concentration-response curves for *C. vulgaris* at the end of 72-h exposure period. Growth inhibition is presented as a percentage of cell numbers estimated by measurements of chlorophyll α fluorescence. The NPs tested were CeO₂ and TiO₂ NPs up to 200 mg/L and Ag PVP-coated NPs up to 10 mg/L.

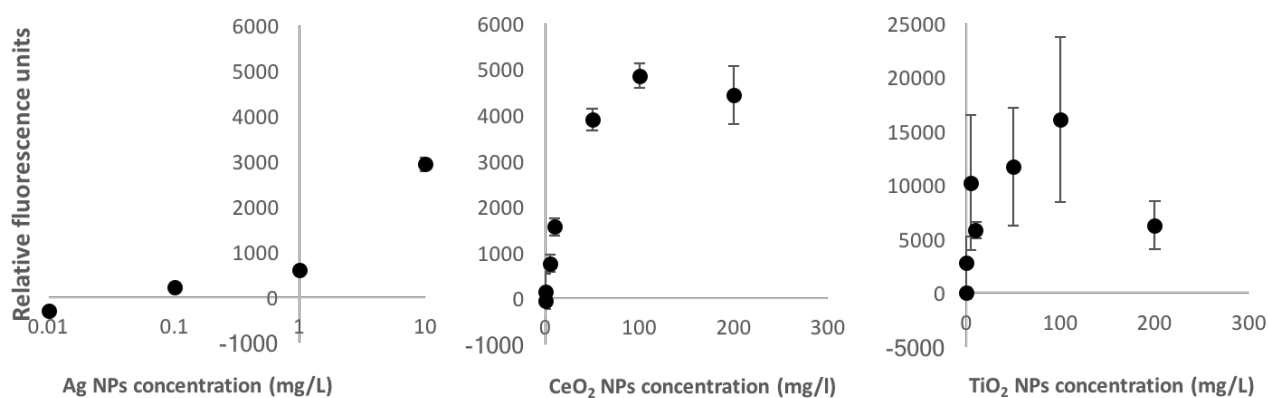


Figure 5.6: Relative fluorescence units of *C. vulgaris* after 72-h exposure to Ag, CeO₂ and TiO₂ NPs (mg/L). The fluorescence has been normalised to control conditions (no NPs added) and to the number of cells per condition.

In conclusion, toxicity of compounds can differ among methodology employed to assess the toxicity. The outcome for dissolved metal ions such as Ag ions can follow the S:V theory, decreasing the toxicity of a compound when the exposure vessel has higher a S:V. The not-water-soluble NP toxicity in the aqueous phase, however, is more challenging to assess, when constant agitation of the solutions is prohibited due to the model organism employed. In the present study, two aqueous phase toxicity tests with fundamental differences in NP exposure design were used to assess NP aqueous toxicity, the fresh water algae toxicity test and the

zebrafish larvae toxicity test. Additionally, the traditional static exposure methods (i.e. glass beakers and 96-well plates) were compared to the modified exposure chamber to assess zebrafish NP acute toxicity with limited sedimentation of the NPs in the aqueous phase. The exposure chamber allowed the zebrafish larvae to get exposed to a concentration of NPs that is closer to the nominal concentration than when larvae are exposed via glass beakers or 96-well plates. The present study indicates that the exposure chamber is able to successfully expose the zebrafish larvae to a homogeneous NP suspension therefore providing an important tool for NP risk characterisation.

Chapter 6 - Conclusions

As nanotechnology is becoming a powerful tool with numerous applications in everyday life, it is only but essential to assess the NP toxicity upon release in the aquatic environment. Evidence suggests that toxicity of NPs in the aqueous phase can be associated with NP physicochemistry and a great challenge in the assessment of NP eco-toxicology is that NP are seldom found in isolation in the aquatic environment. The adsorption of already existing aquatic contaminants onto NPs is of major interest and potentially considerable impact on the environmental remediation as well as on the toxicology level. Chapters 2 and 3 of the present thesis investigated associations between a range of NPs and two representative groups of environmental contaminants, PAHs and metal ions, respectively.

Chapter 2 identified sorption of photo-labile organic compounds (i.e. PAHs) onto semiconductor NPs which under UVA promoted photo-catalysis of the organic compounds. This project is the first to comprehensively investigate the sorption of PAHs onto semiconductor NPs under UVA using bioavailability of adsorbed compound and photo-by-products to study sorption processes at the organism level. Toxicity of adsorbed contaminants in aquatic organisms strongly related to sorption capacity and photo-catalysis efficiency as the NPs under UVA can catalyse organic compounds to potentially toxic photo-by-products. While sorption of both PAHs was suggested in the present study, the presence of NPs reduced anthracene bioavailability while low concentrations of benzo(a)pyrene in the presence of NPs increased the photo-by-product bioavailability in zebrafish. Additional research is needed to fully understand the implications of sorption under UVA radiation in environmentally relevant conditions (e.g. lower concentrations and solar irradiation), environmentally relevant interactions (e.g. presence of bacteria or organic matter) and screening of more biomarkers to identify toxicity at the organism level.

Sorption of copper was confirmed on negatively charged NPs with sorption being closely related to surface area as presented in Chapter 3. While adsorbent surface area has been previously shown to play important role in sorption, this research provided a comprehensive assessment of co-contaminant sorption onto NPs, employing nine NPs with different physicochemical properties and assessing sorption using four different methodologies including analytical chemistry, algae growth inhibition, zebrafish mortality and zebrafish gene

expression. While the chemistry of the surface of NPs during sorption was not investigated, the presence of all NPs suggested no additional effect or a protective role against copper in *C. vulgaris* and larval zebrafish, and sorption capacity increased with higher surface area (i.e. smaller diameter NPs).

An indirect effect of metallic NPs was indicated in chapter 4 investigating the aquatic toxicity of perovskite, a new generation, photovoltaic NP. The lead dissolution out of lead-halide perovskite NPs was identified responsible for perovskite NP toxicity in zebrafish and *C. vulgaris*. Many studies have described perovskite chemistry in the aqueous phase, however, this is the first study to investigate perovskite NP toxicity in the aqueous phase. The perovskite NPs dissolved lead in aqueous and dietary exposure in zebrafish inducing metal bioavailability specific biomarkers without significantly changing distribution of zebrafish gut microbiota after a 14-d dietary exposure in contrast to lead ions that were used as a positive control. This study provided an example of indirect effects of NPs in the aquatic environment as well as possible routes of exposure to perovskite NPs. A further step would be the replacement of lead as the metal cation in the perovskite solar cells with a cation of lower toxicity and production of environmentally safe solar cell materials.

A particular concern in nanotoxicology is the lack of aqueous dispersion of most NPs during many *in vivo* toxicity assays. Chapter 5 presented an exposure chamber designed to assess toxicity of NPs in the aqueous phase and enhance exposure conditions as NPs are continuously in dispersion throughout the exposure duration. It was shown that controlled conditions of NP exposure in the aqueous phase leads to consistent results and higher toxicity of NP in zebrafish larvae. Results indicated that NP toxicity depends on NP aqueous dispersion. The designed exposure chamber can provide the start for a standardised methodology that would limit variation in results among laboratories and will enable to critically compare data and conduct correct risk assessment. It would be interesting to further investigate the physicochemistry of NP during the controlled conditions provided by the present exposure chamber using other aquatic model organisms that previously were assessed in static exposure conditions, thus a better understanding of the link between toxicity and NP physicochemistry can be developed.

Finally, the results of the present thesis support the bioavailability and gene expression as sensitive and environmentally relevant tools for investigation of NPs toxicity in the aqueous phase. Bioavailability of adsorbent successfully identified sorption of co-contaminants onto NPs and metal and lead-specific biomarkers attributed lead-halide perovskite NPs toxicity to

lead ion dissolution. Specific biomarkers can provide information on knowledge gaps and in combination with careful characterization of the physicochemical properties of NPs can provide insights on the relationship between NP physicochemistry and environmentally relevant toxicity. A long-term observation of NP behaviour in the aquatic environment and investigation of NP toxicity in association with other environmental components in the aquatic environment can provide information with respect to environmental management and sustainable nanotechnology.

Appendix A

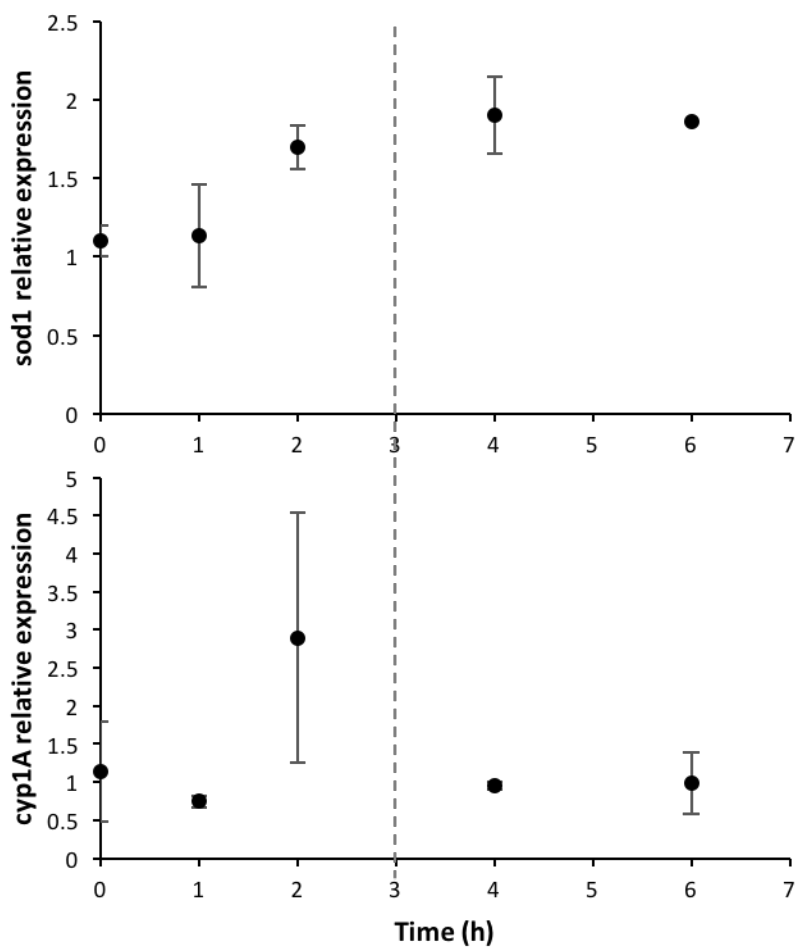


Figure A.1: Preliminary study on the *sod1* and *cyp1A* expression after 6 $\mu\text{g/L}$ of anthracene under 5 W/m^2 UVA radiation. *Sod1* expression increases with time reaching highest expression (2-fold induction) at 4 h after the end of UVA exposure. *Cyp1A* increases with maximum 3-fold induction at 2 h after the end of UVA. The sampling of the following experiments was conducted 3 h after UVA radiation so induced expression of both biomarkers could be observed.

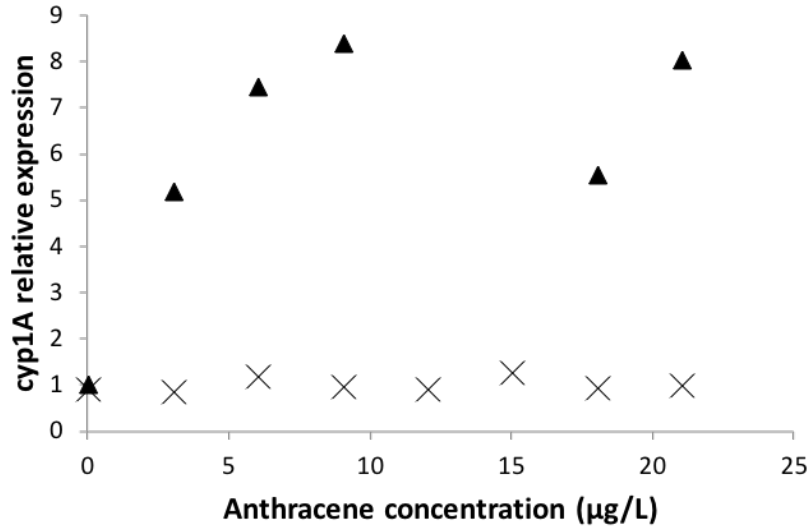


Figure A.2: *Cyp1A* gene expression of zebrafish larvae exposed to anthracene (black triangles) and anthracene and 0.2 mg/L of NM105 mixture (x). No induction of *cyp1A* was observed in the presence of 0.2 mg/L of NPs. Concentration-response curves were analysed by glm ($p < 0.001$) and treatments were compared with pair-wise contrast statements ($p < 0.001$). Data represent one replicate and a pool of 20 larvae.

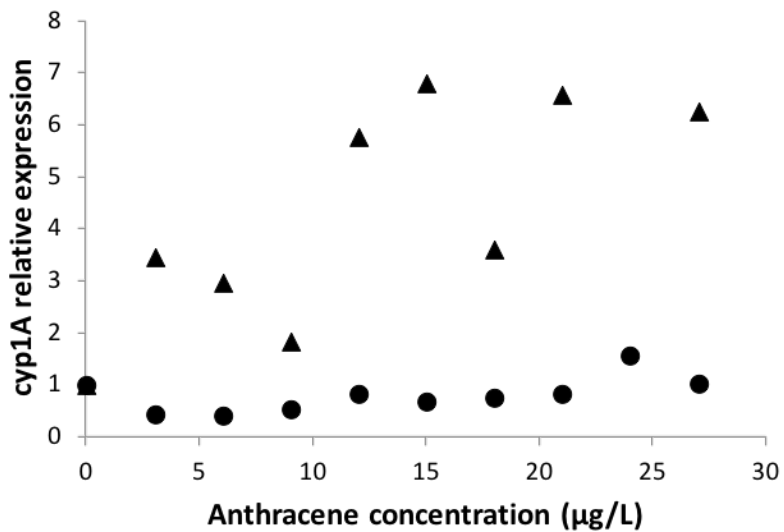


Figure A.3: *Cyp1A* gene expression of zebrafish larvae exposed to anthracene (black triangles) and anthracene and 0.2 mg/L of Si NPs mixture (black circles). No induction of *cyp1A* was observed in the presence of 0.2 mg/L of NPs. Concentration-response curves were analysed by glm ($p < 0.001$) and treatments were compared with pair-wise contrast statements ($p < 0.001$). Data represent one replicate and a pool of 20 larvae.

Appendix B

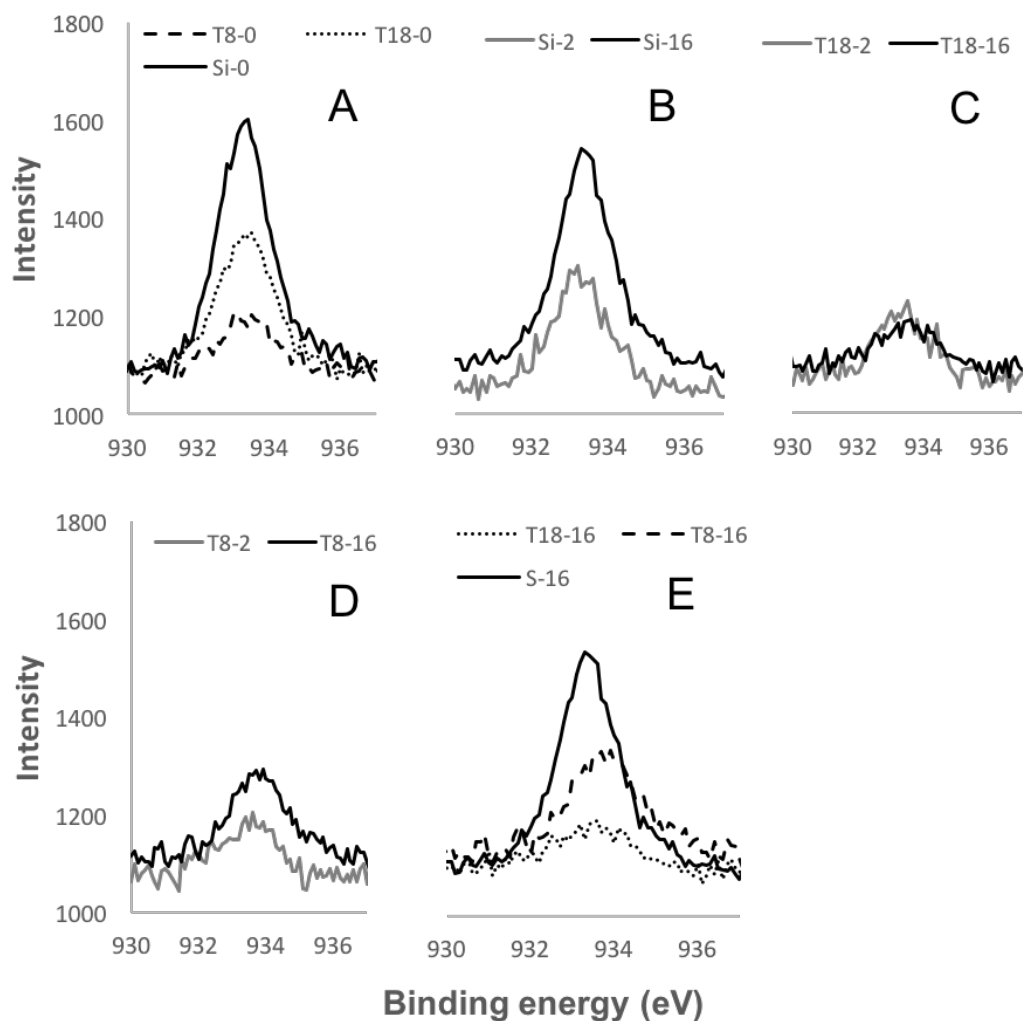


Figure B.1: The photoelectron peaks of 933 eV corresponds to Cu 2p detected by XPS. (A) comparison of Cu measurements with 0 mg/L of NPs (B) Cu and 2mg/L Si NPs (grey line), Cu and 16 mg/L Si NPs (black line), (C) Cu and 2 mg/L TiO₂ 18 nm NPs (grey line), Cu and 16 mg/L TiO₂ 18 nm NPs (black line), (D) Cu and 2 mg/L TiO₂ 4-8 nm NPs (grey line), Cu and 16 mg/L TiO₂ 4-8 nm NPs (black line), (E) comparison of Cu and 16 mg/L of NPs.

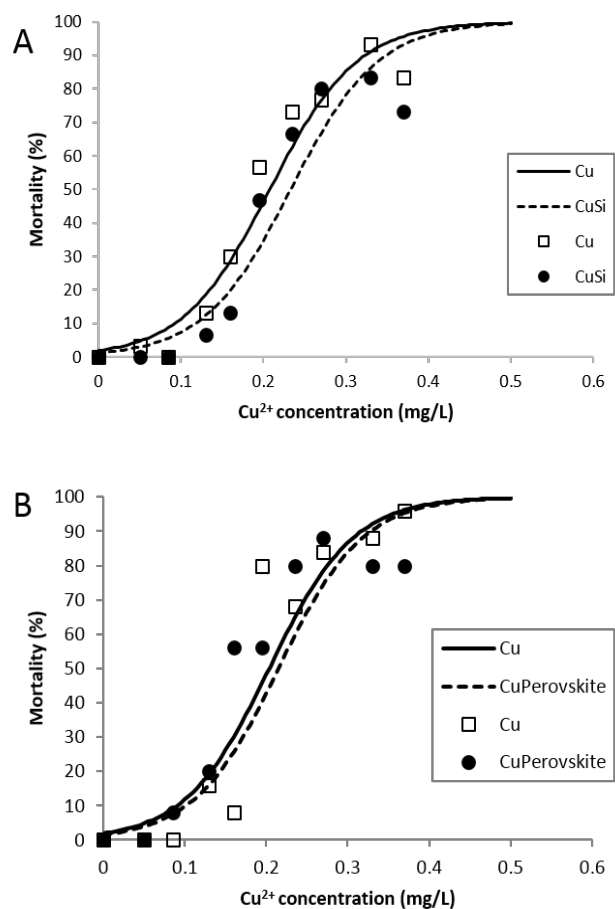


Figure B.2: zebrafish larvae mortality curves of Cu and Cu + NPs (CuSi, CuPerovskite). The solid lines and white squares represent the dose response curves when larvae exposed to Cu and the dashed line and black circles represent the response when exposed to Cu and Si (A) and Perovskite (B). There were no significant differences in the dose response curves between Cu and Cu with NPs indicating no sorption of Cu on the NPs on Cu bioavailability (likelihood ratio test, $p > 0.05$).

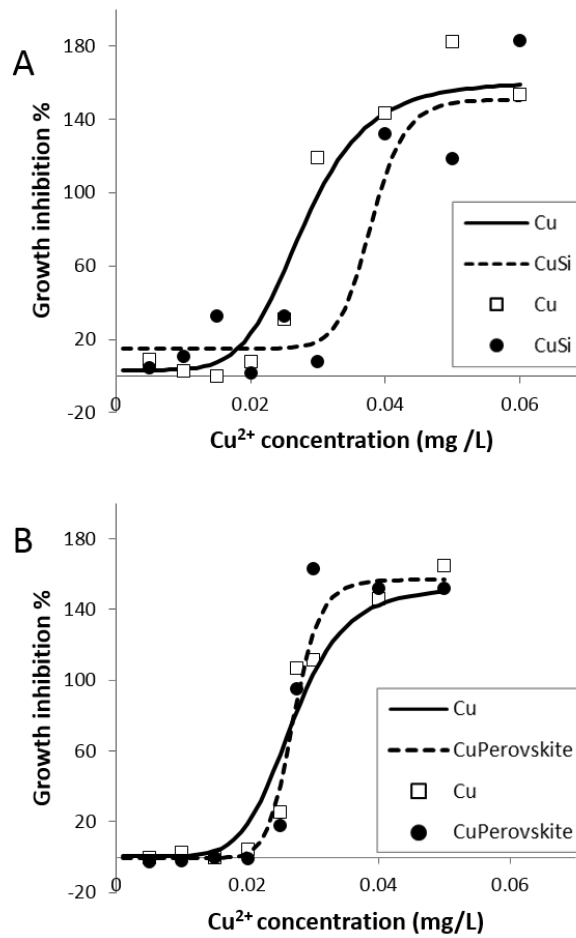


Figure B.3: Growth inhibition curves of Cu and Cu + NPs (CuSi, CuPerovskite). The solid lines and white squares represent the concentration response curves when algae were exposed to Cu and the dashed line and black circles represent the response when exposed to Cu and Si (A) and Perovskite (B). There were no significant differences in the concentration-response curves between Cu and Cu with NPs indicating no sorption of Cu on the NP on Cu bioavailability (likelihood ratio test, $p > 0.05$).

Appendix C

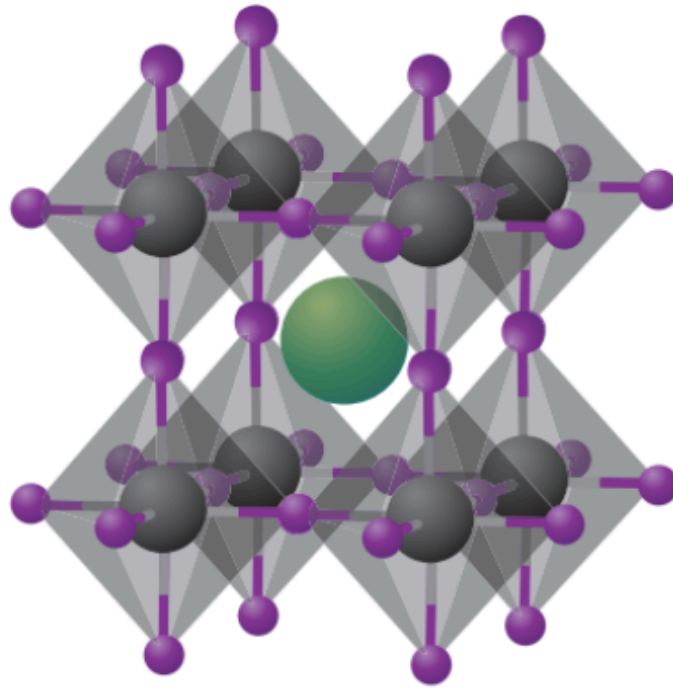


Figure C.1: The structure of a metal halide perovskite solar cell follows the generic formula ABX_3 . Organic or inorganic cations occupy position A (green), metal cations and halides occupy positions B (grey) and X (purple), respectively. Picture taken from (Grätzel, 2014)

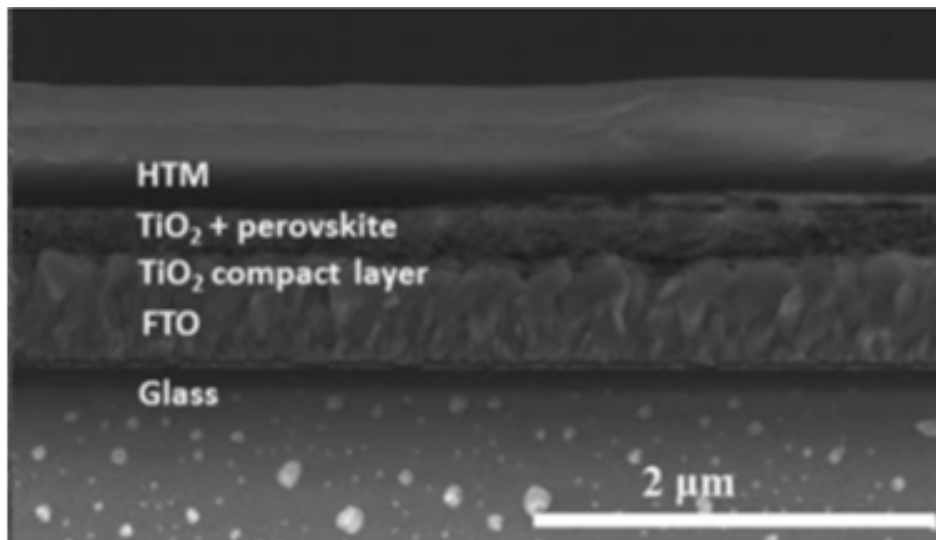


Figure C.2: A cross section of a corresponding device showing the TiO₂ and perovskite layer in entirely inert atmosphere. Picture taken from (Aruoja et al., 2009; Hoefler et al., 2017).

Table C.1: Wet weight (mg), peduncle length (mm) and sex (female or male) of dietary exposure experiment presented in Chapter 4. Fish in the following table were exposed to perovskite nanoparticles (MALI, MALB or FALB) or lead nitrate. Samples were collected at 0, 48 and 96 h after the start of dietary exposure.

Sample name	Concentration/ Treatment	Exposure time (h)	Wet weight (mg)	Peduncle length (mm)	Sex
16.0.1	0 µg/g	0	404	28	M
16.0.2	0 µg/g	0	530	27	F
16.0.3	0 µg/g	0	710	31	F
16.0.4	0 µg/g	0	660	33	M
16.0.5	0 µg/g	0	610	34	F
16.0.6	0 µg/g	0	500	29	M
16.0.7	0 µg/g	0	380	30	M
16.0.8	0 µg/g	0	520	31	M
1.48.1	ctrl	48	610	30	M
1.48.2	ctrl	48	810	33	F
2.48.1	MALI	48	620	32	F
2.48.2	MALI	48	480	25	M
3.48.1	MALB	48	570	31	M
3.48.2	MALB	48	420	26	F
4.48.1	FALB	48	830	36	F
4.48.2	FALB	48	410	29	M
5.48.1	LEAD NIT	48	420	28	M
5.48.2	LEAD NIT	48	440	28	F
6.48.1	MALB	48	1000	32	F
6.48.2	MALB	48	410	29	M
7.48.1	FALB	48	420	28	M
7.48.2	FALB	48	630	27	F
8.48.1	LEAD NIT	48	670	32	F
8.48.2	LEAD NIT	48	530	30	M
9.48.1	ctrl	48	460	29	M
9.48.2	ctrl	48	550	31	F
10.48.1	MALI	48	510	27	F
10.48.2	MALI	48	590	30	M
11.48.1	LEAD NIT	48	470	28	M
11.48.2	LEAD NIT	48	460	26	F
12.48.1	ctrl	48	610	34	F
12.48.2	ctrl	48	540	30	M
13.48.1	MALI	48	580	29	M
13.48.2	MALI	48	750	31	F
14.48.1	MALB	48	580	30	M

14.48.2	MALB	48	540	28	F
15.48.1	FALB	48	530	29	M
15.48.2	FALB	48	810	30	F
1.96.1	ctrl	96	600	30	F
1.96.2	ctrl	96	610	31	M
2.96.1	MALI	96	580	30	M
2.96.2	MALI	96	780	31	F
3.96.2	MALB	96	530	31	M
3.96.1	MALB	96	460	27	F
4.96.2	FALB	96	670	31	F
4.96.1	FALB	96	550	29	M
5.96.1	LEAD NIT	96	680	29	F
5.96.2	LEAD NIT	96	530	29	M
6.96.1	MALB	96	650	30	M
6.96.2	MALB	96	820	30	F
7.96.1	FALB	96	700	30	F
7.96.2	FALB	96	650	32	M
8.96.1	LEAD NIT	96	560	30	M
8.96.2	LEAD NIT	96	910	30	F
9.96.1	ctrl	96	510	27	F
9.96.2	ctrl	96	460	29	M
10.96.1	MALI	96	450	27	M
10.96.2	MALI	96	630	29	F
11.96.1	LEAD NIT	96	660	27	F
11.96.2	LEAD NIT	96	680	30	M
12.96.1	ctrl	96	650	31	M
12.96.2	ctrl	96	550	28	F
13.96.1	MALI	96	700	32	F
13.96.2	MALI	96	490	29	M
14.96.1	MALB	96	770	30	F
14.96.2	MALB	96	1200	32	F
15.96.1	FALB	96	730	30	F
15.96.2	FALB	96	490	29	M
AVERAGE			600.206	29.720588	

Table C.2: Wet weight (mg), peduncle length (mm), gut condition (empty, full or half full) and sex (female or male) of dietary exposure experiment presented in Chapter 4. Fish in the following table were exposed to perovskite nanoparticles (MALI, MALB or FALB) or lead nitrate. Samples were collected at 14 d after the start of dietary exposure.

Sample name	Treatment	Exposure time (d)	Wet weight (mg)	Peduncle length (mm)	Gut	Sex
1.14.1	ctrl	14	890	35	full	F
2.14.1	MALI	14	560	33	full	M
3.14.1	MALB	14	730	31	1/2 full	F
4.14.1	FALB	14	590	29	1/2 full	F
5.14.1	LEAD NIT	14	410	28	1/2 full	M
6.14.1	MALB	14	730	31	1/2 full	M
7.14.1	FALB	14	59	31	full	M
8.14.1	LEAD NIT	14	880	32	1/2 full	F
9.14.1	ctrl	14	710	31	full	F
10.14.1	MALI	14	590	29	full	F
11.14.1	LEAD NIT	14	500	26	full	M
12.14.1	ctrl	14	970	32	full	F
13.14.1	MALI	14	500	26	1/2 full	M
14.14.1	MALB	14	720	29	1/2 full	F
15.14.1	FALB	14	700	30	full	F
1.14.2	ctrl	14	1270	35	1/2 full	M
2.14.2	MALI	14	630	29	1/2 full	M
3.14.2	MALB	14	670	29	full	M
4.14.2	FALB	14	790	31	full	F
5.14.2	LEAD NIT	14	780	35	empty	F
6.14.2	MALB	14	920	32	full	M
7.14.2	FALB	14	620	29	full	M
8.14.2	LEAD NIT	14	670	30	1/2 full	M
9.14.2	ctrl	14	720	31	full	M
10.14.2	MALI	14	680	29	full	M
11.14.2	LEAD NIT	14	770	30	full	F
12.14.2	ctrl	14	1230	34	full	F

13.14.2	MALI	14	900	31	full	F
14.14.2	MALB	14	490	25	full	F
15.14.2	FALB	14	710	30	full	M
1.14.3	ctrl	14	480	30	full	M
2.14.3	MALI	14	450	28	full	M
3.14.3	MALB	14	600	32	1/2 full	M
4.14.3	FALB	14	490	26	1/2 full	M
5.14.3	LEAD NIT	14	970	29	full	F
6.14.3	MALB	14	110	33	full	F
7.14.3	FALB	14	610	30	full	M
8.14.3	LEAD NIT	14	710	30	full	F
9.14.3	ctrl	14	810	35	full	M
10.14.3	MALI	14	450	29	1/2 full	M
11.14.3	LEAD NIT	14	620	28	1/2 full	M
12.14.3	ctrl	14	590	29	full	M
13.14.3	MALI	14	610	29	full	F
14.14.3	MALB	14	750	31	1/2 full	M
15.14.3	FALB	14	560	28	1/2 full	M
1.14.4	ctrl	14	1020	33	1/2 full	F
2.14.4	MALI	14	680	29	1/2 full	M
3.14.4	MALB	14	690	26	1/2 full	M
4.14.4	FALB	14	500	27	1/2 full	M
5.14.4	LEAD NIT	14	640	30	full	M
6.14.4	MALB	14	680	31	full	M
7.14.4	FALB	14	600	32	full	M
8.14.4	LEAD NIT	14	750	34	1/2 full	M
9.14.4	ctrl	14	530	29	full	M
10.14.4	MALI	14	630	31	full	F
11.14.4	LEAD NIT	14	460	25	empty	M
12.14.4	ctrl	14	500	28	empty	M
13.14.4	MALI	14	650	31	empty	M
14.14.4	MALB	14	500	27	1/2 full	M
15.14.4	FALB	14	770	31	1/2 full	M

4.14.5	FALB	14	640	32	full	M
6.14.5	MALB	14	410	25	1/2 full	M
12.14.5	ctrl	14	700	29	1/2 full	M
13.14.5	MALI	14	680	31	full	F

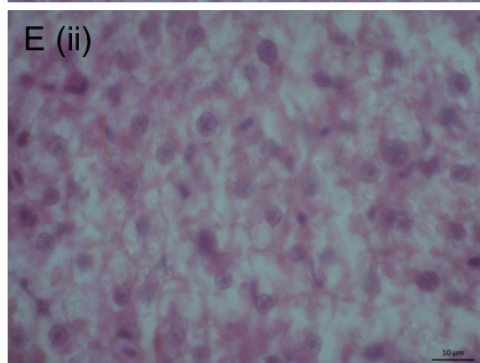
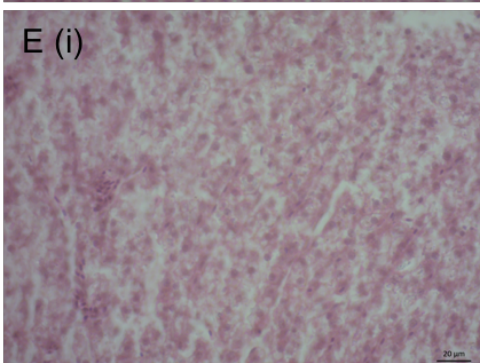
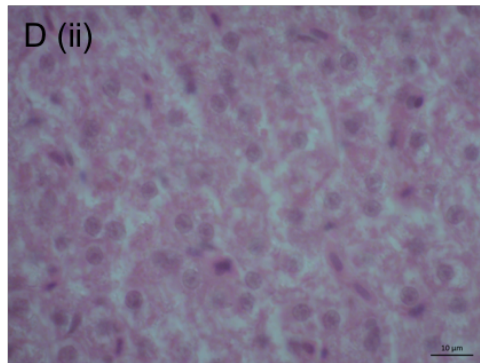
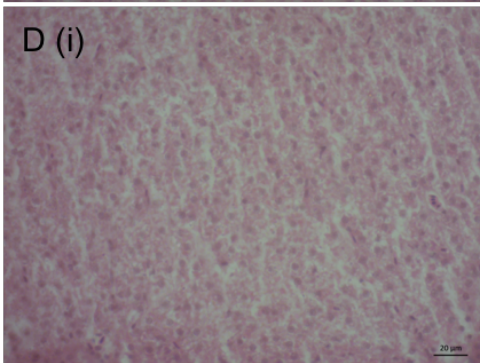
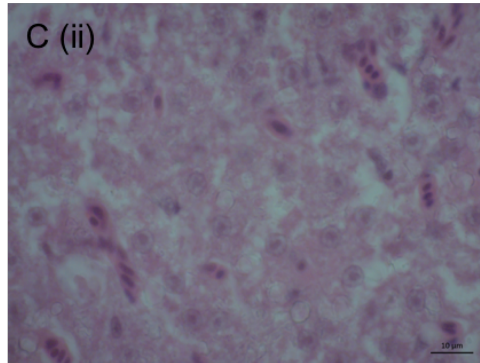
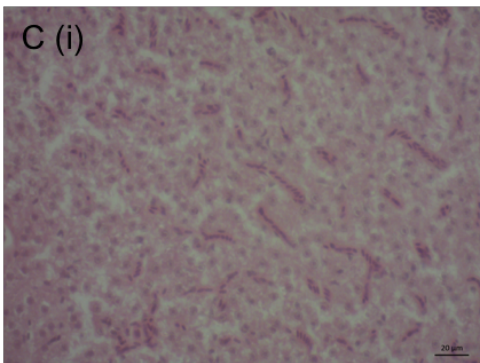
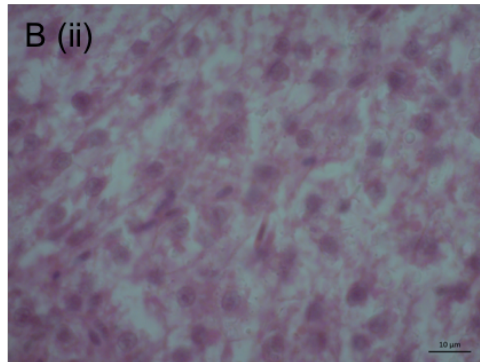
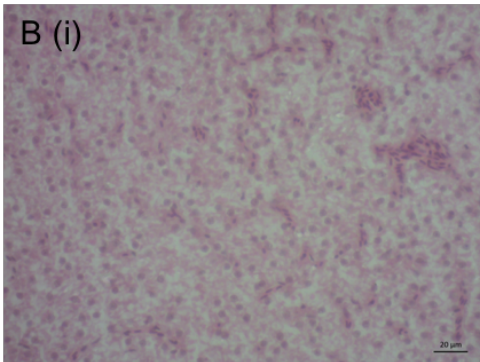
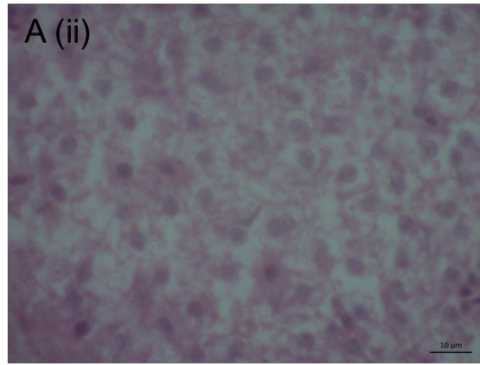
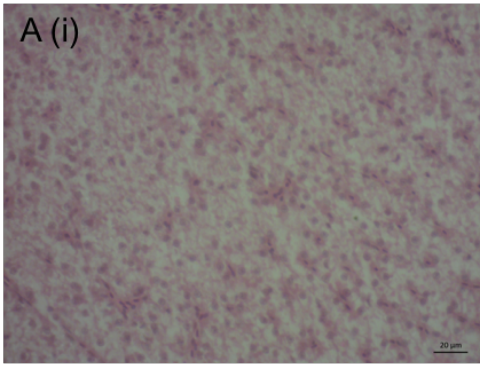


Figure C.3: Liver tissue sections (8 mm) after H&E staining, viewed in x40 (i) and x100 (ii) from fish fed with control food (A), Pb-spiked food (B), MALI NP (C), MALB NP (D) and FALB NP-spiked food(E).

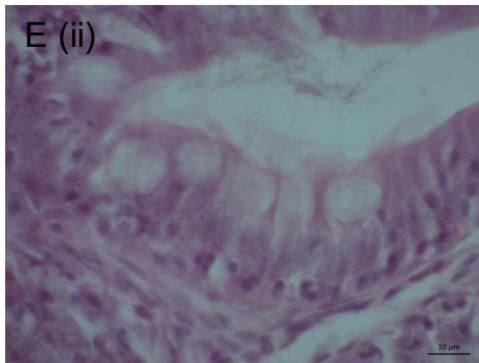
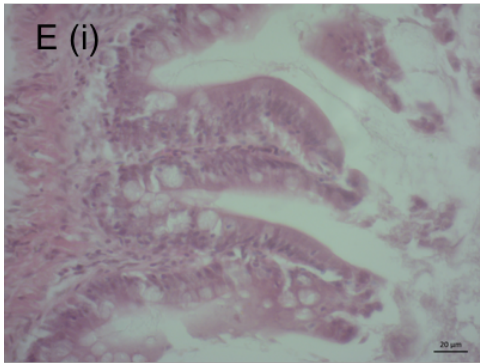
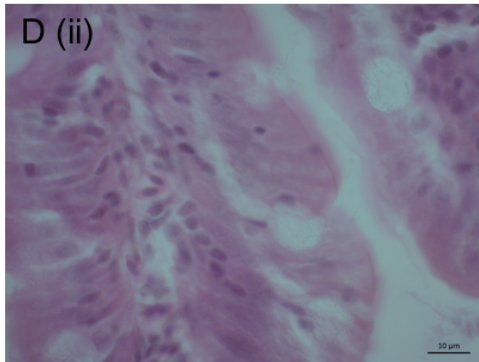
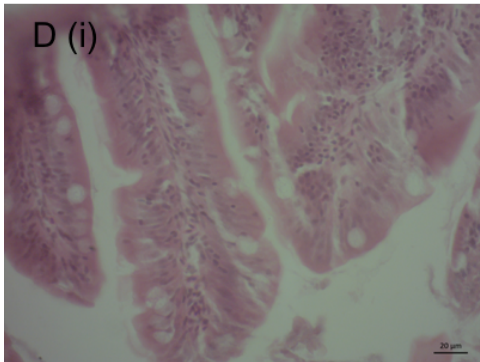
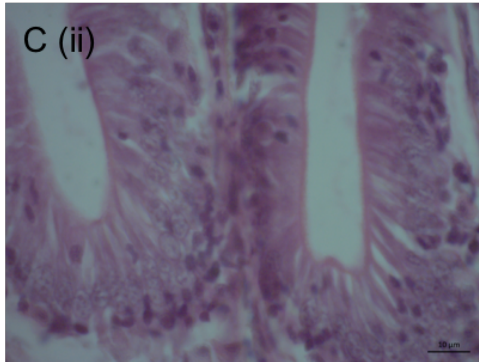
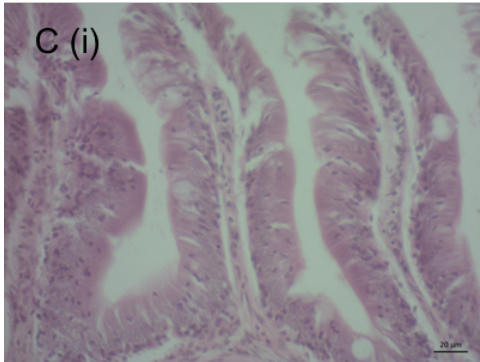
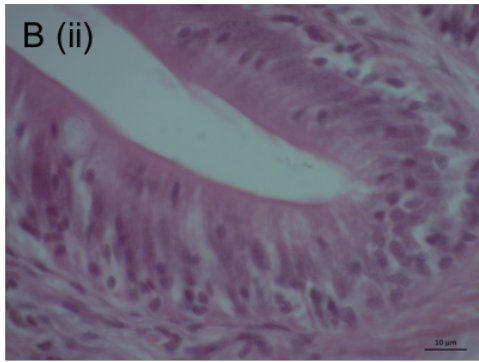
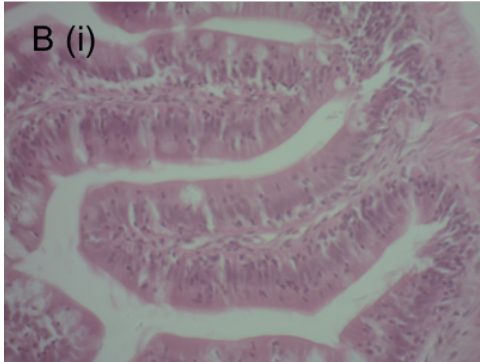
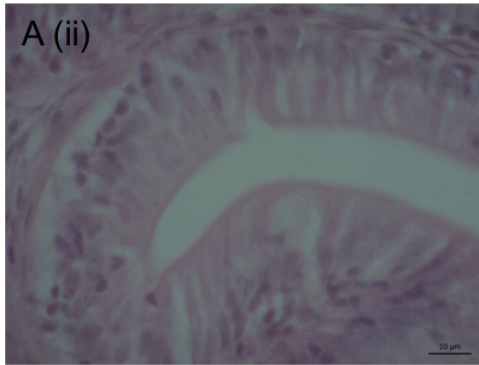
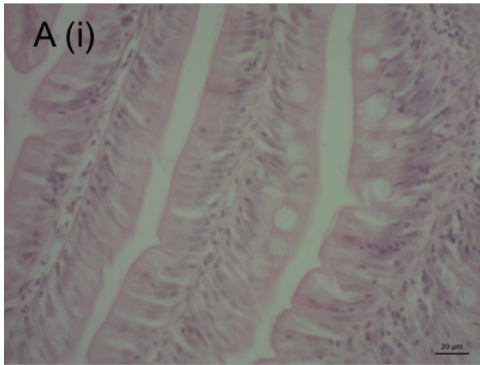


Figure C.4: Gut lumen tissue sections (8 mm) after H&E staining, viewed in x40 (i) and x100 (ii) from fish fed with control food (A), Pb-spiked food (B), MALI NP (C), MALB NP (D) and FALB NP-spiked food(E).

Appendix D

Table D.1: The list of nanoparticles used in the present PhD study, but not necessarily all reported in this thesis, included NPs used for the Round Robin exercise (gold nano-spheres and nano-rods), and NPs that belong to the FNN energy value chain (silicon, boron doped silicon and perovskites NPs) and which have demonstrated great potential for application on photovoltaic panels because of their low cost and their high theoretical energy efficiency, as well as titanium dioxide, PVP coated silver, and cerium dioxide NPs.

Sample Label	Material	Dispersion(solvent)	Test conducted
FNN_RR_GNP1	Au	H ₂ O	Round Robin
FNN_RR_GNP2	Au	H ₂ O	Round Robin
FNN_RR_GNR1	Au	H ₂ O	Round Robin
FNN_IUTA_SiO ₂ @Si_01	Si	H ₂ O	Acute toxicity
FNN_IUTA_Si@B_2.5%_01	B doped Si	H ₂ O	Acute toxicity, Copper sorption study
FNN_IUTA_Si@B_2%_01	B doped Si	H ₂ O	Acute toxicity, Copper sorption study
FNN_IUTA_Si@B_1.5%_01	B doped Si	H ₂ O	Acute toxicity, Copper sorption study
FNN_IUTA_Si@B_1%_01	B doped Si	H ₂ O	Acute toxicity, Copper sorption study
FNN_IUTA_Si_01	Si	H ₂ O	Acute toxicity, Copper sorption study, PAHs sorption study
FNN_EPFL_Perovskite_01	CH ₃ NH ₃ PbI ₃	H ₂ O	Acute toxicity, Copper sorption study, Perovskite eco-toxicity study
FNN_PUM_Ag_#1	Ag coated with PVP	H ₂ O	Acute toxicity, exposure chamber
FNN_EPFL_TiO ₂ _01	TiO ₂	H ₂ O	Acute toxicity
FNN_ICN_CeO ₂ _#002	CeO ₂	HTM 10 mM in H ₂ O (Hexamethylenetetramine)	Acute toxicity, exposure chamber
FNN_ICN_TiO ₂ _#010	TiO ₂	TMAOH (Tetramethylammonium hydroxide) 10 mM in H ₂ O	Acute toxicity, exposure chamber
FNN_EPFLA_MAFA(67pc)L I #05	CH ₃ NH ₃ (0.33)CH ₃ NH ₃ (0.67)PbI ₃	H ₂ O	Acute toxicity, Perovskite eco-toxicity study
FNN_EPFLA_FALB	CH ₃ NH ₃ PbBr ₃	H ₂ O	Acute toxicity, Perovskite eco-toxicity study
FNN_EPFLA_MALB	CH ₃ NHNH ₃ PbBr ₃	H ₂ O	Acute toxicity, Perovskite eco-toxicity study
FNN_EPFLA_FALI	CH ₃ NHNH ₃ PbI ₃	H ₂ O	Acute toxicity, Perovskite eco-toxicity study

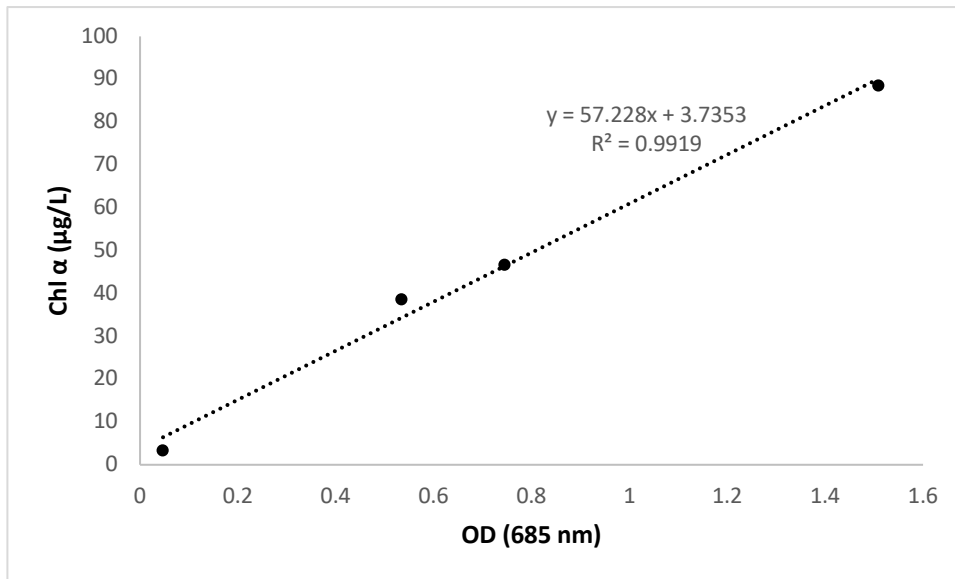


Figure D.1: Correlation of chlorophyll α levels after acetone extraction with optical density (OD) of *Chlorella vulgaris* cultures.

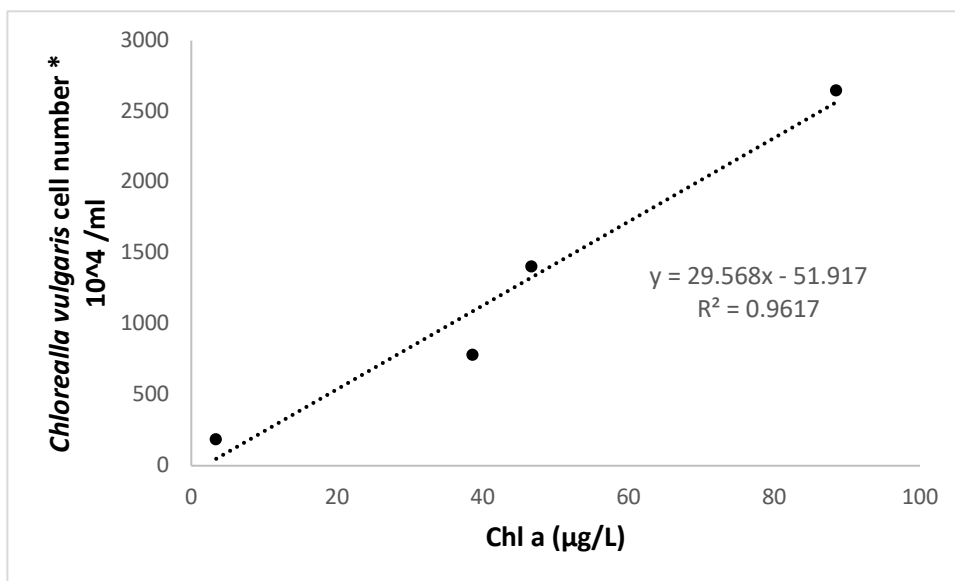


Figure D.2: Correlation of chlorophyll α levels after acetone extraction with *Chlorella vulgaris* cell numbers/ml (multiplied by 10^4).

References

- Alsop, D., Wood, C.M., 2011. Metal uptake and acute toxicity in zebrafish: common mechanisms across multiple metals. *Aquatic Toxicology* 105, 385-393.
- Alves, L.C., Wood, C.M., 2006. The chronic effects of dietary lead in freshwater juvenile rainbow trout (*Oncorhynchus mykiss*) fed elevated calcium diets. *Aquatic Toxicology* 78, 217-232.
- OECD (Organization of Cultural and Economic Development), 1981. Alga, growth inhibition test (201) OECD Guideline for Testing of Chemicals . , Paris, France.
- OECD (Organization of Cultural and Economic Development), 2013. OECD Guideline for Testing of Chemicals: Fish, Early-life Stage Toxicity Test (210), Paris, France.
- Aristidou, N., Sanchez-Molina, I., Chotchuangchutchaval, T., Brown, M., Martinez, L., Rath, T., Haque, S.A., 2015. The role of oxygen in the degradation of methylammonium lead trihalide perovskite photoactive layers. *Angewandte Chemie International Edition* 54, 8208-8212.
- Aruoja, V., Dubourguier, H.-C., Kasemets, K., Kahru, A., 2009. Toxicity of nanoparticles of CuO, ZnO and TiO₂ to microalgae *Pseudokirchneriella subcapitata*. *Science of the Total Environment* 407, 1461-1468.
- Asharani, P.V., Yi, L.W., Gong, Z.Y., Valiyaveetil, S., 2011. Comparison of the toxicity of silver, gold and platinum nanoparticles in developing zebrafish embryos. *Nanotoxicology* 5, 43-54.
- Augugliaro, V., Bellardita, M., Loddo, V., Palmisano, G., Palmisano, L., Yurdakal, S., 2012. Overview on oxidation mechanisms of organic compounds by TiO₂ in heterogeneous photocatalysis. *Journal of Photochemistry and Photobiology C: Photochemistry Reviews* 13, 224-245.
- Babayigit, A., Thanh, D.D., Ethirajan, A., Manca, J., Muller, M., Boyen, H.G., Conings, B., 2016. Assessing the toxicity of Pb- and Sn-based perovskite solar cells in model organism *Danio rerio*. *Scientific Reports* 6, 11.

- Bar-Ilan, O., Albrecht, R.M., Fako, V.E., Furgeson, D.Y., 2009. Toxicity assessments of multisized gold and silver nanoparticles in zebrafish embryos. *Small* 5, 1897-1910.
- Barron, M.G., Heintz, R., Rice, S.D., 2004. Relative potency of PAHs and heterocycles as aryl hydrocarbon receptor agonists in fish. *Marine Environmental Research* 58, 95-100.
- Baumann, J., Sakka, Y., Bertrand, C., Köser, J., Filser, J., 2014. Adaptation of the *Daphnia sp.* acute toxicity test: miniaturization and prolongation for the testing of nanomaterials. *Environmental Science and Pollution Research* 21, 2201-2213.
- Baun, A., Hartmann, N.B., Grieger, K., Kusk, K.O., 2008a. Ecotoxicity of engineered nanoparticles to aquatic invertebrates: a brief review and recommendations for future toxicity testing. *Ecotoxicology* 17, 387-395.
- Baun, A., Sorensen, S.N., Rasmussen, R.F., Hartmann, N.B., Koch, C.B., 2008b. Toxicity and bioaccumulation of xenobiotic organic compounds in the presence of aqueous suspensions of aggregates of nano-C₆₀. *Aquatic Toxicology* 86, 379-387.
- Benmessaoud, I.R., Mahul-Mellier, A.-L., Horváth, E., Maco, B., Spina, M., Lashuel, H.A., Forró, L., 2016. Health hazards of methylammonium lead iodide based perovskites: cytotoxicity studies. *Toxicology Research* 5, 407-419.
- Bian, S.-W., Mudunkotuwa, I.A., Rupasinghe, T., Grassian, V.H., 2011. Aggregation and dissolution of 4 nm ZnO nanoparticles in aqueous environments: influence of pH, ionic strength, size, and adsorption of humic acid. *Langmuir* 27, 6059-6068.
- Boran, H., Boyle, D., Altinok, I., Patsiou, D., Henry, T.B., 2016. Aqueous Hg²⁺ associates with TiO₂ nanoparticles according to particle size, changes particle agglomeration, and becomes less bioavailable to zebrafish. *Aquatic Toxicology* 174, 242-246.
- Bosveld, A.T., de Bie, P.A., Van den Brink, N.W., Jongepier, H., Klomp, A.V., 2002. In vitro EROD induction equivalency factors for the 10 PAHs generally monitored in risk assessment studies in The Netherlands. *Chemosphere* 49, 75-83.
- Boyle, D., Al-Bairuty, G.A., Henry, T.B., Handy, R.D., 2013. Critical comparison of intravenous injection of TiO₂ nanoparticles with waterborne and dietary exposures concludes minimal environmentally-relevant toxicity in juvenile rainbow trout *Oncorhynchus mykiss*. *Environmental Pollution* 182, 70-79.

- Boyle, D., Boran, H., Atfield, A.J., Henry, T.B., 2015. Use of an exposure chamber to maintain aqueous phase nanoparticles dispersions for improved toxicity testing in fish. *Environmental Toxicology and Chemistry* 34, 583-588.
- Brame, J.A., Hong, S.W., Lee, J., Lee, S.-H., Alvarez, P.J., 2013. Photocatalytic pre-treatment with food-grade TiO₂ increases the bioavailability and bioremediation potential of weathered oil from the Deepwater Horizon oil spill in the Gulf of Mexico. *Chemosphere* 90, 2315-2319.
- Brubaker, W.W., Hites, R.A., 1998. OH reaction kinetics of polycyclic aromatic hydrocarbons and polychlorinated dibenzo-p-dioxins and dibenzofurans. *The Journal of Physical Chemistry A* 102, 915-921.
- Buseck, P.R., Tshipursky, S.J., Hettich, R., 1992. Fullerenes from the geological environment. *Science* 257, 215-217.
- Cardinale, B.J., Bier, R., Kwan, C., 2012. Effects of TiO₂ nanoparticles on the growth and metabolism of three species of freshwater algae. *Journal of Nanoparticle Research* 14, 913.
- Chen, C., Lei, P., Ji, H., Ma, W., Zhao, J., Hidaka, H., Serpone, N., 2004. Photocatalysis by titanium dioxide and polyoxometalate/TiO₂ cocatalysts. Intermediates and mechanistic study. *Environmental Science & Technology* 38, 329-337.
- Christmann, M., Boisseau, C., Kitzinger, R., Berac, C., Allmann, S., Sommer, T., Aasland, D., Kaina, B., Tomicic, M.T., 2016. Adaptive upregulation of DNA repair genes following benzo (a) pyrene diol epoxide protects against cell death at the expense of mutations. *Nucleic Acid Research* 44, 10727-10743.
- Crespo, S., Nonnotte, G., Colin, D., Leray, C., Nonnotte, L., Aubree, A., 1986. Morphological and functional alterations induced in trout intestine by dietary cadmium and lead. *Journal of Fish Biology* 28, 69-80.
- Dabrowski, A., 2001. Adsorption - from theory to practice. *Advances in Colloid and Interface Science* 93, 135-224.
- Dai, L., 2006. Carbon nanotechnology: recent developments in chemistry, physics, materials science and device applications. Elsevier.

- Dalai, S., Pakrashi, S., Bhuvaneshwari, M., Iswarya, V., Chandrasekaran, N., Mukherjee, A., 2014. Toxic effect of Cr (VI) in presence of n-TiO₂ and n-Al₂O₃ particles towards freshwater microalgae. *Aquatic Toxicology* 146, 28-37.
- Della Torre, C., Parolini, M., Del Giacco, L., Ghilardi, A., Ascagni, M., Santo, N., Maggioni, D., Magni, S., Madaschi, L., Prosperi, L., 2017. Adsorption of B (α) P on carbon nanopowder affects accumulation and toxicity in zebrafish (*Danio rerio*) embryos. *Environmental Science: Nano* 4, 1132-1146.
- Diamond, S.A., Mount, D.R., Mattson, V.R., Heinis, L.J., 2006. Photoactivated polycyclic aromatic hydrocarbon toxicity in medaka (*Oryzias latipes*) embryos: Relevance to environmental risk in contaminated sites. *Environmental Toxicology and Chemistry* 25, 3015-3023.
- Dos Santos, C.R., Cavalcante, A.L.M., Hauser-Davis, R.A., Lopes, R.M., Da Costa, R.D.C.O., 2016. Effects of sub-lethal and chronic lead concentrations on blood and liver ALA-D activity and hematological parameters in Nile tilapia. *Ecotoxicology and Environmental Safety* 129, 250-256.
- Fan, W.H., Cui, M.M., Shi, Z.W., Tan, C., Yang, X.P., 2012. Enhanced Oxidative Stress and Physiological Damage in *Daphnia magna* by Copper in the Presence of Nano-TiO₂. *Journal of Nanomaterials*, 7.
- Fan, W.H., Peng, R.S., Li, X.M., Ren, J.Q., Liu, T., Wang, X.R., 2016. Effect of titanium dioxide nanoparticles on copper toxicity to *Daphnia magna* in water: Role of organic matter. *Water Research* 105, 129-137.
- Fang, Q., Shi, X., Zhang, L., Wang, Q., Wang, X., Guo, Y., Zhou, B., 2015. Effect of titanium dioxide nanoparticles on the bioavailability, metabolism, and toxicity of pentachlorophenol in zebrafish larvae. *Journal of Hazardous Materials* 283, 897-904.
- Farkas, J., Bergum, S., Nilsen, E.W., Olsen, A.J., Salaberria, I., Ciesielski, T.M., Baczek, T., Konieczna, L., Salvenmoser, W., Jenssen, B.M., 2015. The impact of TiO₂ nanoparticles on uptake and toxicity of benzo(a)pyrene in the blue mussel (*Mytilus edulis*). *Science of the Total Environment* 511, 469-476.
- Fu, P.P., Xia, Q., Sun, X., Yu, H., 2012. Phototoxicity and Environmental Transformation of Polycyclic Aromatic Hydrocarbons (PAHs)-Light-Induced Reactive Oxygen Species,

- Lipid Peroxidation, and DNA Damage. *Journal of Environmental Science and Health Part C-Environmental Carcinogenesis & Ecotoxicology Reviews* 30, 1-41.
- Gilbert, B., Ono, R.K., Ching, K.A., Kim, C.S., 2009. The effects of nanoparticle aggregation processes on aggregate structure and metal uptake. *Journal of Colloid and Interface Science* 339, 285-295.
- Glomstad, B., Altin, D., Sørensen, L., Liu, J., Jenssen, B.M., Booth, A.M., 2016. Carbon nanotube properties influence adsorption of phenanthrene and subsequent bioavailability and toxicity to *Pseudokirchneriella subcapitata*. *Environmental Science & Technology* 50, 2660-2668.
- Gohardani, O., Elola, M.C., Elizetxea, C., 2014. Potential and prospective implementation of carbon nanotubes on next generation aircraft and space vehicles: a review of current and expected applications in aerospace sciences. *Progress in Aerospace Sciences* 70, 42-68.
- Gottschalk, F., Sun, T.Y., Nowack, B., 2013. Environmental concentrations of engineered nanomaterials: Review of modeling and analytical studies. *Environmental Pollution* 181, 287-300.
- Griffitt, R.J., Hyndman, K., Denslow, N.D., Barber, D.S., 2009. Comparison of molecular and histological changes in zebrafish gills exposed to metallic nanoparticles. *Toxicological Sciences* 107, 404-415.
- Griffitt, R.J., Luo, J., Gao, J., Bonzongo, J.C., Barber, D.S., 2008. Effects of particle composition and species on toxicity of metallic nanomaterials in aquatic organisms. *Environmental Toxicology and Chemistry* 27, 1972-1978.
- Grätzel, M., 2014. The light and shade of perovskite solar cells. *Nat. Mater* 13, 838-842.
- Guadagnini, R., Halamoda Kenzaoui, B., Walker, L., Pojana, G., Magdolenova, Z., Bilanicova, D., Saunders, M., Juillerat-Jeanneret, L., Marcomini, A., Huk, A., 2015. Toxicity screenings of nanomaterials: challenges due to interference with assay processes and components of classic *in vitro* tests. *Nanotoxicology* 9, 13-24.
- Haider, A., Kang, I.-K., 2015. Preparation of silver nanoparticles and their industrial and biomedical applications: a comprehensive review. *Advances in Materials Science and Engineering* 2015.

- Hamilton, I.M., Dill, L.M., 2002. Monopolization of food by zebrafish (*Danio rerio*) increases in risky habitats. *Canadian Journal of Zoology* 80, 2164-2169.
- Han, Y., Meyer, S., Dkhissi, Y., Weber, K., Pringle, J.M., Bach, U., Spiccia, L., Cheng, Y.-B., 2015. Degradation observations of encapsulated planar CH₃NH₃PbI₃ perovskite solar cells at high temperatures and humidity. *Journal of Materials Chemistry A* 3, 8139-8147.
- Harper, S., Usenko, C., Hutchison, J.E., Maddux, B.L.S., Tanguay, R.L., 2008. *In vivo* biodistribution and toxicity depends on nanomaterial composition, size, surface functionalisation and route of exposure. *Journal of Experimental Nanoscience* 3, 195-206.
- Hartmann, N.B., Von der Kammer, F., Hofmann, T., Baalousha, M., Ottofuelling, S., Baun, A., 2010. Algal testing of titanium dioxide nanoparticles-Testing considerations, inhibitory effects and modification of cadmium bioavailability. *Toxicology* 269, 190-197.
- Henry, T.B., Wileman, S.J., Boran, H., Sutton, P., 2013. Association of Hg²⁺ with Aqueous (C₆₀)_n Aggregates Facilitates Increased Bioavailability of Hg²⁺ in Zebrafish (*Danio rerio*). *Environmental Science & Technology* 47, 9997-10004.
- Hoefler, S.F., Trimmel, G., Rath, T., 2017. Progress on lead-free metal halide perovskites for photovoltaic applications: a review. *Monatshefte für Chemie-Chemical Monthly*, 1-32.
- Holden, P.A., Gardea-Torresdey, J.L., Klaessig, F., Turco, R.F., Mortimer, M., Hund-Rinke, K., Cohen Hubal, E.A., Avery, D., Barceló, D., Behra, R., Cohen, Y., Deydier-Stephan, L., Ferguson, P.L., Fernandes, T.F., Herr Harthorn, B., Henderson, W.M., Hoke, R.A., Hristozov, D., Johnston, J.M., Kane, A.B., Kapustka, L., Keller, A.A., Lenihan, H.S., Lovell, W., Murphy, C.J., Nisbet, R.M., Petersen, E.J., Salinas, E.R., Scheringer, M., Sharma, M., Speed, D.E., Sultan, Y., Westerhoff, P., White, J.C., Wiesner, M.R., Wong, E.M., Xing, B., Steele Horan, M., Godwin, H.A., Nel, A.E., 2016. Considerations of environmentally relevant test conditions for improved evaluation of ecological hazards of engineered nanomaterials. *Environmental Science and Technology* 50, 6124-6145.
- Honary, S., Zahir, F., 2013. Effect of zeta potential on the properties of nano-drug delivery systems - a review (Part 2). *Tropical Journal of Pharmaceutical Research* 12, 265-273.

- Hurum, D.C., Agrios, A.G., Gray, K.A., Rajh, T., Thurnauer, M.C., 2003. Explaining the enhanced photocatalytic activity of Degussa P25 mixed-phase TiO₂ using EPR. *Journal of Physical Chemistry B* 107, 4545-4549.
- ISO (International Standards Organization), 2008. Nano-technologies terminology and definitions for nano-objects. Nanoparticle, Nanofibre and Nanoplate, Geneva, Switzerland.
- Jacobsen, N., Pojano, G., Wallin, H., Jensen, K., 2010. Nanomaterial dispersion protocol for toxicological studies in ENPRA. Internal ENPRA Project Report. The National Research Centre for the Working Environment, 6.
- Jang, M.-H., Kim, W.-K., Lee, S.-K., Henry, T.B., Park, J.-W., 2014. Uptake, tissue distribution, and depuration of total silver in common carp (*Cyprinus carpio*) after aqueous exposure to silver nanoparticles. *Environmental Science & Technology* 48, 11568-11574.
- Ji, J., Long, Z., Lin, D., 2011. Toxicity of oxide nanoparticles to the green algae *Chlorella sp.* *Chemical Engineering Journal* 170, 525-530.
- Johnson, F., 1998. The genetic effects of environmental lead. *Mutation Research/Reviews in Mutation Research* 410, 123-140.
- Kalman, J., Paul, K.B., Khan, F.R., Stone, V., Fernandes, T.F., 2015. Characterisation of bioaccumulation dynamics of three differently coated silver nanoparticles and aqueous silver in a simple freshwater food chain. *Environmental Chemistry* 12, 662-672.
- Kim, H.S., Kwack, S.J., Lee, B.M., 2000. Lipid peroxidation, antioxidant enzymes, and benzo [a] pyrene-quinones in the blood of rats treated with benzo [a] pyrene. *Chemico-Biological Interactions* 127, 139-150.
- Kim, K.T., Truong, L., Wehmas, L., Tanguay, R.L., 2013. Silver nanoparticle toxicity in the embryonic zebrafish is governed by particle dispersion and ionic environment. *Nanotechnology* 24, 8.
- Kim, M.-S., Hong, K.-M., Chung, J.G., 2003. Removal of Cu (II) from aqueous solutions by adsorption process with anatase-type titanium dioxide. *Water Research* 37, 3524-3529.
- Kovriznych, J.A., Sotnikova, R., Zeljenkova, D., Rollerova, E., Szabova, E., Wimmerova, S., 2013. Acute toxicity of 31 different nanoparticles to zebrafish (*Danio rerio*) tested in

- adulthood and in early life stages - comparative study. *Interdisciplinary Toxicology* 6, 67-73.
- Kołodziejczak-Radzimska, A., Jesionowski, T., 2014. Zinc oxide—from synthesis to application: a review. *Materials* 7, 2833-2881.
- Lee, M.M., Teuscher, J., Miyasaka, T., Murakami, T.N., Snaith, H.J., 2012. Efficient hybrid solar cells based on meso-superstructured organometal halide perovskites. *Science* 338, 643-647.
- Lee, R.F., 2003. Photo-oxidation and photo-toxicity of crude and refined oils. *Spill Science & Technology Bulletin* 8, 157-162.
- Lee, S., Choi, H., Suh, S., Doo, I.-S., Oh, K.-Y., Choi, E.J., Taylor, A.T.S., Low, P.S., Lee, Y., 1999. Oligogalacturonic acid and chitosan reduce stomatal aperture by inducing the evolution of reactive oxygen species from guard cells of tomato and *Commelina communis*. *Plant Physiology* 121, 147-152.
- Li, G., Lv, L., Fan, H.T., Ma, J.Y., Li, Y.Q., Wan, Y., Zhao, X.S., 2010. Effect of the agglomeration of TiO₂ nanoparticles on their photocatalytic performance in the aqueous phase. *Journal of Colloid and Interface Science* 348, 342-347.
- Li, M., Luo, Z., Yan, Y., Wang, Z., Chi, Q., Yan, C., Xing, B., 2016a. Arsenate accumulation, distribution, and toxicity associated with titanium dioxide nanoparticles in *Daphnia magna*. *Environmental Science & Technology* 50, 9636-9643.
- Li, S.B., Pan, X., Wallis, L.K., Fan, Z.Y., Chen, Z.L., Diamond, S.A., 2014. Comparison of TiO₂ nanoparticle and graphene-TiO₂ nanoparticle composite phototoxicity to *Daphnia magna* and *Oryzias latipes*. *Chemosphere* 112, 62-69.
- Li, X., Zhou, S., Fan, W., 2016b. Effect of nano-Al₂O₃ on the toxicity and oxidative stress of copper towards *Scenedesmus obliquus*. *International Journal of Environmental Research and Public Health* 13, 575.
- Liang, L., Lv, J., Luo, L., Zhang, J., Zhang, S., 2011. Influences of surface-coated fulvic and humic acids on the adsorption of metal cations to SiO₂ nanoparticles. *Colloids and Surfaces A: Physicochemical and Engineering Aspects* 389, 27-32.

- Lin, D., Ji, J., Long, Z., Yang, K., Wu, F., 2012. The influence of dissolved and surface-bound humic acid on the toxicity of TiO₂ nanoparticles to *Chlorella sp.* Water Research 46, 4477-4487.
- Linsebigler, A.L., Lu, G., Yates Jr, J.T., 1995. Photocatalysis on TiO₂ surfaces: principles, mechanisms, and selected results. Chemical Reviews 95, 735-758.
- Lu, K., Dong, S., Petersen, E.J., Niu, J., Chang, X., Wang, P., Lin, S., Gao, S., Mao, L., 2017. Biological uptake, distribution, and depuration of radio-labeled graphene in adult zebrafish: effects of graphene size and natural organic matter. ACS Nano 11, 2872-2885.
- Ma, H.B., Brennan, A., Diamond, S.A., 2012. Phototoxicity of TiO₂ nanoparticles under solar radiation to two aquatic species: *Daphnia magna* and *Japanese medaka*. Environmental Toxicology and Chemistry 31, 1621-1629.
- Mallakin, A., Dixon, D.G., Greenberg, B.M., 2000. Pathway of anthracene modification under simulated solar radiation. Chemosphere 40, 1435-1441.
- Marrugan, A., 2004. Measuring biological diversity. Victoria, Australia: Blackwell Scienc Ltd a Blackwell Publishing company.
- Meyer, J.S., 2005. Toxicity of dietborne metals to aquatic organisms. Allen Press/ACG Publishing.
- Miller, K.P., Ramos, K.S., 2001. Impact of cellular metabolism on the biological effects of benzo [a] pyrene and related hydrocarbons. Drug Metabolism Reviews 33, 1-35.
- Moreno-Garrido, I., Pérez, S., Blasco, J., 2015. Toxicity of silver and gold nanoparticles on marine microalgae. Marine Environmental Research 111, 60-73.
- Mount, D.R., Barth, A.K., Garrison, T.D., Barten, K.A., Hockett, J.R., 1994. Dietary and waterborne exposure of rainbow trout (*Oncorhynchus mykiss*) to copper, cadmium, lead and zinc using a live diet. Environmental Toxicology and Chemistry 13, 2031-2041.
- Navarro, E., Baun, A., Behra, R., Hartmann, N.B., Filser, J., Miao, A.-J., Quigg, A., Santschi, P.H., Sigg, L., 2008. Environmental behavior and ecotoxicity of engineered nanoparticles to algae, plants, and fungi. Ecotoxicology 17, 372-386.
- Nur, Y., Lead, J.R., Baalousha, M., 2015. Evaluation of charge and agglomeration behavior of TiO₂ nanoparticles in ecotoxicological media. Science of the Total Environment 535, 45-53.

- Oukarroum, A., Bras, S., Perreault, F., Popovic, R., 2012. Inhibitory effects of silver nanoparticles in two green algae, *Chlorella vulgaris* and *Dunaliella tertiolecta*. *Ecotoxicology and Environmental Safety* 78, 80-85.
- Pan, B., Lin, D.H., Mashayekhi, H., Xing, B.S., 2008. Adsorption and hysteresis of bisphenol A and 17 alpha-ethinyl estradiol on carbon nanomaterials. *Environmental Science & Technology* 42, 5480-5485.
- Park, H.G., Yeo, M.K., 2013. Comparison of gene expression changes induced by exposure to Ag, Cu-TiO₂, and TiO₂ nanoparticles in zebrafish embryos. *Molecular & Cellular Toxicology* 9, 129-139.
- Park, J.W., Henry, T.B., Ard, S., Menn, F.M., Compton, R.N., Sayler, G.S., 2011. The association between nC₍₆₀₎ and 17 alpha-ethinylestradiol (EE2) decreases EE2 bioavailability in zebrafish and alters nanoaggregate characteristics. *Nanotoxicology* 5, 406-416.
- Park, J.W., Henry, T.B., Menn, F.M., Compton, R.N., Sayler, G., 2010. No bioavailability of 17 alpha-ethinylestradiol when associated with nC₍₆₀₎ aggregates during dietary exposure in adult male zebrafish (*Danio rerio*). *Chemosphere* 81, 1227-1232.
- Paul, T., Miller, P.L., Strathmann, T.J., 2007. Visible-light-mediated TiO₂ photocatalysis of fluoroquinolone antibacterial agents. *Environmental Science & Technology* 41, 4720-4727.
- Perraudin, E., Budzinski, H., Villenave, E., 2007. Identification and quantification of ozonation products of anthracene and phenanthrene adsorbed on silica particles. *Atmospheric Environment* 41, 6005-6017.
- Petersen, E.J., Henry, T.B., Zhao, J., MacCuspie, R.I., Kirschling, T.L., Dobrovolskaia, M.A., Hackley, V., Xing, B.S., White, J.C., 2014. Identification and avoidance of potential artifacts and misinterpretations in nanomaterial ecotoxicity measurements. *Environmental Science & Technology* 48, 4226-4246.
- Peterson, J.W., Gu, B.H., Seymour, M.D., 2015. Surface interactions and degradation of a fluoroquinolone antibiotic in the dark in aqueous TiO₂ suspensions. *Science of the Total Environment* 532, 398-403.

- Peterson, S.M., Zhang, J., Weber, G., Freeman, J.L., 2011. Global gene expression analysis reveals dynamic and developmental stage-dependent enrichment of lead-induced neurological gene alterations. *Environmental Health Perspectives* 119, 615.
- Pigeot-Remy, S., Dufour, F., Herissan, A., Ruaux, V., Mauge, F., Hazime, R., Foronato, C., Guillard, C., Chaneac, C., Durupthy, O., Colbeau-Justin, C., Cassaignon, S., 2017. Bipyrnidal anatase TiO₂ nanoparticles, a highly efficient photocatalyst? Towards a better understanding of the reactivity. *Applied Catalysis B-Environmental* 203, 324-334.
- Rabitto, I., Costa, J.A., de Assis, H.S., Pelletier, E., Akaishi, F., Anjos, A., Randi, M., Ribeiro, C.O., 2005. Effects of dietary Pb (II) and tributyltin on neotropical fish, *Hoplias malabaricus*: histopathological and biochemical findings. *Ecotoxicology and Environmental Safety* 60, 147-156.
- Rodea-Palomares, I., Gonzalo, S., Santiago-Morales, J., Leganés, F., García-Calvo, E., Rosal, R., Fernández-Pinas, F., 2012. An insight into the mechanisms of nanoceria toxicity in aquatic photosynthetic organisms. *Aquatic Toxicology* 122, 133-143.
- Rosenfeldt, R.R., Seitz, F., Schulz, R., Bundschuh, M., 2014. Heavy metal uptake and toxicity in the presence of titanium dioxide nanoparticles: a factorial approach using *Daphnia magna*. *Environmental Science & Technology* 48, 6965-6972.
- Rosenfeldt, R.R., Seitz, F., Senn, L., Schilde, C., Schulz, R., Bundschuh, M., 2015. Nanosized titanium dioxide reduces copper toxicity - the role of organic material and the crystalline phase. *Environmental Science & Technology* 49, 1815-1822.
- Rothenberg, G., 2008. Heterogeneous catalysis. *Catalysis: Concepts and Green Applications*, 127-187.
- Schloss, P.D., Gevers, D., Westcott, S.L., 2011. Reducing the effects of PCR amplification and sequencing artifacts on 16S rRNA-based studies. *PloS One* 6, e27310.
- Schwab, F., Bucheli, T.D., Camenzuli, L., Magrez, A., Knauer, K., Sigg, L., Nowack, B., 2013. Diuron sorbed to carbon nanotubes exhibits enhanced toxicity to *Chlorella vulgaris*. *Environmental Science & Technology* 47, 7012-7019.
- Selck, H., Handy, R.D., Fernandes, T.F., Klaine, S.J., Petersen, E.J., 2016. Nanomaterials in the aquatic environment: An EU-USA perspective on the status of ecotoxicity testing,

- research priorities and challenges ahead. *Environmental Toxicology and Chemistry/SETAC* 35, 1055.
- Semple, K.T., Doick, K.J., Jones, K.C., Burauel, P., Craven, A., Harms, H., 2004. Peer reviewed: defining bioavailability and bioaccessibility of contaminated soil and sediment is complicated. ACS Publications.
- Silva, A.R., Martins, P.M., Teixeira, S., Carabineiro, S.A.C., Kuehn, K., Cuniberti, G., Alves, M.M., Lanceros-Mendez, S., Pereira, L., 2016. Ciprofloxacin wastewater treated by UVA photocatalysis: contribution of irradiated TiO₂ and ZnO nanoparticles on the final toxicity as assessed by *Vibrio fischeri*. *Rsc Advances* 6, 95494-95503.
- Silva, J.C.C., Teodoro, J.A.R., Afonso, R.J.d.C.F., Aquino, S.F., Augusti, R., 2014. Photolysis and photocatalysis of ibuprofen in aqueous medium: characterization of by-products via liquid chromatography coupled to high-resolution mass spectrometry and assessment of their toxicities against *Artemia Salina*. *Journal of Mass Spectrometry* 49, 145-153.
- Strümpel, C., McCann, M., Beaucarne, G., Arkhipov, V., Slaoui, A., Švrček, V., Del Cañizo, C., Tobias, I., 2007. Modifying the solar spectrum to enhance silicon solar cell efficiency—An overview of available materials. *Solar Energy Materials and Solar Cells* 91, 238-249.
- Sun, T.Y., Gottschalk, F., Hungerbühler, K., Nowack, B., 2014. Comprehensive probabilistic modelling of environmental emissions of engineered nanomaterials. *Environmental Pollution* 185, 69-76.
- Sun, Y., Zhang, G., He, Z., Wang, Y., Cui, J., Li, Y., 2016. Effects of copper oxide nanoparticles on developing zebrafish embryos and larvae. *International Journal of Nanomedicine* 11, 905.
- Suttioparnit, K., Jiang, J., Sahu, M., Suvachittanont, S., Charinpanitkul, T., Biswas, P., 2011. Role of surface area, primary particle size, and crystal phase on titanium dioxide nanoparticle dispersion properties. *Nanoscale Res Lett* 6, 27.
- Tan, C., Wang, W.-X., 2014. Modification of metal bioaccumulation and toxicity in *Daphnia magna* by titanium dioxide nanoparticles. *Environmental Pollution* 186, 36-42.
- The R Core Team., 2015. R : A language and environment for statistical computing., version 3.2.1 ed. R Foundation for Statistical Computing, Vienna, Austria.

- Thit, A., Skjolding, L.M., Selck, H., Sturve, J., 2017. Effects of copper oxide nanoparticles and copper ions to zebrafish (*Danio rerio*) cells, embryos and fry. *Toxicology in Vitro* 45, 89-100.
- Thomas, S., Stephen, R., 2010. Rubber nanocomposites: preparation, properties and applications. John Wiley & Sons.
- Tian, S., Zhang, Y., Song, C., Zhu, X., Xing, B., 2014. Titanium dioxide nanoparticles as carrier facilitate bioaccumulation of phenanthrene in marine bivalve, ark shell (*Scapharca subcrenata*). *Environmental Pollution* 192, 59-64.
- Tuominen, M., Schultz, E., Sillanpää, M., 2013. Toxicity and stability of silver nanoparticles to the green alga *Pseudokirchneriella subcapitata* in boreal freshwater samples and growth media. *Nanomaterials and the Environment* 1, 48-57.
- Van Hoecke, K., Quik, J.T.K., Mankiewicz-Boczek, J., De Schamphelaere, K.A.C., Elsaesser, A., Van der Meeren, P., Barnes, C., McKerr, G., Howard, C.V., Van De Meent, D., Rydzynski, K., Dawson, K.A., Salvati, A., Lesniak, A., Lynch, I., Silversmit, G., De Samber, B., Vincze, L., Janssen, C.R., 2009. Fate and effects of CeO₂ nanoparticles in aquatic ecotoxicity tests. *Environmental Science & Technology* 43, 4537-4546.
- Vicario-Parés, U., Castañaga, L., Lacave, J.M., Oron, M., Reip, P., Berhanu, D., Valsami-Jones, E., Cajaraville, M.P., Orbea, A., 2014. Comparative toxicity of metal oxide nanoparticles (CuO, ZnO and TiO₂) to developing zebrafish embryos. *Journal of Nanoparticle Research* 16, 2550.
- Vinodhini, R., Narayanan, M., 2008. Bioaccumulation of heavy metals in organs of fresh water fish *Cyprinus carpio* (common carp). *International Journal of Environmental Science & Technology* 5, 179-182.
- Von Moos, N., Koman, V.B., Santschi, C., Martin, O.J., Maurizi, L., Jayaprakash, A., Bowen, P., Slaveykova, V.I., 2016. Pro-oxidant effects of nano-TiO₂ on *Chlamydomonas reinhardtii* during short-term exposure. *Rsc Advances* 6, 115271-115283.
- Wang, G., Fowler, B.A., 2008. Roles of biomarkers in evaluating interactions among mixtures of lead, cadmium and arsenic. *Toxicology and Applied Pharmacology* 233, 92-99.

- Wang, X., Tao, S., Xing, B., 2009. Sorption and competition of aromatic compounds and humic acid on multiwalled carbon nanotubes. *Environmental Science & Technology* 43, 6214-6219.
- Xu, N., Shi, Z., Fan, Y., Dong, J., Shi, J., Hu, M.Z.-C., 1999. Effects of particle size of TiO₂ on photocatalytic degradation of methylene blue in aqueous suspensions. *Industrial & Engineering Chemistry Research* 38, 373-379.
- Yablonovitch, E., 1993. Photonic band-gap structures. *JOSA B* 10, 283-295.
- Yang, K., Wang, X.L., Zhu, L.Z., Xing, B.S., 2006. Competitive sorption of pyrene, phenanthrene, and naphthalene on multiwalled carbon nanotubes. *Environmental Science & Technology* 40, 5804-5810.
- Yang, L., Liya, E.Y., Ray, M.B., 2008. Degradation of paracetamol in aqueous solutions by TiO₂ photocatalysis. *Water research* 42, 3480-3488.
- Yang, W.-W., Miao, A.-J., Yang, L.-Y., 2012. Cd²⁺ Toxicity to a green alga *Chlamydomonas reinhardtii* as influenced by its adsorption on TiO₂ engineered nanoparticles. *PLoS One* 7, e32300.
- Yu, H., 2002. Environmental carcinogenic polycyclic aromatic hydrocarbons: photochemistry and phototoxicity. *Journal of Environmental Science and Health - Part C Environmental Carcinogenesis and Ecotoxicology Reviews* 20, 149-183.
- Zhang, L., Li, P., Gong, Z., Li, X., 2008. Photocatalytic degradation of polycyclic aromatic hydrocarbons on soil surfaces using TiO₂ under UV light. *Journal of Hazardous Materials* 158, 478-484.
- Zhang, W., Xiong, B., Chen, L., Lin, K., Cui, X., Bi, H., Guo, M., Wang, W., 2013. Toxicity assessment of *Chlorella vulgaris* and *Chlorella protothecoides* following exposure to Pb (II). *Environmental Toxicology and Pharmacology* 36, 51-57.
- Zhang, Y., Zhou, J., Ning, B., 2007. Photodegradation of estrone and 17β-estradiol in water. *Water Research* 41, 19-26.
- Zhang, Z., Wang, C.-C., Zakaria, R., Ying, J.Y., 1998. Role of particle size in nanocrystalline TiO₂-based photocatalysts. *The Journal of Physical Chemistry B* 102, 10871-10878.

Zhao, W., Ma, W., Chen, C., Zhao, J., Shuai, Z., 2004. Efficient degradation of toxic organic pollutants with Ni₂O₃/TiO₂-x B x under visible irradiation. *Journal of the American Chemical Society* 126, 4782-4783.